

Final Report

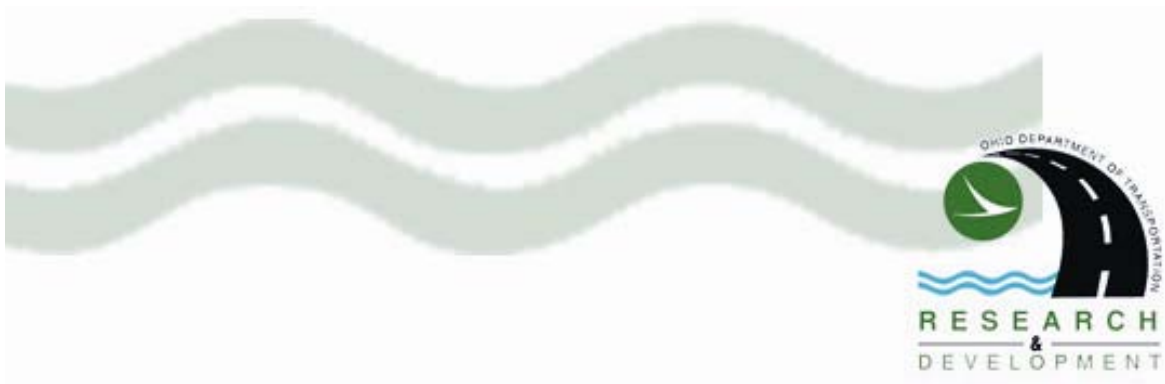
Guidelines for Implementing NCHRP 1-37A M-E Design Procedures in Ohio: Volume 4 - MEPDG Models Validation & Recalibration

Leslie Titus Glover and Jagannath Mallela

Applied Research Associates, Inc.
100 Trade Centre Drive, Suite 200
Champaign, IL 61820

Prepared in cooperation with
the Ohio Department of Transportation, and
the U.S. Department of Transportation,
Federal Highway Administration
State Job Number 134300

November, 2009



1. Report No. FHWA/OH-2009/9D	2. Government Accession No.	3. Recipient's Catalog No.	
4. Title and Subtitle Guidelines for Implementing NCHRP 1-37A M-E Design Procedures in Ohio: Volume 4 – MEPDG Models Validation & Recalibration		5. Report Date November, 2009	
		6. Performing Organization Code	
7. Authors Leslie Titus Glover and Jagannath Mallela		8. Performing Organization Report No.	
9. Performing Organization Name and Address Applied Research Associates, Inc. 100 Trade Centre Dr., Suite 200 Champaign, IL 61820-7233		10. Work Unit No. (TRAIS)	
		11. Contract or Grant No. 134300	
12. Sponsoring Agency Name and Address Office of Research and Development Ohio Department of Transportation 1980 W. Broad St. Columbus, Ohio 43223		13. Type of Report and Period Covered Final Report	
		14. Sponsoring Agency Code	
15. Supplementary Notes			
16. Abstract The development of the Mechanistic-Empirical Pavement Design Guide (MEPDG) under National Cooperative Highway Research Program (NCHRP) projects 1-37A and 1-40D has significantly improved the ability of pavement designers to model and simulate the effects of traffic and climate on future pavement damage, distress, and smoothness. With the adoption of the MEPDG as an American Association of State Highway and Transportation Officials (AASHTO) Interim Guide for Pavement Design, the next step is to integrate the MEPDG into the mainstream of pavement design procedures of State highway agencies across the U.S. The objective of this project was to implement the MEPDG for the Ohio Department of Transportation. More specifically, this study investigated a key requirement for integrating the MEPDG into current ODOT pavement design procedures, that is, evaluating the adequacy of global calibration factors for predicting pavement performance in Ohio and, if needed, developing local calibration factors. Using very limited data from a few LTPP projects located at one site in central Ohio, the study found that the prediction capacities of the MEPDG new hot mix asphalt (HMA) rutting and smoothness (IRI) models and the new jointed plain concrete pavement (JPCP) IRI model needed to be calibrated for Ohio conditions. The HMA alligator cracking model was not evaluated because of lack of adequate data. The results of a limited recalibration of these models are presented in this report. Further evaluation and recalibration is recommended using a more comprehensive database containing both HMA and JPCP projects that reflect Ohio pavement design and construction practices as well as climate and subgrade conditions.			
17. Key Words Pavement, mechanistic, design, concrete, asphalt, calibration, MEPDG		18. Distribution Statement No restriction. This document is available to the public through the National Technical Information Service, 5285 Port Royal Road, Springfield, VA 22161	
19. Security Classif.(of this report) Unclassified	20. Security Classif. (of this page) Unclassified	21. No. of Pages 87	22. Price

SI* (MODERN METRIC) CONVERSION FACTORS

APPROXIMATE CONVERSIONS TO SI UNITS

Symbol	When You Know	Multiply By	To Find	Symbol
LENGTH				
in	inches	25.4	millimeters	mm
ft	feet	0.305	meters	m
yd	yards	0.914	meters	m
mi	miles	1.61	kilometers	km
AREA				
in ²	square inches	645.2	square millimeters	mm ²
ft ²	square feet	0.093	square meters	m ²
yd ²	square yard	0.836	square meters	m ²
ac	acres	0.405	hectares	ha
mi ²	square miles	2.59	square kilometers	km ²
VOLUME				
fl oz	fluid ounces	29.57	milliliters	mL
gal	gallons	3.785	liters	L
ft ³	cubic feet	0.028	cubic meters	m ³
yd ³	cubic yards	0.765	cubic meters	m ³
NOTE: volumes greater than 1000 L shall be shown in m ³				
MASS				
oz	ounces	28.35	grams	g
lb	pounds	0.454	kilograms	kg
T	short tons (2000 lb)	0.907	megagrams (or "metric ton")	Mg (or "t")
TEMPERATURE (exact degrees)				
°F	Fahrenheit	5 (F-32)/9 or (F-32)/1.8	Celsius	°C
ILLUMINATION				
fc	foot-candles	10.76	lux	lx
fl	foot-Lamberts	3.426	candela/m ²	cd/m ²
FORCE and PRESSURE or STRESS				
lbf	poundforce	4.45	newtons	N
lbf/in ²	poundforce per square inch	6.89	kilopascals	kPa
APPROXIMATE CONVERSIONS FROM SI UNITS				
Symbol	When You Know	Multiply By	To Find	Symbol
LENGTH				
mm	millimeters	0.039	inches	in
m	meters	3.28	feet	ft
m	meters	1.09	yards	yd
km	kilometers	0.621	miles	mi
AREA				
mm ²	square millimeters	0.0016	square inches	in ²
m ²	square meters	10.764	square feet	ft ²
m ²	square meters	1.195	square yards	yd ²
ha	hectares	2.47	acres	ac
km ²	square kilometers	0.386	square miles	mi ²
VOLUME				
mL	milliliters	0.034	fluid ounces	fl oz
L	liters	0.264	gallons	gal
m ³	cubic meters	35.314	cubic feet	ft ³
m ³	cubic meters	1.307	cubic yards	yd ³
MASS				
g	grams	0.035	ounces	oz
kg	kilograms	2.202	pounds	lb
Mg (or "t")	megagrams (or "metric ton")	1.103	short tons (2000 lb)	T
TEMPERATURE (exact degrees)				
°C	Celsius	1.8C+32	Fahrenheit	°F
ILLUMINATION				
lx	lux	0.0929	foot-candles	fc
cd/m ²	candela/m ²	0.2919	foot-Lamberts	fl
FORCE and PRESSURE or STRESS				
N	newtons	0.225	poundforce	lbf
kPa	kilopascals	0.145	poundforce per square inch	lbf/in ²

*SI is the symbol for the International System of Units. Appropriate rounding should be made to comply with Section 4 of ASTM E380. (Revised March 2003)

**Guidelines for Implementing NCHRP 1-37A
M-E Design Procedures in Ohio:
Volume 4 – MEPDG Models Validation &
Recalibration**

Final Report

Prepared by

Leslie Titus Glover and Jagannath Mallela

Applied Research Associates, Inc.
100 Trade Centre Drive, Suite 200
Champaign, IL 61820

Credit Reference: Prepared in cooperation with the Ohio Department of Transportation and the U.S. Department Transportation, Federal Highway Administration.

Disclaimer Statement: The contents of this report reflect the views of the authors who are responsible for the facts and the accuracy of the data presented herein. The contents do not necessarily reflect the official views or policies of the Ohio Department of Transportation or the Federal Highway Administration. This report does not constitute a standard, specification or regulation.

November, 2009

ACKNOWLEDGEMENTS

The authors express their deep gratitude to the Ohio Department of Transportation (ODOT). We are particularly grateful to Mr. Roger Green, Mr. Aric Morse, Mr. David Powers, Ms. Vicki Fout, and Ms. Monique Evans for their useful, timely, and constructive comments throughout the planning and execution of this research project.

The authors also gratefully acknowledge the contributions of Dr. Suri Sadasivam of ARA Inc. for his assistance with preparing the project reports and Dr. Susanne Aref, the project's statistical consultant, for her guidance in model recalibration.

TABLE OF CONTENTS

CHAPTER 1. INTRODUCTION.....	1
Background	1
Scope.....	1
Organization of Report.....	2
CHAPTER 2. NEW HMA AND NEW JPCP PERFORMANCE PREDICTION MODELS	3
New HMA Pavements.....	3
Alligator Cracking	3
Transverse Cracking.....	5
Rutting 6	
Smoothness (IRI).....	8
New JPCP	9
Transverse Slab Cracking	9
Transverse Joint Faulting.....	11
Smoothness (IRI).....	12
CHAPTER 3. LTPP PROJECTS USED FOR ANALYSIS	15
Overview of Candidate LTPP Projects for Model Evaluation and Recalibration	15
Identification of Suitable LTPP HMA Projects.....	21
Identification of Suitable LTPP JPCP Projects.....	21
Detailed Description of the LTPP Sections Selected for MEPDG Model Validation	24
Data Types, Data Sources, and Data Processing.....	25
Design (Analysis) Life.....	25
Analysis Parameters.....	27
Traffic 30	
Climatic Data Input.....	37
Pavement Surface Layer Thermal Properties	38
Design Features for HMA and JPCP LTPP Sections	38
Structure Definition.....	39
Performance Data	42
Summary.....	44

TABLE OF CONTENTS, CONTINUED

CHAPTER 4. VALIDATION/RECALIBRATION OF SELECTED MEPDG MODELS	45
Framework for MEPDG Model Validation	45
Determine Model Prediction Capability	46
Estimate Model Accuracy.....	46
Determine Bias	47
New HMA Pavement Models	48
HMA Alligator Cracking.....	48
HMA Transverse Cracking	48
HMA Rutting	51
HMA Smoothness (IRI).....	55
New JPCP	60
Transverse Slab Cracking	60
Transverse Joint Faulting.....	62
JPCP Smoothness (IRI).....	64
CHAPTER 5. SENSITIVITY ANALYSIS OF RECALIBRATED MEPDG MODELS	69
Introduction.....	69
Sensitivity Analysis Results for New HMA Pavements Recalibrated Models	69
Effect of Base Type on MEPDG Predicted HMA Pavement Performance.....	69
Effect of Climate.....	71
Effect of HMA Thickness.....	72
Effect of Subgrade Type.....	72
Effect of HMA In-Situ Air Voids.....	75
Sensitivity Analysis Results for New JPCP Recalibrated Models	78
Effect of Climate.....	78
Effect of PCC Flexural Strength and Modulus of Elasticity	78
Effect of Subgrade Type.....	80
CHAPTER 6. SUMMARY AND CONCLUSIONS.....	83
Summary.....	83
New HMA	83
New JPCP.....	83
Conclusions	85
REFERENCES	87

LIST OF FIGURES

Figure 1.	Layout of the Ohio SHRP Test Road (Sargand et. al., 2007).....	17
Figure 2.	Map showing selected Ohio LTPP projects used for model validation.	18
Figure 3.	Layout of the Ohio SPS-2 projects showing specific construction periods. (Sargand et. al., 2007).....	22
Figure 4.	MEPDG general information requirements.	27
Figure 5.	MEPDG initial IRI input screen and backcast initial IRI.	29
Figure 6.	Hourly estimates of truck traffic for lane 11.....	33
Figure 7.	Estimates of truck traffic for each single axle load grouping for lane 11.	33
Figure 8.	Estimates of truck traffic for each tandem axle load grouping for lane 11.	34
Figure 9.	MEPDG traffic volume inputs.....	35
Figure 10.	Monthly truck volume adjustment factors.	35
Figure 11.	Lateral truck wander and mean number axles/truck.....	36
Figure 12.	Single axle distribution for class 9 trucks.....	36
Figure 13.	Tandem axle distribution for class 9 trucks.....	37
Figure 14.	Climatic data input for project 39_0112.	38
Figure 15.	Field tested and MEPDG computed flexible pavement in-situ subgrade resilient modulus.	41
Figure 16.	Field tested and MEPDG computed JPCP in-situ subgrade k-value.....	41
Figure 17.	Plot of alligator and longitudinal cracking progression for project 0106.....	42
Figure 18.	Plot of alligator and longitudinal cracking progression for project 0903.....	43
Figure 19.	Histogram showing distribution of measured transverse “thermal” cracking.	49
Figure 20.	Histogram showing distribution of measured total rutting.	52
Figure 21.	Plot of measured versus MEPDG predicted HMA pavement total rutting.....	52
Figure 22.	Plot of measured versus MEPDG predicted HMA pavement total rutting.....	54
Figure 23.	Histogram showing distribution of measured total IRI.	56
Figure 24.	Plot of measured versus MEPDG predicted HMA pavement IRI.	56
Figure 25.	Plot of measured versus MEPDG predicted HMA pavement IRI.	59
Figure 26.	Histogram showing distribution of measured transverse slab cracking.	61
Figure 27.	Histogram showing distribution of measured transverse joint faulting for all projects evaluated.....	62
Figure 28.	Plot of measured versus MEPDG predicted JPCP faulting.....	63
Figure 29.	Histogram showing distribution of measured JPCP IRI.	64
Figure 30.	Plot of measured versus MEPDG predicted HMA pavement IRI.	65
Figure 31.	Plot of measured versus recalibrated JPCP IRI model predicted IRI.	67
Figure 32.	Plot showing the effect of base type on predicted rutting.....	70
Figure 33.	Plot showing the effect of base type on predicted IRI.	70
Figure 34.	Plot showing the effect of climate on predicted rutting.	71
Figure 35.	Plot showing the effect of climate on predicted IRI.	72

LIST OF FIGURES, CONTINUED

Figure 36. Plot showing the effect of HMA thickness on predicted rutting.....	73
Figure 37. Plot showing the effect of HMA thickness on predicted IRI.....	73
Figure 38. Plot showing the effect of subgrade type on predicted rutting.....	74
Figure 39. Plot showing the effect of subgrade type on predicted IRI.....	75
Figure 40. Plot showing the effect of HMA air voids in bottom layer on predicted rutting.....	76
Figure 41. Plot showing the effect of HMA air voids in bottom layer on predicted IRI.....	76
Figure 42. Plot showing the effect of HMA air voids in top layer on predicted rutting.....	77
Figure 43. Plot showing the effect of HMA air voids in top layer on predicted IRI.....	77
Figure 44. Plot showing the effect of climate on predicted JPCP IRI.	79
Figure 45. Plot showing the effect of PCC flexural strength and elastic modulus on predicted JPCP IRI.	79
Figure 46. Plot showing the effect of joint spacing on predicted JPCP IRI.....	80
Figure 47. Plot showing the effect of subgrade type on predicted JPCP IRI.....	81

LIST OF TABLES

Table 1.	LTPP projects identified for potential use in MEPDG validation in Ohio.....	16
Table 2.	Detailed summary of project type and design features.....	19
Table 3.	Design and station limits of replacement sections.	22
Table 4.	Predominant sources of data used for MEPDG performance models verification in Ohio.....	26
Table 5.	Summary of construction dates and analysis periods for all selected LTPP projects.	28
Table 6.	Summary of initial IRI estimated for all projects analyzed.....	30
Table 7.	Example of daily single and tandem axle load spectra summary for Mondays in November 1996.	32
Table 8.	GPS coordinates of Ohio LTPP sections selected for use in validation/calibration.....	37
Table 9.	JPCP pavement projects design features.	39
Table 10.	Summary of NCHRP 1-40D new HMA pavement and new JPCP model statistics.....	46
Table 11.	Comparison of measured and predicted transverse cracking.....	50
Table 12.	Comparison of measured and predicted transverse cracking by binder type.	50
Table 13.	Statistical comparison of measured and predicted rutting data.	53
Table 14.	Statistical comparison of measured and recalibrated rutting model predicted rutting data.	55
Table 15.	Statistical comparison of measured and MEPDG predicted IRI data.	57
Table 16.	Statistical comparison of measured and predicted recalibrated HMA model IRI data.....	59
Table 17.	Comparison of measured and predicted transverse slab cracking.....	61
Table 18.	Statistical comparison of measured and MEPDG predicted transverse joint faulting data.	63
Table 19.	Statistical comparison of measured and MEPDG predicted JPCP IRI data. ...	65
Table 20.	Statistical comparison of measured and predicted recalibrated JPCP model IRI data.....	68
Table 21.	Recommended Subgrade/Embankment Resilient Modulus Input (at optimum density and moisture) for Rigid Pavements and Rehabilitation of Rigid Pavements.....	81

THIS PAGE INTENTIONALLY LEFT BLANK

CHAPTER 1. INTRODUCTION

Background

National Cooperative Highway Research Program (NCHRP) Projects 1-37A and 1-40D collectively developed a mechanistic-based pavement design guide that utilizes existing state-of-the-practice mechanistic pavement design/analysis algorithms and calibrated the design procedure using field performance data. Version 1.0 of the Mechanistic-Empirical Pavement Design Guide (MEPDG) was completed in 2007 (Darter et al., 2007) and adopted as an American Association of State Highway and Transportation Officials (AASHTO) interim pavement design standard in 2008 (AASHTO, 2008).

The MEPDG was calibrated using data derived mostly from the Long Term Pavement Performance (LTPP) database. The LTPP database contains pavement design, materials, climate, traffic, and performance data from several hundred flexible and rigid experimental pavement projects situated throughout the United States. These data were used to develop “nationally calibrated” performance models under NCHRP Projects 1-37A and 1-40D.

It was noted in NCHRP Project 1-37A that model validation and, perhaps, local calibration may be needed for specific geographic areas if (1) the inference space used in the national calibration exercise did not adequately represent local site and design factors and (2) significant differences were found between the predicted and measured distresses and smoothness using local data.

Given this, it should be pointed out that local calibration should be performed only after a rigorous validation study indicates that there is a bias or error in pavement performance predictions for a local condition. Also, since the MEPDG has a sound mechanistic basis, the validation can be performed with relatively fewer data points than a purely empirical approach.

Thus, for this project, a validation exercise was performed as the first step to determine if the nationally calibrated models were sufficiently accurate when used to predict the performance of the real-world pavements in Ohio.

Scope

Although both new and rehabilitated pavements were of interest to the Ohio Department of Transportation (ODOT), the model validation effort was limited to new or reconstructed hot mix asphalt (HMA) pavements and jointed plain concrete pavements (JPCP) because the data required for validation were available for only these two pavement types. Data were not available at this time for HMA overlaid rubblized

portland cement concrete (PCC) and unbonded JPCP overlays of existing PCC pavements – the common rehabilitation types of interest to ODOT.

The following performance indicators were of relevance to this local model validation/calibration effort:

- Flexible pavements.
 - Total rut depth.
 - Transverse “thermal” cracking.
 - Load-related alligator cracking, bottom initiated cracks.
 - Smoothness (measured as International Roughness Index [IRI]).
- JPCP
 - Mean transverse joint faulting.
 - Load-related transverse slab cracking (includes both bottom and surface initiated cracks).
 - Smoothness (IRI).

These models predict the predominant structural and functional distresses that occur on the selected pavement types in Ohio. Although HMA longitudinal cracking is of interest to the ODOT, an active research is ongoing under the NCHRP program to develop models for predicting top-down, longitudinal cracking in HMA layers. Therefore, a decision was made not to consider longitudinal cracking models in this implementation.

Validation involved verifying whether the nationally calibrated models accurately predicted the performance of selected pavements from Ohio which had readily available, high-quality traffic, foundation, design, materials, and performance data. Based on the results of the validation study, deficient MEPDG models were recalibrated.

Organization of Report

This report presents the results of validation and recalibration of selected MEPDG models for new HMA pavement and JPCP in Ohio. Chapter 2 describes the MEPDG models selected for validation and recalibration. Chapter 3 describes the LTPP projects used in this study. Chapter 4 describes the model validation and recalibration effort. Sensitivity of the recalibrated models is presented in chapter 5. Chapter 6 discusses the summary and conclusions from this effort.

CHAPTER 2. NEW HMA AND NEW JPCP PERFORMANCE PREDICTION MODELS

This section presents a brief description of the MEPDG models listed in chapter 1. Detailed descriptions of these models and the entire MEPDG design procedure have been presented in several publications, including AASHTO's MEPDG Manual of Practice (AASHTO, 2008) and the reports developed under NCHRP Project 1-37A (ARA, 2004) and NCHRP 1-40D (Darter et al., 2007).

New HMA Pavements

Alligator Cracking

Alligator cracking initiates at the bottom of the HMA layers and propagates to the surface with continued application of heavy truck traffic. Alligator cracking prediction in the MEPDG begins with the computation incrementally of HMA bottom up fatigue damage. This is done using a grid pattern throughout the HMA layers at critical depths to determine the location within the HMA layer subjected to the highest amount of horizontal tensile strain – the mechanistic parameters used to relate applied loading to fatigue damage. An incremental damage index, ΔDI , is calculated by dividing the actual number of axle loads by the allowable number of axle loads (note that computation of damage is based on Miner's hypothesis) within a specific time increment and axle load interval for each axle type (Miner, 1945). The cumulative damage index for each critical location is determined by summing the incremental damage over time and traffic using equation 1 (AASHTO, 2008):

$$DI = \sum (\Delta DI)_{j,m,l,p,T} = \sum \left(\frac{n}{N_{f-HMA}} \right)_{j,m,l,p,T} \quad (1)$$

where:

n	=	Actual number of axle load applications within a specific time period
j	=	Axle load interval
m	=	Axle load type (single, tandem, tridem, quad, or special axle configuration)
l	=	Truck type using the truck classification groups included in the MEPDG
p	=	Month
T	=	Median temperature for the five temperature intervals or quintiles used to subdivide each month, °F
N_{f-HMA}	=	Allowable number of axle load applications for a flexible pavement and HMA overlays

The allowable number of axle load applications needed for the incremental damage index computation is shown in equation 2 (AASHTO, 2008).

$$N_{f-HMA} = k_{f1}(C)(C_H)\beta_{f1}(\epsilon_t)^{k_{f2}\beta_{f2}}(E_{HMA})^{k_{f3}\beta_{f3}} \quad (2)$$

where:

- N_{f-HMA} = Allowable number of axle load applications for a flexible pavement and HMA overlays
- ϵ_t = Tensile strain at critical locations and calculated by the structural response model, in/in
- E_{HMA} = Dynamic modulus of the HMA measured in compression, psi
- k_{f1}, k_{f2}, k_{f3} = Global field calibration parameters (from the NCHRP 1-40D re-calibration; $k_{f1} = 0.007566$, $k_{f2} = -3.9492$, and $k_{f3} = -1.281$)
- $\beta_{f1}, \beta_{f2}, \beta_{f3}$ = Local or mixture specific field calibration constants; for the global calibration effort, these constants were set to 1.0

$$C = 10^M \quad (3)$$

$$M = 4.84 \left(\frac{V_{be}}{V_a + V_{be}} - 0.69 \right) \quad (4)$$

- V_{be} = Effective asphalt content by volume, percent
- V_a = Percent air voids in the HMA mixture
- C_H = Thickness correction term as follows:

$$C_H = \frac{1}{0.000398 + \frac{0.003602}{1 + e^{(11.02 - 3.49H_{HMA})}}} \quad (5)$$

- H_{HMA} = Total HMA thickness, in

Alligator cracking is calculated from the cumulative damage over time (equation 1) using the relationship presented as equation 6 (AASHTO, 2008).

$$FC_{Bottom} = \left(\frac{1}{60} \right) \left(\frac{C_4}{1 + e^{(C_1 C_1' + C_2 C_2' \text{Log}(DI_{Bottom}))}} \right) \quad (6)$$

where:

- FC_{Bottom} = Area of alligator cracking that initiates at the bottom of the HMA layers, percent of total lane area

DI_{Bottom} = Cumulative damage index at the bottom of the HMA layers
 $C_{1,2,4}$ = Transfer function regression constants; $C_4= 6,000$; $C_1=1.00$;
and $C_2=1.00$

$$C_1^* = -2C_2^* \quad (7)$$

$$C_2^* = -2.40874 - 39.748(1 + H_{HMA})^{-2.856} \quad (8)$$

where: H_{HMA} = Total HMA thickness, in

Transverse Cracking

For the MEPDG, the amount of crack propagation induced by a given thermal cooling cycle is predicted using the Paris Law of crack propagation (AASHTO, 2008).

$$\Delta C = A(\Delta K)^n \quad (9)$$

where:

ΔC = Change in the crack depth due to a cooling cycle
 ΔK = Change in the stress intensity factor due to a cooling cycle
 A, n = Fracture parameters for the HMA mixture

Experimental results indicate that reasonable estimates of A and n can be obtained from the indirect tensile creep-compliance and strength of the HMA in accordance with equations 10 and 11 (AASHTO, 2008).

$$A = 10^{k_t, \beta_t (4.389 - 2.52 \text{Log}(E_{HMA} \sigma_m^n))} \quad (10)$$

where:

$$\eta = 0.8 \left[1 + \frac{1}{m} \right] \quad (11)$$

k_t = Coefficient determined through global calibration for each input level (Level 1 = 5.0; Level 2 = 1.5; and Level 3 = 3.0)
 E_{HMA} = HMA indirect tensile modulus, psi
 σ_m = Mixture tensile strength, psi
 m = The m-value derived from the indirect tensile creep compliance curve measured in the laboratory
 β_t = Local or mixture calibration factor

Stress intensity factor, K , was incorporated in the MEPDG through the use of a simplified equation developed from theoretical finite element studies (equation 12).

$$K = \sigma_{tip} (0.45 + 1.99(C_o)^{0.56}) \quad (12)$$

where:

- σ_{ip} = Far-field stress from pavement response model at depth of crack tip, psi
 C_o = Current crack length, ft

The amount of transverse cracking is predicted by the MEPDG using an assumed relationship between the probability distribution of the log of the crack depth to HMA layer thickness ratio and the percent of cracking. Equation 13 shows the expression used to determine the amount of thermal cracking (AASHTO, 2008).

$$TC = \beta_{t1} N \left[\frac{1}{\sigma_d} \text{Log} \left(\frac{C_d}{H_{HMA}} \right) \right] \quad (13)$$

where:

- TC = Thermal cracking, ft/mi
 β_{t1} = Regression coefficient determined through global calibration (400)
 $N[z]$ = Standard normal distribution evaluated at $[z]$
 σ_d = Standard deviation of the log of the depth of cracks in the pavement (0.769), in
 C_d = Crack depth, in
 H_{HMA} = Thickness of HMA layers, in

Rutting

Rutting is caused by the plastic or permanent vertical deformation in the HMA, unbound base/subbase layers, and subgrade/foundation soil. For the MEPDG, rutting is predicted by calculating incrementally the plastic vertical strain accumulated in each pavement layer due to applied axle loading. In other words, rutting is the sum of all plastic vertical strain at the mid-depth of each pavement layer within the pavement structure, accumulated over a given analysis period. The rate of pavement layer plastic deformation could vary significantly over a given time increment since (1) the pavement layer properties change with temperature (summer versus winter months) and moisture (wet versus dry) and (2) applied traffic could be very different.

The MEPDG model for calculating total rutting is based on the universal “strain hardening” relationship developed from data obtained from repeated load permanent deformation triaxial tests of both HMA mixtures and unbound aggregate materials and subgrade soils in the laboratory. The laboratory derived relationship was then calibrated to match field measured rut depth.

For all HMA mixtures types, the MEPDG field calibrated form of the laboratory derived relationship from repeated load permanent deformation tests is shown in equation 14.

$$\Delta_{p(HMA)} = \varepsilon_{p(HMA)} h_{HMA} = \beta_{1r} k_z \varepsilon_{r(HMA)} 10^{k_{1r}} n^{k_{2r} \beta_{2r}} T^{k_{3r} \beta_{3r}} \quad (14)$$

where:

$\Delta_{p(HMA)}$	=	Accumulated permanent or plastic vertical deformation in the HMA layer/sublayer, in
$\varepsilon_{p(HMA)}$	=	Accumulated permanent or plastic axial strain in the HMA layer/sublayer, in/in
$\varepsilon_{r(HMA)}$	=	Resilient or elastic strain calculated by the structural response model at the mid-depth of each HMA sublayer, in/in
$h_{(HMA)}$	=	Thickness of the HMA layer/sublayer, in
n	=	Number of axle load repetitions
T	=	Mix or pavement temperature, °F
k_z	=	Depth confinement factor
$k_{1r,2r,3r}$	=	Global field calibration parameters (from the NCHRP 1-40D recalibration; $k_{1r} = -3.35412$, $k_{2r} = 0.4791$, $k_{3r} = 1.5606$)
$\beta_{1r}, \beta_{2r}, \beta_{3r}$	=	Local or mixture field calibration constants; for the global calibration, these constants were all set to 1.0

$$k_z = (C_1 + C_2 D) 0.328196^D \quad (15)$$

$$C_1 = -0.1039(H_{HMA})^2 + 2.4868H_{HMA} - 17.342 \quad (16)$$

$$C_2 = 0.0172(H_{HMA})^2 - 1.7331H_{HMA} + 27.428 \quad (17)$$

D = Depth below the surface, in

H_{HMA} = Total HMA thickness, in

Equation 18 shows the field-calibrated mathematical equation used to calculate plastic vertical deformation within all unbound pavement sublayers and the foundation or embankment soil.

$$\Delta_{p(soil)} = \beta_{s1} k_{s1} \varepsilon_v h_{soil} \left(\frac{\varepsilon_o}{\varepsilon_r} \right) e^{-\left(\frac{\rho}{n} \right)^\beta} \quad (18)$$

where:

$\Delta_{p(Soil)}$	=	Permanent or plastic deformation for the layer/sublayer, in.
n	=	Number of axle load applications
ε_o	=	Intercept determined from laboratory repeated load permanent deformation tests, in/in
ε_r	=	Resilient strain imposed in laboratory test to obtain material properties ε_o , β , and ρ , in/in

ε_v	=	Average vertical resilient or elastic strain in the layer/sublayer and calculated by the structural response model, in/in
h_{Soil}	=	Thickness of the unbound layer/sublayer, in
k_{s1}	=	Global calibration coefficients; $k_{s1}=1.673$ for granular materials and 1.35 for fine-grained materials
β_{s1}	=	Local calibration constant for the rutting in the unbound layers; the local calibration constant was set to 1.0 for the global calibration effort

$$\text{Log}\beta = -0.61119 - 0.017638(W_c) \quad (19)$$

$$\rho = 10^9 \left(\frac{C_o}{1 - (10^9)^\beta} \right)^{\frac{1}{\beta}} \quad (20)$$

$$C_o = \text{Ln} \left(\frac{a_1 M_r^{b_1}}{a_9 M_r^{b_9}} \right) = 0.0075 \quad (21)$$

W_c	=	Water content, percent
M_r	=	Resilient modulus of the unbound layer or sublayer, psi
$a_{1,9}$	=	Regression constants; $a_1=0.15$ and $a_9=20.0$
$b_{1,9}$	=	Regression constants; $b_1=0.0$ and $b_9=0.0$

Smoothness (IRI)

The design premise included in the MEPDG for predicting smoothness degradation is that the development of surface distress will result in a reduction in smoothness (increasing IRI). Equations 22 and 23 were developed from data collected within the LTPP program and are embedded in the MEPDG to predict the IRI over time for new HMA pavements (AASHTO, 2008).

$$\text{IRI} = \text{IRI}_o + 0.0150(\text{SF}) + 0.400(\text{FC}_{\text{Total}}) + 0.0080(\text{TC}) + 40.0(\text{RD}) \quad (22)$$

where:

IRI_o	=	Initial IRI after construction, in/mi
SF	=	Site factor, refer to equation 23
FC_{Total}	=	Area of fatigue cracking (combined alligator, longitudinal, and reflection cracking in the wheel path), percent of total lane area. All load related cracks are combined on an area basis – length of cracks is multiplied by 1 foot to convert length into an area basis
TC	=	Length of transverse cracking (including the reflection of

RD = transverse cracks in existing HMA pavements), ft/mi.
Average rut depth, in

The site factor (SF) is calculated in accordance with the following equation.

$$SF = FROSTH + SWELL * AGE^{1.5} \quad (23)$$

where:

FROSTH = $\text{LN}([\text{PRECIP}+1]*\text{FINES}*\text{FI}+1)$
 SWELLP = $\text{LN}([\text{PRECIP}+1]*\text{CLAY}*\text{PI}+1)$
 FINES = FSAND + SILT
 AGE = pavement age, years
 PI = subgrade soil plasticity index
 PRECIP = mean annual precipitation, in.
 FI = mean annual freezing index, deg. F Days
 FSAND = amount of fine sand particles in subgrade
 (percent of particles between 0.074 and 0.42 mm)
 SILT = amount of silt particles in subgrade
 (percent of particles between 0.074 and 0.002 mm)
 CLAY = amount of clay size particles in subgrade
 (percent of particles less than 0.002 mm)

New JPCP

Transverse Slab Cracking

The MEPDG considers both bottom-up and top-down modes of transverse “slab” cracking in JPCP. Under typical service conditions, the potential for either mode of cracking is present in all slabs – any given slab may crack either from bottom-up or top-down, but not both. Therefore, the predicted bottom-up and top-down cracking are not particularly meaningful by themselves, and combined cracking is reported excluding the possibility of both modes of cracking occurring on the same slab. The percentage of slabs with transverse cracks (including all severities) in a given traffic lane is used as the measure of transverse cracking and is predicted using the following globally calibrated equation for both bottom-up and top-down cracking (AASHTO, 2008):

$$CRK = \frac{1}{1 + (DI_F)^{-1.98}} \quad (24)$$

where:

CRK = Predicted amount of bottom-up or top-down cracking (fraction).
 DI_F = Fatigue damage calculated using the procedure described in this section.

The general expression for fatigue damage accumulations considering all critical factors for JPCP transverse cracking is as follows (based on Miner's hypothesis): (Miner, 1945)

$$DI_F = \sum \frac{n_{i,j,k,l,m,n,o}}{N_{i,j,k,l,m,n,o}} \quad (25)$$

where:

- DI_F = Total fatigue damage (top-down or bottom-up)
- $n_{i,j,k,\dots}$ = Applied number of load applications at condition i, j, k, l, m, n
- $N_{i,j,k,\dots}$ = Allowable number of load applications at condition i, j, k, l, m, n
- i = Age (accounts for change in PCC modulus of rupture and elasticity, slab/base contact friction, deterioration of shoulder LTE)
- j = Month (accounts for change in base elastic modulus and effective dynamic modulus of subgrade reaction)
- k = Axle type (single, tandem, and tridem for bottom-up cracking; short, medium, and long wheelbase for top-down cracking)
- l = Load level (incremental load for each axle type)
- m = Equivalent temperature difference between top and bottom PCC surfaces.
- n = Traffic offset path
- o = Hourly truck traffic fraction

The applied number of load applications ($n_{i,j,k,l,m,n}$) is the actual number of axle type k of load level l that passed through traffic path n under each condition (age, season, and temperature difference). The allowable number of load applications is the number of load cycles at which fatigue failure is expected and is a function of the applied stress and PCC strength. The allowable number of load applications is determined using the following globally calibrated PCC fatigue equation:

$$\log(N_{i,j,k,l,m,n}) = C_1 \cdot \left(\frac{MR_i}{\sigma_{i,j,k,l,m,n}} \right)^{C_2} \quad (26)$$

where:

- $N_{i,j,k,\dots}$ = Allowable number of load applications at condition i, j, k, l, m, n .
- MR_i = PCC modulus of rupture at age i , psi.
- $\sigma_{i,j,k,\dots}$ = Applied stress at condition i, j, k, l, m, n
- C_1 = Calibration constant, 2.0
- C_2 = Calibration constant, 1.22

The fatigue damage calculation is a process of summing damage from each damage increment. Once top-down and bottom-up damage are estimated, the corresponding cracking is computed using equation 24 and the total combined cracking determined using equation 27.

$$TCRACK = (CRK_{Bottom-up} + CRK_{Top-down} - CRK_{Bottom-up} \cdot CRK_{Top-down}) \cdot 100 \quad (27)$$

where:

- $TCRACK$ = Total transverse cracking (percent, all severities).
 $CRK_{Bottom-up}$ = Predicted amount of bottom-up transverse cracking (fraction).
 $CRK_{Top-down}$ = Predicted amount of top-down transverse cracking (fraction).

Equation 27 assumes that a slab may crack from either bottom-up or top-down, but not both.

Transverse Joint Faulting

The mean transverse joint faulting is predicted incrementally on a monthly basis. The magnitude of increment is based on current faulting level, the number of axle loads applied, pavement design features, material properties, and climatic conditions. Total faulting is determined as a sum of faulting increments from all previous months (i.e., since traffic opening) using the following equations (AASHTO, 2008):

$$Fault_m = \sum_{i=1}^m \Delta Fault_i \quad (28)$$

$$\Delta Fault_i = C_{34} * (FAULTMAX_{i-1} - Fault_{i-1})^2 * DE_i \quad (29)$$

$$FAULTMAX_i = FAULTMAX_0 + C_7 * \sum_{j=1}^m DE_j * \text{Log}(1 + C_5 * 5.0^{EROD})^{C_6} \quad (30)$$

$$FAULTMAX_0 = C_{12} * \delta_{curling} * \left[\text{Log}(1 + C_5 * 5.0^{EROD}) * \text{Log}\left(\frac{P_{200} * WetDays}{P_s}\right) \right]^{C_6} \quad (31)$$

where:

- $Fault_m$ = Mean joint faulting at the end of month m , in.
 $\Delta Fault_i$ = Incremental change (monthly) in mean transverse joint faulting during month i , in.
 $FAULTMAX_i$ = Maximum mean transverse joint faulting for month i , in.
 $FAULTMAX_0$ = Initial maximum mean transverse joint faulting, in.
 $EROD$ = Base/subbase erodibility factor.
 $\delta_{curling}$ = Maximum mean monthly slab corner upward deflection PCC due to temperature curling and moisture warping.
 P_s = Overburden on subgrade, lb.
 P_{200} = Percent subgrade material passing No. 200 sieve.
 $WetDays$ = Average annual number of wet days (greater than 0.1 inch rainfall).

DE_i = Differential energy of subgrade deformation accumulated during month i

$$DE = \frac{k}{2} * (w_L + w_{UL})(w_L - w_{UL}) \quad (32)$$

K = modulus of subgrade reaction, psi/in.
 w_L is the corner deflection under the loaded slab.
 w_{UL} is the corner deflection under the loaded slab.

$C_{1,2,3,4,5,6,7,12,34}$ = Global calibration constants ($C_1 = 1.29$; $C_2 = 1.1$; $C_3 = 0.001725$; $C_4 = 0.0008$; $C_5 = 250$; $C_6 = 0.4$; $C_7 = 1.2$; and C_{12} and C_{34} are defined by equations 33 and 34).

$$C_{12} = C_1 + C_2 * FR^{0.25} \quad (33)$$

$$C_{34} = C_3 + C_4 * FR^{0.25} \quad (34)$$

FR = Base freezing index defined as percentage of time the top base temperature is below freezing (32 °F) temperature.

Since the maximum faulting development occurs during nighttime when the PCC slab is curled upward and joints are opened and the load transfer efficiencies are lower, only axle load repetitions applied from 8 p.m. to 8 a.m. are considered in the faulting analysis.

Smoothness (IRI)

In the MEPDG, JPCP smoothness is predicted as a function of the initial as-constructed smoothness and any change in pavement longitudinal profile over time and traffic due to distress development and progression and foundation movements. The IRI model was calibrated and validated using LTPP data that represented variety of design, materials, foundations, and climatic conditions. The following is the final globally calibrated model (AASHTO, 2008):

$$IRI = IRI_I + C1*CRK + C2*SPALL + C3*TFAULT + C4*SF \quad (35)$$

where:

IRI = Predicted IRI, in/mi
 IRI_I = Initial smoothness measured as IRI, in/mi
 CRK = Percent slabs with transverse cracks (all severities)
 $SPALL$ = Percentage of joints with spalling (medium and high severities)
 $TFAULT$ = Total joint faulting cumulated per mi, in
 $C1$ = 0.8203
 $C2$ = 0.4417
 $C3$ = 0.4929

$$\begin{aligned}
C4 &= 25.24 \\
SF &= \text{Site factor} \\
SF &= AGE (1+0.5556*FI) (1+P_{200})*10^{-6} \quad (36)
\end{aligned}$$

where:

$$\begin{aligned}
AGE &= \text{Pavement age, yr.} \\
FI &= \text{Freezing index, } ^\circ\text{F-days.} \\
P_{200} &= \text{Percent subgrade material passing No. 200 sieve.}
\end{aligned}$$

The transverse cracking and faulting are obtained using the MEPDG models described earlier. The transverse joint spalling is determined in accordance with equation 37, which was calibrated using LTPP and other data (AASHTO, 2008).

$$SPALL = \left[\frac{AGE}{AGE + 0.01} \right] \left[\frac{100}{1 + 1.005^{(-12*AGE+SCF)}} \right] \quad (37)$$

where:

$$\begin{aligned}
SPALL &= \text{Percentage joints spalled (medium- and high-severities)} \\
AGE &= \text{Pavement age since construction, years} \\
SCF &= \text{Scaling factor based on site-, design-, and climate-related}
\end{aligned}$$

$$\begin{aligned}
SCF = & -1400 + 350 \cdot AC_{PCC} \cdot (0.5 + PREFORM) + 3.4 f'c \cdot 0.4 \\
& - 0.2 (FT_{cycles} \cdot AGE) + 43 H_{PCC} - 536 WC_{PCC} \quad (38)
\end{aligned}$$

$$\begin{aligned}
AC_{PCC} &= \text{PCC air content, percent} \\
AGE &= \text{Time since construction, years} \\
PREFORM &= \text{1 if preformed sealant is present; 0 if not} \\
f'c &= \text{PCC compressive strength, psi} \\
FT_{cycles} &= \text{Average annual number of freeze-thaw cycles} \\
H_{PCC} &= \text{PCC slab thickness, in} \\
WC_{PCC} &= \text{PCC water/cement ratio}
\end{aligned}$$

THIS PAGE INTENTIONALLY LEFT BLANK.

CHAPTER 3. LTPP PROJECTS USED FOR ANALYSIS

Overview of Candidate LTPP Projects for Model Evaluation and Recalibration

The LTPP database contains design, materials, construction, site (i.e., traffic, climate, and subgrade), and performance information for a wide variety of experimental pavement project types in Ohio; however, only those from the new HMA pavement and new JPCP experiments were relevant to this effort (LTPP, 2008). Table 1 is a detailed listing of the relevant projects from the LTPP Specific Pavement Studies (SPS) 1, SPS 2, SPS 8, SPS 9, and General Pavement Studies (GPS) 3 experiments that were potential candidates for use in this study. Figure 1 and Figure 2 show the layout and geographic locations of these projects, and Table 2 presents the basic design information.

The SPS projects were located on a 3.3-mi section of U.S. Route 23 in Delaware County, 25 miles north of Columbus. Its flat topography and uniform soil conditions and weather made the site ideal for pavement experiments (Sargand et al., 2007).

- Three of the four LTPP experiments at this site are located on new traffic lanes built in the median of U.S. 23 as follows:
 - The new northbound lane contains an LTPP SPS-2 experiment, which compares the performance of different structural designs for PCC pavements.
 - The new southbound lane contains an SPS-1 experiment, which compares different structural designs for asphalt concrete pavements.
 - The new southbound lane also includes an SPS-9 experiment to validate the SuperPave binder specification and to evaluate the performance of SuperPave mixes relative to the ODOT's own asphalt mix.
- Two LTPP SPS-8 experiments (HMA and JPCP) intended to isolate the effects of weather on PCC and HMA pavements are located on a southbound on-ramp to the old lanes of U.S. 23 and are now serving as low-volume frontage roads.
- The SPS-1, SPS-2, and SPS-9 pavements carried an average annual daily traffic (AADT) of 26,000 vehicles, 20 percent of which are trucks when opened to traffic in 1996.

The LTPP GPS-3 projects, LTPP 39_3013 and 39_3801, were constructed in 1970 and 1983, respectively. LTPP 39_3013 is located on the southbound (outer lane) of US 68, southeast of Cincinnati, approximately 1.7 mi north of St-125 and south of Hamer Road. LTPP 39_3801 is located on the southbound (outer lane) of US 7, south of Wheeling, approximately 0.46 mi south of St-147.

Table 1. LTPP projects identified for potential use in MEPDG validation in Ohio (LTPP, 2008).

SHRP ID	Pavement Type	County	Functional Class	Route Signing	Route No.	Direction of Travel	Mile Point	Elev., ft	Location Info
0100 ¹	HMA over various base types ⁵	Delaware	Rural Principal Arterial	US	23	South	20.9	950	North of Delaware
0200 ²	JPCP over various base types ⁶	Delaware	Rural Principal Arterial	US	23	North	17.6	955	North of Delaware
0800 ³	HMA and JPCP over aggregate base	Delaware	Rural Local Collector	US	23	South		950	Onramp onto Us-23 from City of Norton
0900 ⁴	HMA over aggregate base	Delaware	Rural Principal Arterial	US	23	South	18.5	955	South of S-229 (Norton Road); North of Delaware.
3013	New JPCP over cement treated base	Brown	Rural Minor Arterial	US	68	South	21.7	960	1.7 mi N. of St-125 -- W. of US-62 -- 0.48 mi S. of Hamer Rd. -- SE of Cincinnati
3801	New JPCP over cement treated base	Belmont	Urban Other Principal Arterial	US	7	South	12.33	655	0.46 mi S. of St-147 -- 1750' N. of Bridge over R.R. -- S. of Wheeling, Oh. -- S. of Bellaire

1. Includes 12 regular LTPP, 2 supplemental, and 5 replacement (i.e., replaced the originally built sections due to premature failures) new HMA projects.
2. Includes 12 regular LTPP projects and 7 supplemental new JPCP projects.
3. Includes 2 regular new HMA, 2 regular new JPCP, and 2 new HMA replacement projects.
4. Includes 3 regular new SuperPave HMA projects.
5. Base types include dense graded aggregate (DGAB), lean concrete (LCB), asphalt treated (ATB) and permeable asphalt treated (PATB) materials.

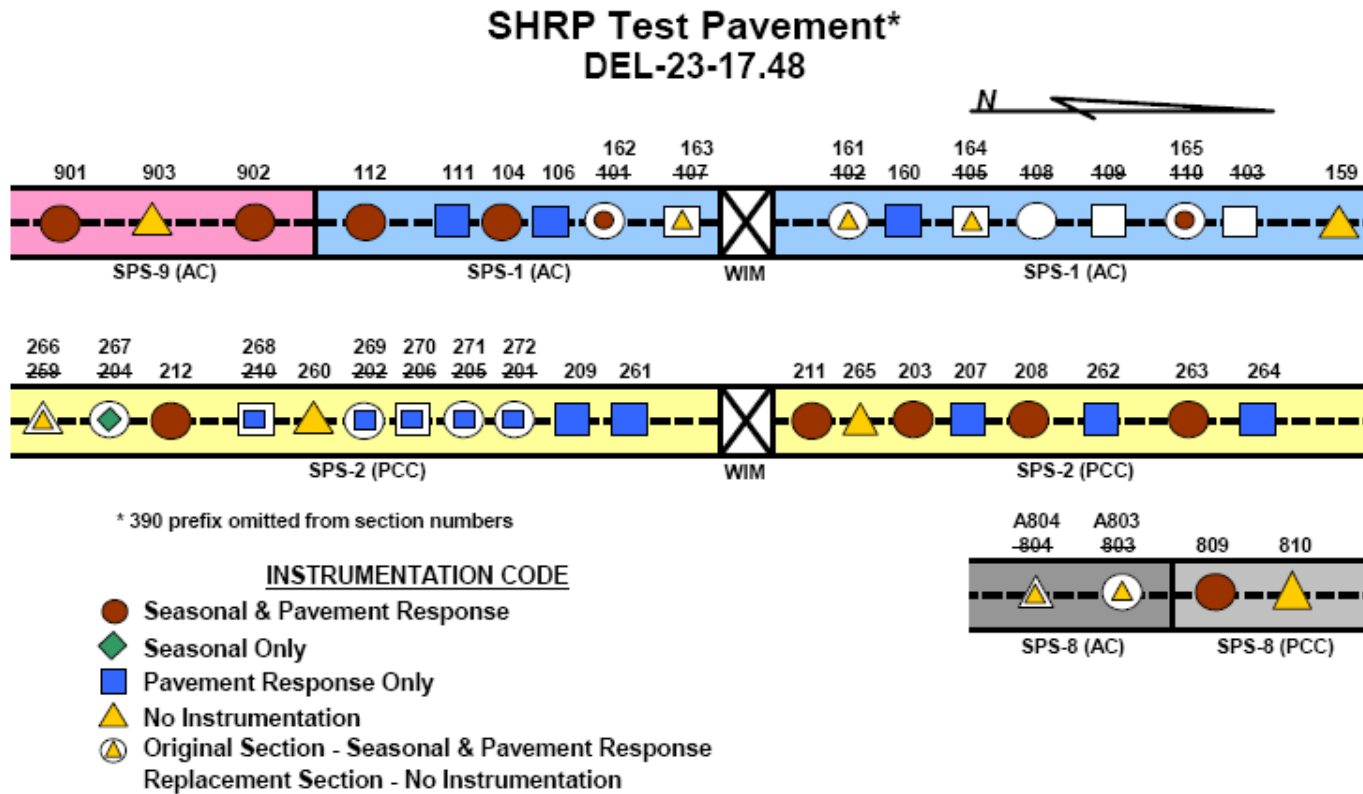


Figure 1. Layout of the Ohio Strategic Highway Research Program (SHRP) Test Road (Sargand et al., 2007).



Figure 2. Map showing selected Ohio LTPP projects used for model validation.

Table 2. Detailed summary of project type and design features
(Sargand et al., 2007).

SPS-1 (Southbound)				
Section	Station	AC Thickness (in.)	Base Type and Thickness	Drains
390101	355+00-350+00	7	8" DGAB	No
390102	375+00-370+00	4	12" DGAB	No
390103	420_75-415+75	4	8" ATB	No
390104	341+00-336+00	7	12" ATB	No
390105	392+50-387+50	4	4" ATB/4" DGAB	No
390106	348+00-343+00	7	8" ATB/4" DGAB	No
390107	363+00-358+00	4	4" PATB/4"DGAB	Yes
390108	399+75-394+75	7	4" ATB/8" DGAB	Yes
390109	406+50-401+50	7	4" PATB/12" DGAB	Yes
390110	413+50-408+50	7	4" ATB/4" PATB	Yes
390111	333+00-328+00	4	8" ATB/4" PATB	Yes
390112	325+00-320+00	4	12" ATB/4" PATB	Yes
390159	433+00-428+00	4	15" ATB/4" PCTB/6" DGAB	Yes
390160	382+00-377+00	4	11" ATB/4"DGAB	Yes
SPS-8 (Ramp)				
Section	Station	AC Thickness (in.)	Base Type and Thickness	Drain
390803	19+19-14+90	4	8" DGAB	No
390804	13+50-8+50	7	12" DGAB	No
SPS-9 (Southbound)				
Section	Station	AC Thickness (in.)	Base Type and Thickness	Drain
390901	282+5-277+75	4 (AC-20)	12" ATB/4" PATB/6" DGAB	Yes
390902	302+50-297+50	4 (PG58-28)	12" ATB/4" PATB/6" DGAB	Yes
390903	291+00-286+00	4 (PG64-28)	12" ATB/4" PATB/6" DGAB	Yes

Table 2. Detailed summary of project type and design features, continued (Sargand et al., 2007).

SPS-2 (Northbound)						
Section	Station	PCC Layer		Lane Width (ft.)	Base Type and Thickness	Drain
		Strength (psi)	Thickness (in.)			
390201	343+00-348+00	ODOT	8	12	6" DGAB	No
390202	319+00-324+00	900	8	14	6" DGAB	No
390203	384+00-389+00	ODOT	11	14	6" DGAB	No
390204	275+50-280+50	900	11	12	6" DGAB	No
390205	335+75-340+75	ODOT	8	12	6" LCB	No
390206	327+50-332+50	900	8	14	6" LCB	No
390207	391+25-396+25	ODOT	11	14	6" LCB	No
390208	397+75-402+75	900	11	12	6" LCB	No
390209	350+25-355+25	ODOT	8	12	4" PATB/4" DGAB	Yes
390210	303+50-308+50	900	8	14	4" PATB/4" DGAB	Yes
390211	369+00-374+00	ODOT	11	14	4" PATB/4" DGAB	Yes
390212	294+00-299+00	900	11	12	4" PATB/4" DGAB	Yes
390259	265+50-270+50	900	11	12	6" DGAB	Yes
390260	311+50-316+50	ODOT	11	12	4" PATB/4" DGAB	Yes
390261	357+75-362+75	ODOT	11	14	4" PCTB/4" DGAB	Yes
390262	405+25-410+25	ODOT	11	12	4" PCTB/4" DGAB	Yes
390263	414+50-419+50	ODOT	11	14	6" DGAB	Yes
390264	422+50-427+50	ODOT	11	12	6" DGAB	Yes
390265	376+10-381+10	ODOT	11	12	4" PATB/4" DGAB	Yes
SPS-8 (Ramp)						
Section	Station	PCC Layer		Lane Width (ft.)	Base Type and Thickness	Drain
		Strength (psi)	Thickness (in.)			
390809	25+90-20+90	550	8	11	6" DGAB	No
390810	32+50-27+50	550	11	11	6" DGAB	No
Section	Station	PCC Layer		Lane Width (ft)	Base Type and Thickness	Drain
		Strength (psi)	Thickness (in)			
393013	21.7	880	8.3	12	4" Soil Cement	No
393801	12.33	750	9.2	12	4.4' CTB	Yes

*Strength = 14-day PCC flexural strength.

Conditions and performance of the experimental pavements are monitored by several thousand sensors. Pavement sensors measure horizontal strain, vertical displacement, vertical pressure, pavement temperature, frost depth, and moisture. Weigh-in-motion (WIM) sensors in the northbound and southbound lanes of U.S. 23 measure the truck counts, weights, and speeds. A weather station measures air temperature, precipitation, wind, relative humidity, and solar radiation.

Identification of Suitable LTPP HMA Projects

Of the 19 LTPP HMA sections originally constructed, the following 6 failed and were replaced soon after they were constructed and opened to traffic (Sargand et al., 2007):

- Four SPS-1 projects: 390101, 390102, 390105, and 390107. All four projects were replaced with more robust pavement sections of interest to ODOT with underdrains.
- Two SPS-8 HMA projects: 390803 and 390804. They were replaced with identical designs, except that lime was added to the subgrade to improve the stiffness of that layer. No underdrains were added to the SPS-8 replacement sections.

Table 3 summarizes the pavement buildup, design features, and station limits of the replacement sections. In Section 390164, PG 64-28 binder was used in both the TI and TII mixes, a bituminous prime coat was used between the permeable asphalt treated base (PATB) and the TII layers, and a tack coat was used between the TII and TI layers. No reclaimed material was used in the TI or TII mixes. Unstapled Tensar BX1100 fabric was placed between the subgrade and DGAB (Sargand et al., 2007).

In 2002, the SPS-1 sections in the southbound lanes were closed because of an imminent failure in Section 390103 and significant rutting in Sections 390108, 390109, and 390110. These four contiguous sections were replaced in 2003 with a new HMA pavement designed for extended service (390165).

The six failed original projects were excluded from analysis. The six replacement projects (39A803, 39A804, 390161, 390162, 390163, and 390164) also were excluded from analysis because of a lack of adequate materials and performance data.

Identification of Suitable LTPP JPCP Projects

JPCP projects from the LTP SPS-2 and GPS-3 experiments were identified for analysis. The SPS-2 sections were constructed in two phases – most of the sections at the south end of the project were constructed in August/September 1996, while the others were constructed in October 1996. The section layout is presented in Figure 3.

Table 3. Design and station limits of replacement sections.
(Sargand et al., 2007).

New SHRP Section	Replaced SHRP Section	Station Limits		Pavement Buildup	Design Features
		Start	End		
39A803	390803	19+90	14+90	1.75" TI/ 2.25" TII/ 8" DGAB over lime stabilized subgrade	No Recycled Material
39A804	390804	13+50	8+50	1.75" TI/ 5.25" TII/ 12" DGAB over lime stabilized subgrade	No Recycled Material
390161	390102	375+00	370+00	1.25" TI/ 1.75" TII/ 12"ATB/4" PATB/ 6" DGAB	SUPERPAVE Level I Design & 20% RAP in both TI and TII. Underdrains installed
390162	390107	363+00	358+00	1.25" TI/ 1.75" TII/ 12"ATB/ 4" PATB/ 6" DGAB	No Recycled Material & Gravel Coarse Agg. In Both T1 and TII. Underdrains installed
390163	390101	355+00	350+00	1.25" TIH/ 1.75" TII/ 12"ATB/ 4" PATB/ 6" DGAB	No Recycled Material in TIH, Polymer added to TIH. Underdrains installed
390164	390105	392+50	387+50	1.75" TI/ 5.25" TII/ 4"PATB/ 8"DGAB/ Geogrid	Geogrid - Tensor BX1100 Underdrains installed
390165	390103	420+75	415+75	1.5"TI/ 1.75"-TII/ 9.5" ATB/4"304NJ/6" DGAB/16" cement stabilized soil	
	390108	399+75	394+75		
	390109	406+50	401+50		
	390110	413+50	408+50		

TI - Asphalt Concrete Surface Course TIH – TI w/coarse aggregate TII - Asphalt Concrete Intermediate Course

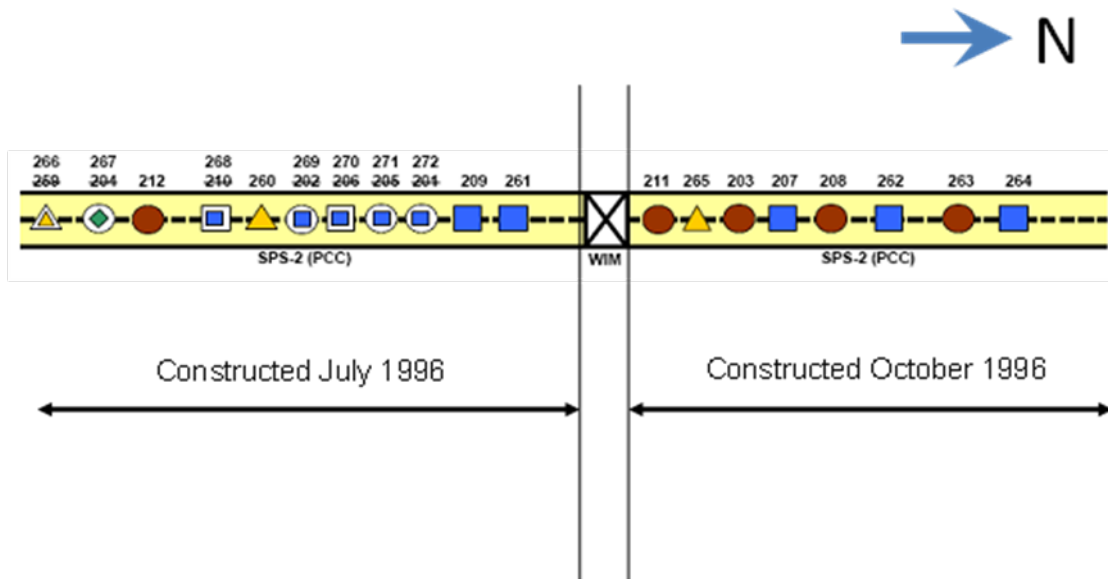


Figure 3. Layout of the Ohio SPS-2 projects showing specific construction periods.
(Sargand et al., 2007)

According to Sargand et al. (2007), Sections 0205 and 0206 showed signs of pumping at both the transverse joints and pavement/shoulder longitudinal joint. Also, both sections contained a longitudinal crack that started near the pavement edge and passed continuously through several slabs as it moved to the right wheel path and back near the pavement edge. By 2006, numerous transverse cracks had developed in projects 0201, 0204, 0205, 0206, 0210, 0212, and 0259. Section 0206 had extensive transverse cracking.

A review of pertinent data and characteristics of the severely cracked and uncracked SPS-2 sections revealed the following:

- Six of the eight severely cracked sections had high strength (780 psi average or as-built 14-day strength) concrete as specified by the SHRP experiment. It must be noted that higher strengths were obtained by increasing the cement contents in the mix design. The remaining 11 sections had ODOT standard concrete mix design (550 psi nominal 14-day strength).
- Five of the eight severely cracked sections had an 8-in-thick PCC slab, and the remainder had an 11-in-thick slab.
- Of the eight severely cracked sections, four were built on a dense graded aggregate base (DGAB), three on lean concrete, and one on a PATB.
- Five of the eight sections had standard width lanes (i.e., 12-ft lanes), and the remainder had widened (14-ft) lanes.
- The concrete temperatures at placement for the severely cracked sections (which were very close to the maximum air temperature noted in the daily logs of the inspector) were on average 9°F higher than those for sections that did not crack. The range of temperatures was between 75°F and 85°F for the former sections and between 60°F and 75°F for the latter.
- The post-placement drop in ambient temperature for the severely cracked sections was 25°F, on average, with the maximum drop recorded for section 0205 of 36°F.

It is plausible that relatively large temperature drops after paving coupled with the high internal heat of hydration that is expected to be generated in many of the high strength mixes could have lead to the development of a “thermal shock” leading to:

- High curling stress related tensile stresses and potentially hairline or micro-cracking at the top of the slab. These cracks would have been aggravated over time by traffic loadings resulting in observable macro-cracking.
- High built-in curling gradients.

Rapid loss of moisture at the surface of the concrete due to the high water demand of the high cement factor mixes used also could have contributed to a large effective built-in gradient. Sargand et al. (2007) also noted that curling and warping might be factors contributing to the premature deterioration of some of the SPS-2 concrete pavement sections.

Based on the information gathered, it was realized that the extensive premature cracking observed on some sections of the SPS-2 experiment in Ohio could be linked to factors that typically contribute to early age cracking in concrete pavements and not to traffic alone. (There are sections with design similar to the failed sections at the

experimental site which have undergone similar traffic and environmental loadings but have not failed.) Early age cracking is related primarily to materials, environmental, and construction factors acting singly or in concert (more common) prevalent at the time of construction or within a few weeks after construction before the pavement is opened to traffic. In the case of the SPS-2 experiment, the risk factors that could have led to early cracking or, at the very least, extensive pre-traffic loading of the pavement in the form of built-in stresses include:

- Large ambient temperature swings (trigger factor).
- High surface evaporation rate (trigger factor).
- High cement factor concrete (material variant).
- Shrinkage susceptible mix (material variant).

A more detailed investigation of ambient conditions and materials factors may need to be performed to ensure a more exhaustive effort that covers all the other associated variables. Nevertheless, the larger point here is that traffic-induced fatigue damage is perhaps not the only force that caused the premature failures. No doubt, repeated traffic load applications could have aggravated the built-in stresses or early age hairline cracking built in to the pavement at the time of construction. Since the MEPDG would need a more precise set of inputs than are available to accurately model the pavement sections that have prematurely cracked, they have been excluded from the model validation analysis undertaken in this study. Moreover, for local validation and calibration purposes, it is desirable to adopt sections that exhibit more typical accumulation of distress.

The failed SPS-2 sections were replaced with SPS-2 projects 390266, 390267, 390268, 390269, 390270, 390271, and 390272 (see Figure 3). These sections also were excluded from the analysis due to a lack of adequate performance data.

Finally, the two GPS-3 projects identified were included in analysis.

Detailed Description of the LTPP Sections Selected for MEPDG Model Validation

The candidate projects shortlisted for analysis are listed below:

- New HMA SPS-1 and SPS-9 pavement (13 projects).
 - 390103
 - 390104
 - 390106
 - 390108
 - 390109
 - 390110
 - 390111
 - 390112
 - 390159
 - 390160
 - 390901
 - 390902
 - 390903

- New JPCP SPS-2 and GPS-3 (14 projects).
 - 390203
 - 390207
 - 390208
 - 390209
 - 390211
 - 390212
 - 390260
 - 390261
 - 390262
 - 390263
 - 390264
 - 390265
 - 393013
 - 393801

Although these projects typically had adequate amounts of good quality data required for analysis, an in-depth review was performed to identify the projects that actually had the data required. A summary of the review and the final list of projects selected for analysis are presented in the following sections.

Data Types, Data Sources, and Data Processing

For the LTPP projects selected, a majority of the required MEPDG inputs were available in the LTPP database. MEPDG national defaults or ODOT-specific defaults were used for the inputs for which data were not available in the LTPP database. Sources of data used in model verification are presented in Table 4. A summary description of these projects is presented in the following sections.

Design (Analysis) Life

The MEPDG requires pavement construction and traffic opening dates along with design life or analysis period. Design life for each project was determined based on construction date. An example of the information required is presented for project 393801 in Figure 4. This project was constructed in September 1983, and the measured performance data are available until 2006. The MEPDG must thus run over a period of 25 years to cover this time period. A summary of pavement construction dates and analysis life is presented in Table 5.

Table 4. Predominant sources of data used for MEPDG performance models verification in Ohio.

Input Group		Input Parameter	Validation Input Level Used	Data Source
Truck Traffic	Axle Load Distributions (single, tandem, tridem)		Level 1	LTPP traffic module and ODOT traffic database
	Truck Volume Distribution		Level 1	LTPP traffic module
	Lane & Directional Truck Distributions		Level 1	
	Tire Pressure		Level 3	MEPDG (national) defaults
	Axle Configuration, Tire Spacing		Level 3	
	Truck wander		Level 3	
Climate		Temperature, Wind Speed, Cloud Cover, Precipitation, Relative Humidity	Level 1 Weather Stations	NCDC*
Material Properties	Unbound Layers & Subgrade	Resilient Modulus - Subgrade All Unbound Layers	Level 1; Backcalculation	LTPP
		Resilient Modulus - Base/subbase	Level 3	Ohio MEPDG related literature or MEPDG defaults
		Classification & Volumetric Properties	Level 1	LTPP
		Moisture-Density Relationships	Level 1	LTPP
		Soil-Water Characteristic Relationships	Level 3	MEPDG defaults
		Saturated Hydraulic Conductivity	Level 3	MEPDG defaults
	HMA	HMA Dynamic Modulus	Level 2	LTPP
		HMA Creep Compliance & Indirect Tensile Strength	Levels 3	Ohio MEPDG related literature or MEPDG defaults
		Volumetric Properties	Level 1	LTPP
		HMA Coefficient of Thermal Expansion	Level 3	MEPDG defaults
	PCC	PCC Elastic Modulus	Level 1 & 2	LTPP
		PCC Flexural Strength	Level 1 & 2	LTPP
		PCC Coefficient of Thermal Expansion	Level 1 & 2	LTPP
All Materials	Unit Weight	Level 1	LTPP	
	Poisson's Ratio	Levels 1 and 3	Ohio MEPDG related literature or MEPDG defaults	
	Other Thermal Properties; conductivity, heat capacity, surface absorptivity	Level 3	MEPDG defaults	

* National Climatic Data Center

General Information

Project Name: 39_3801

Description:

Design Life (years): 25

Base/Subgrade Construction Month: Year:

Pavement Construction Month: September Year: 1983

Traffic open month: December Year: 1983

Type of Design

New Pavement

Flexible Pavement Jointed Plain Concrete Pavement (JPCP) Continuously Reinforced Concrete Pavement (CRCP)

Restoration

Jointed Plain Concrete Pavement (JPCP)

Overlay

Asphalt Concrete Overlay PCC Overlay

OK Cancel

Figure 4. MEPDG general information requirements (example using project 39-3801).

Analysis Parameters

The MEPDG requires terminal distress/IRI values along with initial IRI. For the validation exercise, terminal distress/IRI is not relevant. For all the projects used in analysis, initial IRI was backcast from historical IRI data available for each section. An illustration of how the initial IRI is backcast from historical IRI information is shown for project 39-0101 in Figure 5. For this project, an initial IRI in 1995 was estimated from backcasting to be 75.4 in/mile. Figure 5 also presents the MEPDG input screen for this input category for project 39-0101. A summary of initial IRI values for all the LTPP sections analyzed as part of this study is presented in Table 6.

Although there was a wide range of backcasted initial IRI values, most of the estimated values appear reasonable when compared to common pavement construction practice. This is because most of the pavements evaluated (with the exception of the two GPS-3 projects) were newly constructed and IRI was measured and reported by LTPP within the first year of construction, when the pavement had been subjected to very little deterioration. An exception to this is the GPS-3 project 393013 for which the backcasted initial IRI was relatively high (151 in/mi). This high value was found to be unreasonable and was excluded from IRI analysis.

Table 5. Summary of construction dates and analysis periods for all selected LTPP projects.

LTPP ID	Date Construction Began	Date Construction Completed	Design Life, yrs
390103	30-Aug-95	26-Oct-95	9
390104	17-Aug-95	09-Oct-95	9
390106	17-Oct-95	26-Oct-95	9
390108	15-Sep-95	26-Oct-95	9
390109	18-Sep-95	26-Oct-95	9
390110	15-Sep-95	26-Oct-95	9
390111	21-Aug-95	09-Oct-95	9
390112	21-Aug-95	09-Oct-95	9
390159	23-Sep-95	26-Oct-95	9
390160	23-Sep-95	26-Oct-95	9
390203	17-Oct-95	17-Oct-95	9
390207	30-Oct-95	30-Oct-95	9
390208	06-Nov-95	06-Nov-95	9
390209	23-Oct-95	23-Oct-95	9
390211	19-Oct-95	19-Oct-95	9
390260	02-Oct-95	02-Oct-95	9
390261	26-Sep-95	26-Sep-95	9
390261	19-Oct-95	19-Oct-95	9
390262	27-Sep-95	27-Sep-95	9
390262	11-Oct-95	11-Oct-95	9
390263	16-Oct-95	16-Oct-95	9
390265	25-Sep-95	25-Sep-95	9
390901	09-Oct-95	07-Sep-95	9
390902	09-Oct-95	22-Aug-95	9
390903	09-Oct-95	22-Aug-95	9
393013	—	22-Mar-70	40
393801	—	22-Sep-83	25

Analysis Parameters

Project Name:

Initial IRI (in/mi)

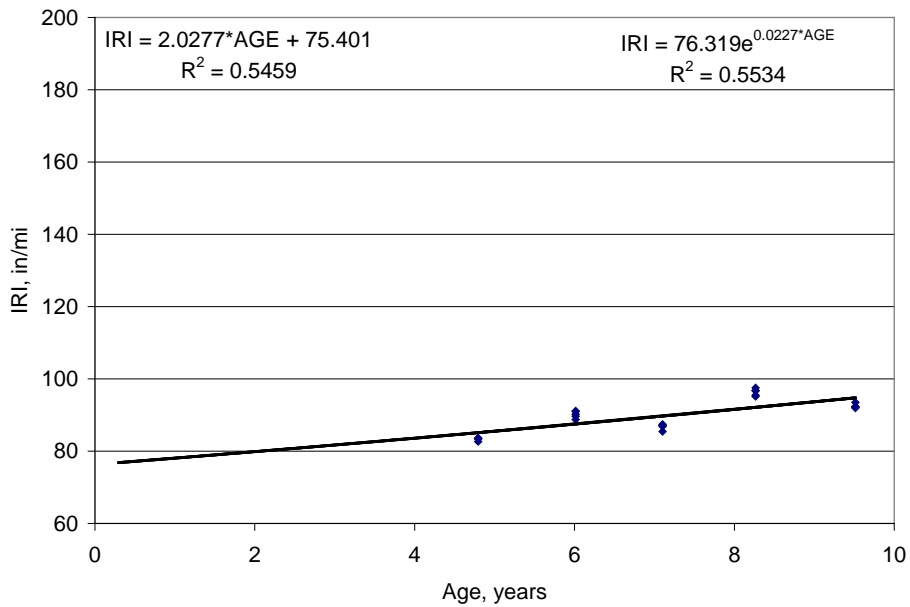
Performance Criteria

Rigid Pavement Flexible Pavement

	Limit	Reliability
<input checked="" type="checkbox"/> Terminal IRI (in/mile)	<input type="text" value="172"/>	<input type="text" value="90"/>
<input checked="" type="checkbox"/> AC Surface Down Cracking Long Cracking (ft/mi)	<input type="text" value="2000"/>	<input type="text" value="90"/>
<input checked="" type="checkbox"/> AC Bottom Up Cracking Alligator Cracking (%)	<input type="text" value="25"/>	<input type="text" value="90"/>
<input checked="" type="checkbox"/> AC Thermal Fracture (ft/mi)	<input type="text" value="1000"/>	<input type="text" value="90"/>
<input checked="" type="checkbox"/> Chemically Stabilized Layer Fatigue Fracture(%)	<input type="text" value="25"/>	<input type="text" value="90"/>
<input checked="" type="checkbox"/> Permanent Deformation - Total Pavement (in)	<input type="text" value="0.75"/>	<input type="text" value="90"/>
<input checked="" type="checkbox"/> Permanent Deformation - AC Only (in)	<input type="text" value="0.25"/>	<input type="text" value="90"/>

OK Cancel

(a)



(b)

Figure 5. MEPDG initial IRI input screen and backcast initial IRI.

Table 6. Summary of initial IRI estimated for all projects analyzed.

LTPP Section ID	Initial IRI, in/mi	LTPP Section ID	Initial IRI, in/mi
39_0101	89.2	39_0203	66.3
39_0102	79.7	39_0207	76.4
39_0103	99.1	39_0208	86.0
39_0104	54.8	39_0209	61.4
39_0105	68.9	39_0211	82.8
39_0106	78.6	39_0260	68.8
39_0107	82.4	39_0261	72.6
39_0108	56.8	39_0262	76.6
39_0109	42.3	39_0263	76.1
39_0110	75.6	39_0264	77.2
39_0111	60.1	39_0265	90.3
39_0112	66.2	39_3013	151.4
39_0160	98.2	39_3801	113.0

Traffic

Many of the traffic inputs for the Ohio LTPP projects were obtained at Level 1, since WIM and automated vehicle classification (AVC) data were available for all the projects. For the SPS-1, SPS-2, and SPS-9 projects, AVC and WIM data were obtained from 1996 to 2005. For the GPS-3, both historic and actual counts of traffic volume were available along with WIM data collected in the 1990's. Because of the differences in traffic data available in the LTPP database and ODOT traffic databases, traffic data processing was done differently for the SPS and GPS projects. A description of the traffic processing effort is presented in the following sections.

SPS 1, 2, & 9 Traffic Data Processing

ODOT provided an actual count of single, tandem, tridem, and quad axles that were applied to the SPS-1, -2, and -9 projects from 1996 through 2005:

- Daily file size tables (provided information on the days for which the north or southbound lanes were open or closed to traffic from 1996 through 2005).
- Vehicle class count data.
- Counts of single, tandem, tridem, and quad axles applied for each of the four lanes (northbound and southbound) based on the following:
 - Day of the month.
 - Month and year.
 - Axle load grouping.

An example of the data provided is presented in Table 7 for single and tandem axles. Note that counts for penta and hex axles also were provided. These were added to the quad axles, as the MEPDG does not directly consider these axle types.

The data presented in Table 7 were used to develop the MEPDG traffic inputs used for analysis; in other words, a traffic file was created containing monthly estimates of average daily counts of all axle types and axle load groupings for each month of the analysis period. The process used to create the traffic analysis file was as follows:

1. Determine mean daily axle counts for each axle type and axle load grouping for each month of the analysis period, 1996 through 2004.
2. Match the mean daily axle counts for each axle type and axle load grouping to the specific days within the given month. In other words, the average axle counts for Mondays in November of 1996 were matched to all Mondays in that given month. The same was done for all the other days for that given month and all the other months within the analysis period.
3. Step 2 assumed that the LTPP pavements were opened to traffic all throughout the analysis period. Information provided by ODOT on the periods for which the test pavements were opened to traffic, however, suggested otherwise. That is, there were prolonged periods when the northbound lanes, or southbound lanes, or both lanes were closed to traffic. Using the information provided by ODOT on traffic closure times, all days for which the northbound lanes, southbound lanes, or both were closed was identified and truck traffic for those days were assumed to be zero.
4. The adjusted traffic estimates in step 3 were summarized in an Excel spreadsheet that was read directly by the MEPDG and used for analysis.

Examples of the data provided for lane 11 are presented in Figure 6 through Figure 8.

Table 7. Example of daily single and tandem axle load spectra summary for Mondays in November 1996.

Single Axle						Tandem Axles					
Wt.	Lane				Sum	Wt.	Lane				Sum
	11	12	52	51			11	12	52	51	
3	12	2	28	308	350	6	8	1	3	8	20
4	30	13	31	831	905	8	22	10	17	11	60
5	78	11	16	531	636	10	112	13	26	43	194
6	93	26	17	250	386	12	309	39	43	70	461
7	57	4	29	131	221	14	335	38	39	175	587
8	108	6	51	92	257	16	258	31	20	211	520
9	167	14	36	102	319	18	172	28	13	237	450
10	465	38	51	181	735	20	179	24	13	250	466
11	578	66	18	205	867	22	148	13	17	156	334
12	442	32	16	364	854	24	110	11	19	138	278
13	84	3	9	276	372	26	99	6	14	123	242
14	58	3	6	379	446	28	95	11	12	114	232
15	37	2	4	234	277	30	146	14	16	109	285
16	57	3	2	173	235	32	179	11	7	110	307
17	56	5	4	131	196	34	295	27	14	95	431
18	81	3	2	80	166	36	171	9	8	101	289
19	61	7	4	65	137	38	46	10	7	105	168
20	15	1	3	43	62	40	25	3	4	86	118
21	12	0	2	50	64	42	5	0	3	124	132
22	2	0	2	32	36	44	2	0	0	111	113
23	3	0	2	45	50	46	0	0	2	126	128
24	2	0	0	36	38	48	1	0	4	103	108
25	0	0	0	33	33	50	0	0	0	81	81
26	2	0	2	25	29	52	0	0	0	51	51
27	1	0	0	25	26	54	0	0	0	62	62
28	1	0	0	13	14	56	0	0	0	31	31
29	0	0	0	17	17	58	0	0	0	18	18
30	0	0	0	15	15	60	0	0	0	12	12
31	0	0	0	11	11	62	0	0	0	8	8
32	0	0	0	2	2	64	0	0	0	5	5
33	0	0	0	3	3	66	0	0	0	1	1
34	0	0	0	0	0	68	0	0	0	0	0
35	0	0	0	0	0	70	0	0	0	0	0
36	0	0	0	0	0	72	0	0	0	0	0
37	0	0	0	0	0	74	0	0	0	0	0
38	0	0	0	0	0	76	0	0	0	0	0
39	0	0	0	0	0	78	0	0	0	0	0
40	0	0	0	0	0	80	0	0	0	0	0
Sum	2502	239	335	4683	7759		2717	299	301	2875	6192

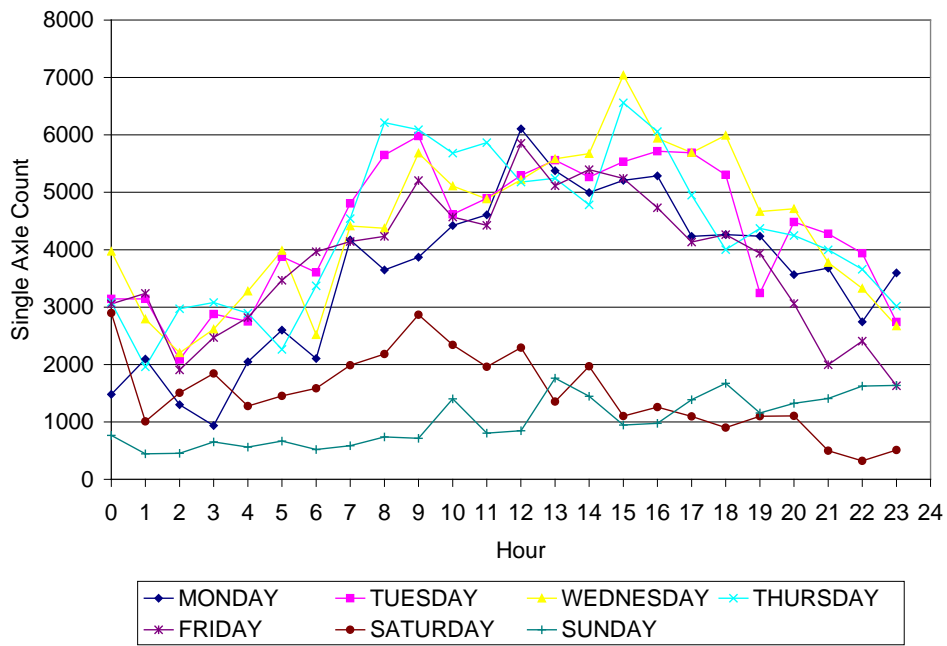


Figure 6. Hourly estimates of truck traffic for lane 11 (November 1996).

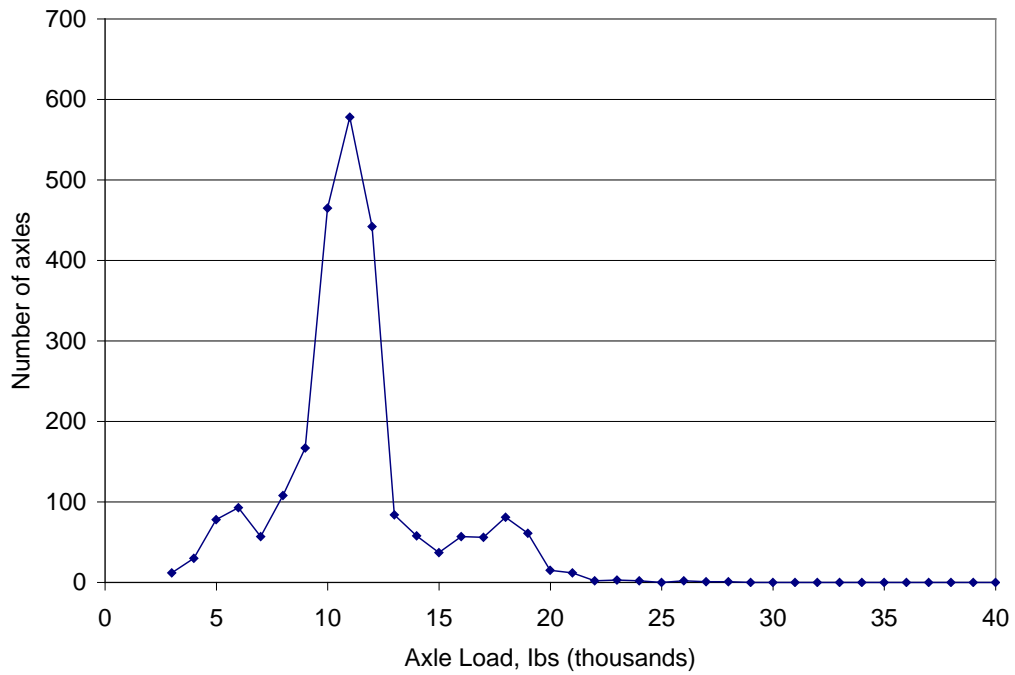


Figure 7. Estimates of truck traffic for each single axle load grouping for lane 11 (November 1996).

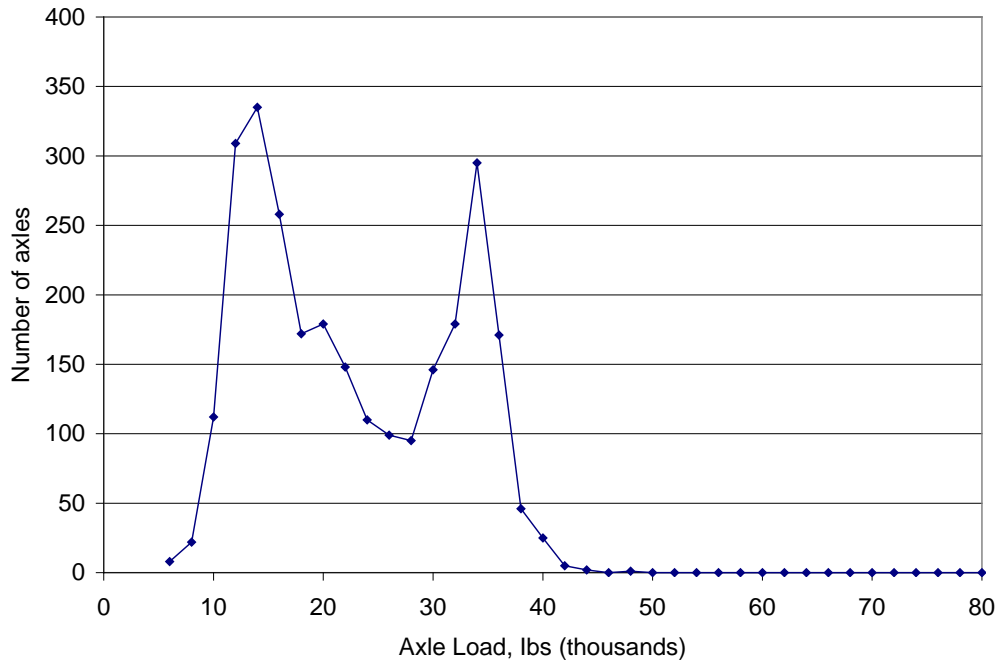


Figure 8. Estimates of truck traffic for each tandem axle load grouping for lane 11 (November 1996).

GPS 3013 & 3801 Traffic Data Processing

For the GPS projects, traffic was estimated in the more conventional manner (that is, providing required user traffic inputs directly to the LTPP). The raw data provided were then used by the MEPDG to produce the traffic analysis files required for analysis.

Traffic Volume

Key traffic volume inputs provided are presented in Figure 9 through Figure 11. Note that the initial average annual daily truck traffic (AADTT) and traffic growth rate for 393013 were 565 and 0 percent linear, respectively, and for 393801 were 195 and 16.8 percent (linear), respectively.

Axle Load Data

The MEPDG also requires single, tandem, tridem, and quad axle load distribution factors for analysis. For all sections analyzed, the single and tandem axle load distributions were developed using WIM data obtained from the LTPP sites. Examples of axle load distribution factors computed for the truck class 9 for projects 39_3013 and 39_3801 are presented in Figure 12 and Figure 13.

Traffic Volume Adjustment Factors

Monthly Adjustment |
 Vehicle Class Distribution |
 Hourly Distribution |
 Traffic Growth Factors

Opening Date: July, 1970
 Design Life (years): 40

AADTT: 565
 % Traffic Design Direction: 100
 % Traffic Design Lane: 100

Vehicle-class specific traffic growth

Default Growth Function

No Growth
 Linear Growth
 Compound Growth

Default growth rate (%):

Note: Vehicle-class distribution factors are needed to view the effects of traffic growth.

39_3013

Traffic Volume Adjustment Factors

Monthly Adjustment |
 Vehicle Class Distribution |
 Hourly Distribution |
 Traffic Growth Factors

Opening Date: December, 1983
 Design Life (years): 25

AADTT: 195
 % Traffic Design Direction: 100
 % Traffic Design Lane: 100

Vehicle-class specific traffic growth

Default Growth Function

No Growth
 Linear Growth
 Compound Growth

Default growth rate (%): 16.79

Note: Vehicle-class distribution factors are needed to view the effects of traffic growth.

39_3801

Figure 9. MEPDG traffic volume inputs.

Traffic Volume Adjustment Factors

Monthly Adjustment |
 Vehicle Class Distribution |
 Hourly Distribution |
 Traffic Growth Factors

AADTT distribution by vehicle class

Class 4	15.4	
Class 5	16.8	
Class 6	15.4	
Class 7	0.7	
Class 8	19.4	
Class 9	28.9	
Class 10	2.0	
Class 11	0.6	
Class 12	0.1	
Class 13	0.7	
Total	100.0	

Note: AADTT distribution must total 100%.

Load Default Distribution

Level 1: Site Specific Distribution
 Level 2: Regional Distribution
 Level 3: Default Distribution

39_3013

Traffic Volume Adjustment Factors

Monthly Adjustment |
 Vehicle Class Distribution |
 Hourly Distribution |
 Traffic Growth Factors

AADTT distribution by vehicle class

Class 4	9.1	
Class 5	8.6	
Class 6	9.6	
Class 7	2.3	
Class 8	6.5	
Class 9	61.3	
Class 10	1.9	
Class 11	0.4	
Class 12	0.1	
Class 13	0.3	
Total	100.1	

Note: AADTT distribution must total 100%.

Load Default Distribution

Level 1: Site Specific Distribution
 Level 2: Regional Distribution
 Level 3: Default Distribution

39_3801

Figure 10. Monthly truck volume adjustment factors.

General Traffic Inputs

Lateral Traffic Wander

Mean wheel location (inches from the lane marking):

Traffic wander standard deviation (in):

Design lane width (ft): (Note: This is not slab width)

Number Axles/Truck Axle Configuration Wheelbase

	Single	Tandem	Tridem	Quad
Class 4	1.62	0.39	0	0
Class 5	2	0	0	0
Class 6	1.02	0.99	0	0
Class 7	1	0.26	0.83	0
Class 8	2.38	0.67	0	0
Class 9	1.13	1.93	0	0
Class 10	1.19	1.09	0.89	0
Class 11	4.29	0.26	0.06	0
Class 12	3.52	1.14	0.06	0
Class 13	2.15	2.13	0.35	0

39_3013

General Traffic Inputs

Lateral Traffic Wander

Mean wheel location (inches from the lane marking):

Traffic wander standard deviation (in):

Design lane width (ft): (Note: This is not slab width)

Number Axles/Truck Axle Configuration Wheelbase

	Single	Tandem	Tridem	Quad
Class 4	1.08	0.28	0.00	0.00
Class 5	2.30	0.02	0.00	0.00
Class 6	1.10	1.06	0.01	0.00
Class 7	1.34	0.14	0.98	0.20
Class 8	2.38	0.44	0.02	0.00
Class 9	1.35	1.73	0.00	0.01
Class 10	1.08	0.91	0.67	0.16
Class 11	5.08	0.59	0.17	0.00
Class 12	6.53	1.62	0.08	0.03
Class 13	2.43	1.11	0.45	0.66

39_3801

Figure 11. Lateral truck wander and mean number axles/truck.

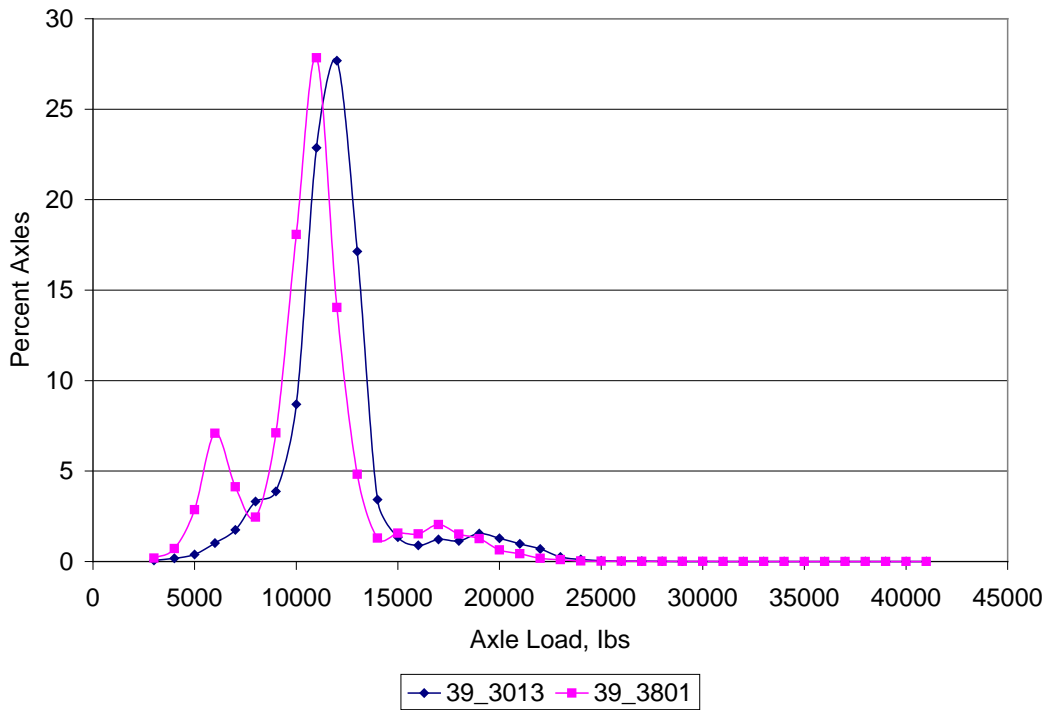


Figure 12. Single axle distribution for class 9 trucks (averaged over all months).

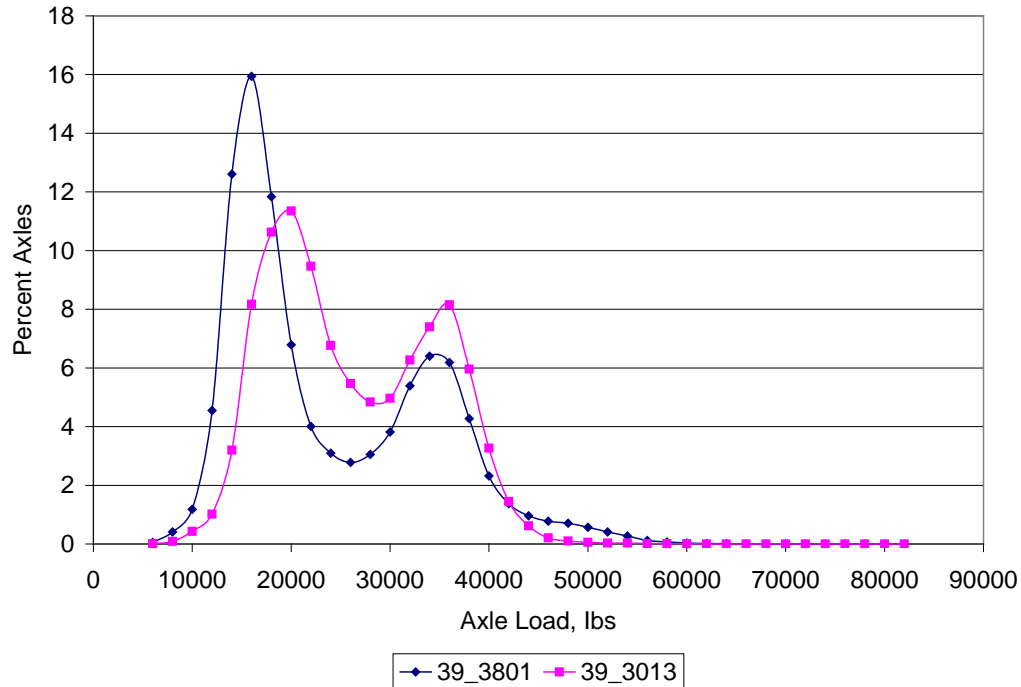


Figure 13. Tandem axle distribution for class 9 trucks (averaged over all months).

Climatic Data Input

The MEPDG requires the location of a project described in terms of longitude, latitude, and elevation in order to develop project-specific climate-related data for analysis. The SPS experiments had a weather station located nearby at the Newark-Heath Airport. This site was therefore used in analyzing all the SPS sections. For the GPS sections, climate data were generated using up to six of the closest weather stations to the section as identified by the MEPDG. Typically, each weather station had 96 to 116 months of climate data. Another piece of information that is required is an estimate of depth to water table level. For this project, a default depth to water table of 10 ft was adopted, based on the value used for national calibration. Details of project locations for all projects analyzed are presented in Table 8. An example of MEPDG coded climate information for project 39_0112 is presented in Figure 14.

Table 8. GPS coordinates of Ohio LTPP sections selected for use in validation/calibration.

LTPP ID	Elevation, ft	Longitude, deg	Latitude, deg	Depth to Water Table, ft
39_0100	955	-83.08	40.43	10
39_0200	955	-83.08	40.43	10
39_0900	950	-83.08	40.43	10
39_3013	960	-83.89	38.88	10
39_3801	655	-80.75	40.00	10

Environment/Climatic

Latitude (degrees.minutes): 40.01
Longitude (degrees.minutes): -82.28
Elevation (ft): 982

Climatic data for a specific weather station.
 Interpolate climatic data for given location.

Seasonal

Depth of water table (ft)	
Annual average	10

Note: Ground water table depth is a positive number measured from the pavement surface.

0.0 miles NEWARK, OH - NEWARK-HEATH AIRPORT Lat: 40.01 Lon: -82.28 Ele: 982 Months: 84 (C)
 20.3 miles LANCASTER, OH - FAIRFIELD COUNTY AIRPORT Lat: 39.46 Lon: -82.4 Ele: 855 Months: 116 (M1)
 22.2 miles COLUMBUS, OH - PORT COLUMBUS INTL AIRPORT Lat: 39.59 Lon: -82.53 Ele: 849 Months: 116 (C)
 31.4 miles ZANESVILLE, OH - ZANESVILLE MUNICIPAL ARPT Lat: 39.56 Lon: -81.53 Ele: 881 Months: 66 (C)
 32.9 miles COLUMBUS, OH - OHIO STATE UNIVERSITY ARPT Lat: 40.05 Lon: -83.05 Ele: 923 Months: 100 (C)
 52.1 miles MARION, OH - MARION MUNICIPAL AIRPORT Lat: 40.37 Lon: -83.04 Ele: 991 Months: 94 (C)

Select stations for generating interpolated climatic files. The best interpolation occurs by selecting stations that are geographically close in differing directions. A station without missing any data is denoted (C)complete. (M#) denotes missing month.
 Press the Generate button after selecting desired weather stations and inputting Elevation and Depth of Water Table. Missing data for a given station will be interpolated from complete stations.

Figure 14. Climatic data input for project 39_0112.

Pavement Surface Layer Thermal Properties

The MEPDG default surface shortwave absorptivity, thermal conductivity, and heat capacity were used for all the layers and for the analyses performed.

Design Features for HMA and JPCP LTPP Sections

The MEPDG requires both HMA and JPCP design features. For new HMA pavements, the relevant design feature is whether to consider an HMA endurance limit in fatigue analysis (applicable to the design of perpetual pavements). This was not considered in analysis, as the pavements being analyzed were not designed as perpetual pavements. For JPCP, the following design features are required:

- The temperature gradient during PCC placement and curing.
- PCC slab transverse joint spacing.
- Transverse joint sealant type.
- Slab width.
- Load transfer mechanism and properties.
- Slab edge support type.
- Base type and base erosion factor.
- PCC-base interface friction type and age at which friction is lost.

Details are presented in Table 9.

Table 9. JPCP project design features.

LTPP ID	Joint Spacing, ft	PCC Slab Edge Support		Transverse Joint Load Transfer	
		Slab Width, ft	Tired PCC Shoulder (Y/N)	Dowel Diameter, in	Dowel Spacing, in
39_0203	15	14	N	1.5	12
39_0207	15	14	N	1.5	12
39_0208	15	12	N	1.5	12
39_0209	15	12	N	1.25	12
39_0211	15	14	N	1.5	12
39_0260	15	12	N	1.5	12
39_0261	15	14	N	1.5	12
39_0262	15	12	N	1.5	12
39_0263	15	14	N	1.5	12
39_0264	15	12	N	1.5	12
39_0265	15	12	N	1.5	12
39_3013	17	12	Y	0	0
39_3801	20	12	Y	1.25	12

1. A built-in temperature gradient of -10°F was used (MEPDG default).
2. A full friction condition was assumed at the PCC-base interface for the entire design period for all base types.
3. A silicone transverse joint sealant type was used.

Structure Definition

The MEPDG requires a definition of the pavement structure along with a detailed description/characterization of the layer materials that make up the pavement structure. Pavement structure is defined by layer material type, position within the structure, and thickness. Material characterization mostly consists of properties needed to support climate modeling, response analysis, and performances prediction.

For all the material groups, detailed information was obtained from the LTPP database and used to characterize the layer material properties including thickness, unit weight, Poisson's ratio, gradation, asphalt mix properties, PCC flexural strength, PCC thermal coefficient of expansion, and PCC modulus of elasticity. Most of the key material properties in the LTPP database were obtained through laboratory testing of mix samples or extracted cores. For other material properties, such as PCC zero stress temperature, thermal conductivity and so on, MEPDG or Ohio-specific defaults were assumed. The sources of key material inputs are as follows:

- **Asphalt mix volumetric properties:** These were obtained through lab testing or asphalt concrete (AC) cores extracted by LTPP. The cores were extracted within 6 to 8 months of placement and after the pavement had been subjected to very little traffic.

- **PCC strength and modulus:** For SPS-2 PCC materials, the 14-, 28-, and 365-day modulus of rupture (flexural strength) and elastic modulus values were measured by LTPP. For the GPS sections, only the long-term (mostly 5 years or more) compressive and tensile strength and elastic modulus were tested and are available. The available data were used to estimate Level 1 MEPDG inputs (14-, 28-, and 90-day MR and E_{PCC}) for SPS projects and Level 3 MEPDG inputs (28-day MR and E_{PCC}) for GPS projects.
- **PCC coefficient of thermal expansion (CTE):** For both the SPS-2 and GPS-3 projects PCC materials, CTE values were measured by LTPP.
- **Unbound aggregate materials and soils inputs for climate modeling:** These were determined using the LTPP lab tested gradation and Atterberg limit values.
- **Resilient modulus of unbound aggregate materials used as base or subbases:** Default MEPDG values were adopted based on the material AASHTO soil classification determined using LTPP lab tested gradation and Atterberg limit values.
- **Subgrade resilient modulus (tested at optimum moisture):** The subgrade lab resilient modulus (M_r) at optimum moisture content is the required input when the Integrated Climatic Model (ICM) is used to determine the seasonal effects over time. This input is then used in the program to backcalculate a k-value for each month which is used in to calculate the stresses and deflections used to compute damage (for JPCP). However, LTPP does not provide the required subgrade lab resilient modulus (M_r) at optimum moisture content. Thus, for both JPCP and HMA pavements, Falling Weight Deflectometer (FWD) data from the LTPP database were used to backcalculate a long-term in-situ subgrade resilient modulus and k-value as appropriate. The point in time chosen for the backcalculation was selected to represent a long-term value (presumably when equilibrium moisture contents are reached in the field) when the subgrade is not either saturated or frozen (summer months). An appropriate subgrade lab resilient modulus (M_r) at optimum moisture content value was then selected through trial and error to obtain an MEPDG estimate of the long-term in situ resilient modulus (for HMA pavements) and k-value (for JPCP) which was similar to the field tested value. Comparisons of long-term, in situ field tested and MEPDG computed flexible subgrade resilient moduli and JPCP subgrade k-values are presented in Figure 15 and Figure 16, respectively.

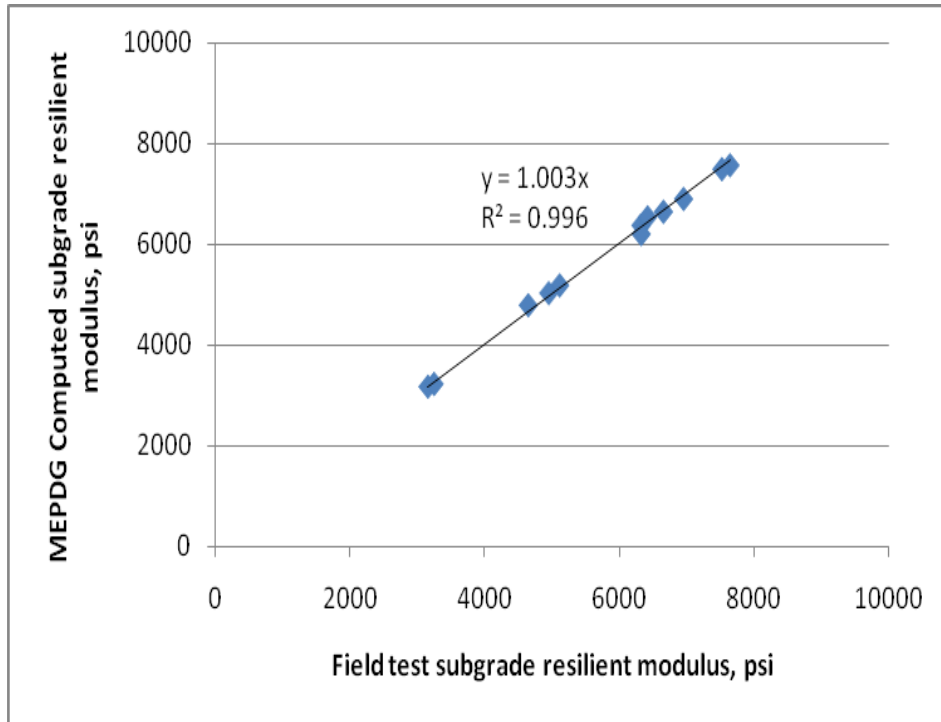


Figure 15. Field tested and MEPDG computed flexible pavement in-situ subgrade resilient modulus.

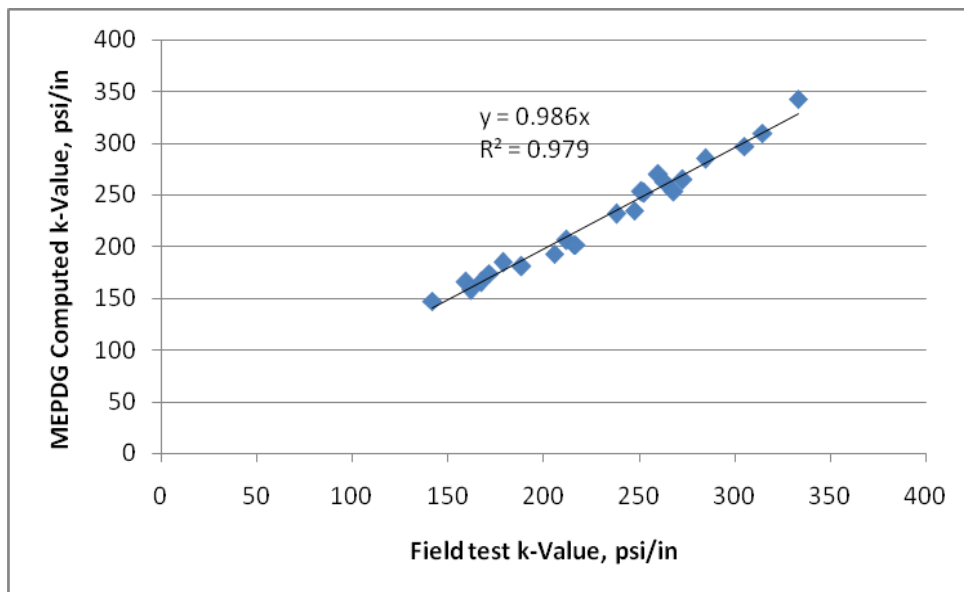


Figure 16. Field tested and MEPDG computed JPCP in-situ subgrade k-value.

Performance Data

The SPS-1 and SPS-2 projects had up to 10 years of distress data on average while the two GPS-2 projects had up to 30 years of distress/IRI data. For the GPS projects, however, distress/IRI was reported for the period 19 to 23 years for section 3013 while the period 6 to 24 years was reported for section 3801.

Generally speaking, all the candidate projects had sufficient amounts of distress/IRI data for use in analysis. Data quality varied as reported in the following sections.

HMA Alligator Cracking

All the SPS-1 and SPS-9 projects experienced both alligator and longitudinal cracking. Several of the SPS-1 sections experienced premature alligator cracking. A review of the historical trends of cracking development versus time for these sections indicated that the wheel path cracking, in many instances, initially manifested in the form of low severity longitudinal cracking which, with repeated traffic applications deteriorated and formed alligator cracking (see Figure 17 and Figure 18).

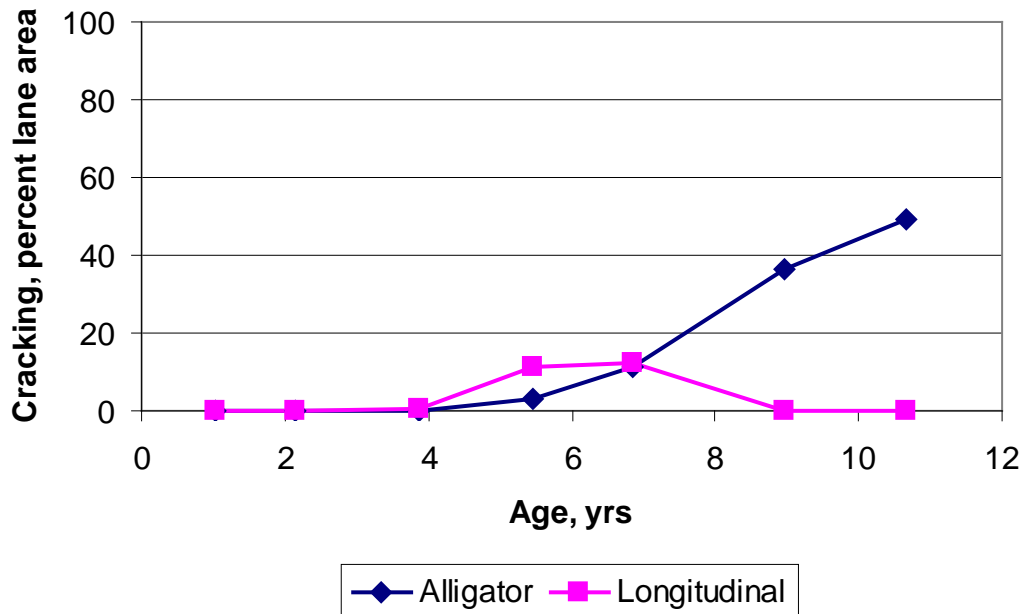


Figure 17. Plot of alligator and longitudinal cracking progression for project 0106.

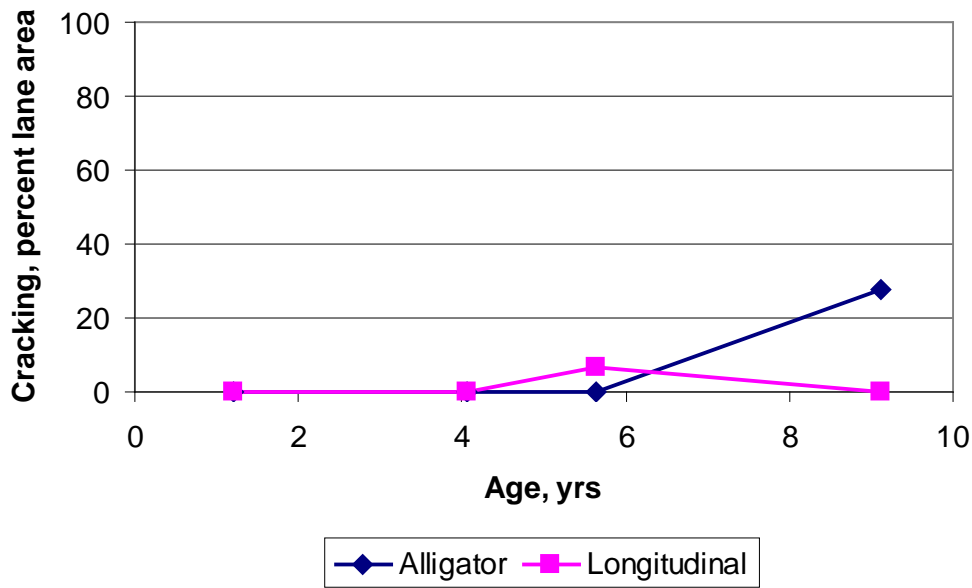


Figure 18. Plot of alligator and longitudinal cracking progression for project 0903.

A detailed forensic investigation of some of the SPS-1 projects indicated that the longitudinal cracking probably was due to defects in construction equipment and may not have been fatigue related (Sargand et al., 2007). Other causes of the premature cracking and failures identified were debonding of the HMA layers due to the infiltration of water between HMA layers and a lack of tack coat between the asphalt layers during construction.

The questionable origins of the alligator cracking recorded for the SPS-1 and SPS-9 sections, and the plausibility that they may not be related to traffic-induced fatigue alone, resulted them in not being considered suitable for further analysis.

Other Distresses/IRI for HMA Pavements

There was a considerable amount of good-quality performance data available for HMA pavements. The data were reviewed for quality by reviewing plots of measured performance versus age for each project. The performance characteristics for HMA pavements included:

- HMA Transverse Cracking
- HMA Rutting
- HMA Smoothness (IRI)

A plot of measured performance versus age was examined for each performance characteristic to determine anomalous data and potential errors. Obvious errors and outliers were removed.

JPCP Performance

In a similar fashion, the performance data of JPCP was reviewed. The performance characteristics for JPCP included:

- JPCP Transverse Cracking
- JPCP Faulting
- JPCP Smoothness (IRI)

Plots of measured performance versus age for examined for each performance characteristic of JPCP, and subsequently errors and outliers were removed.

Summary

Data from as many projects as possible were assembled into a project database and used for analysis. Not all the projects could be used, for a variety of reasons, the most common being:

- Lack of reliable data (SPS-8 projects had no reliable traffic data, reconstructed SPS-1 projects had no reliable performance data).
- Observed anomalies and potential errors in performance data.
- Pavements with materials properties or design features that are not in agreement with current ODOT pavement design philosophy (e.g., joint spacing > 20-ft (e.g., 39-0159 had a permeable cement treated base).

With the exception of the projects that were removed from the project database completely due to early failures, lack of adequate data, and so on, as much information as possible was assembled on a model type basis and used accordingly. In other words, the fact that a given project had no rutting data did not mean that it was not used for validating the transverse cracking models if transverse cracking data were available.

CHAPTER 4. VALIDATION/RECALIBRATION OF SELECTED MEPDG MODELS

Framework for MEPDG Model Validation

This chapter presents a summary of work done to determine selected MEPDG model adequacy under Ohio conditions, specifically the prediction capability, accuracy, and bias of the selected MEPDG models. The work under this effort included:

1. Assembling all relevant data for creating MEPDG input files.
2. Processing assembled data (vehicle class distribution, backcalculated modulus of subgrade reaction, percent JPCP slabs with transverse cracking, etc.) to develop MEPDG input files and time series pavement performance data to be used for model evaluation.
3. Evaluating model adequacy.

Items 1 and 2 were discussed in the previous chapter; this chapter discusses item 3.

Several methods (statistical or otherwise) were used singly or in combination to evaluate model adequacy. Non-statistical methods were applied for situations where measured distress or IRI was mostly zero or close to zero and, therefore, computation of diagnostic statistics such as coefficient of determination (R^2) and standard error of the estimate (SEE) used to determine model adequacy was either not possible or meaningless. For such situations, a simple comparison was made of measured and predicted distress/IRI categorized into as many groups as needed. The range of each group was determined based on engineering judgment. The goal was to determine how often measured and predicted distress/IRI remained in the same group. Measured and predicted distress remaining in the same group implied reasonable and accurate predictions, while measured and predicted distress residing in different groups suggested otherwise.

For situations where the measured distress/IRI values were non-zero, statistical methods were used to determine model adequacy as follows:

1. Execute the MEPDG for each identified LTPP project and predict pavement distresses and IRI.
2. Extract predicted distress and IRI data from the MEPDG outputs that match measured LTPP distress/IRI.
3. Perform statistical analysis to check model adequacy (i.e., prediction capability, accuracy, and bias).
4. Perform local calibration, as needed, for the MEPDG models evaluated.
5. Perform sensitivity analysis of the recalibrated models (discussed in chapter 5)
6. Summarize results including revised model coefficients, where applicable.

The statistical analysis performed is described in greater detail in the following sections.

Determine Model Prediction Capability

The predictive capability of a given performance model was assessed by determining the correlation between measured and MEPDG predicted distress/IRI. The diagnostic statistic used for making this comparison was the coefficient of determination, R^2 . The estimated R^2 was compared with R^2 obtained from NCHRP 1-40D (see Table 10). Engineering judgment was then used to determine the reasonableness of the estimated R^2 as follows:

- Excellent: > 80 percent.
- Very good: 75 to 85 percent.
- Good: 65 to 75 percent.
- Fair: 50 to 65 percent.
- Poor: < 50 percent.

A poor correlation implied the MEPDG distress/IRI prediction model was not predicting distress/IRI reasonably and may need to be recalibrated to improve prediction capability.

Estimate Model Accuracy

The standard error estimate (SEE) was used to determine model accuracy. SEE is the square root of the average squared error of prediction (i.e., the difference between the measured and predicted distress/IRI). SEE is a key measure of the accuracy of prediction models. The estimated SEE was compared with the SEE obtained from NCHRP 1-40D (see Table 10), and engineering judgment was used to determine the reasonableness of the SEE. An SEE value much greater than that reported from NCHRP 1-40D implied distress/IRI predictions was not very accurate. Model prediction accuracy was improved through recalibration in such situations.

Table 10. Summary of NCHRP 1-40D new HMA pavement and new JPCP model statistics.

Pavement Type	Performance Model	Model Statistics		
		Coefficient of Determination, R^2	Standard Error of Estimate, SEE	Number of Data Points, N
New HMA	Alligator cracking	0.275	5.01 percent	405
	Transverse "thermal" cracking	Level 1*: 0.344 Level 2*: 0.218 Level 3*: 0.057	—	—
	Rutting	0.58	0.107 in	334
	IRI	0.56	18.9 in/mi	1926
New JPCP	Transverse "slab" cracking	0.85	4.52 percent	1505
	Transverse joint faulting	0.58	0.033 in	1239
	IRI	0.60	17.1 in/mi	163

*Level of inputs used for calibration.

Determine Bias

Bias was defined as the consistent under- or over-prediction of distress/IRI. Bias was determined by performing linear regression using measured and MEPDG predicted distress/IRI and performing the following two hypothesis tests in the sequence listed. A significance level, α , of 0.05 or 5 percent was assumed for all hypothesis testing.

- Hypothesis 1: Determining whether the linear regression model developed using measured and MEPDG predicted distress/IRI has an intercept of zero:
 - a. Using the results of the linear regression analysis, test the following null and alternative hypotheses to determine if the fitted linear regression model has an intercept of zero:
 - i. H_0 : Model intercept = 0.
 - ii. H_A : Model intercept \neq 0.A rejection of the null hypothesis (p -value $<$ 0.05) implied the linear model had an intercept significantly different from zero at the 5 percent significant level. Thus, predicted MEPDG distress/IRI prediction is biased. In such a situation, the identified bias is removed through recalibration.

- Hypothesis 2: Determine whether the linear regression model developed using measured and MEPDG predicted distress/IRI has a slope of 1.0:
 - a. Using the results of the linear regression analysis, test the following null and alternative hypothesis to determine if the fitted linear regression model has an slope of 1.0:
 - i. H_0 : Model slope = 1.0.
 - ii. H_A : Model slope \neq 1.0.A rejection of the null hypothesis (p -value $<$ 0.05) implies that the linear model has a slope significantly different from 1.0 at the 5 percent significant level. Thus, predicted MEPDG distress/IRI prediction is biased. In such a situation, the identified bias is removed through recalibration.

A third hypothesis test (paired t-test) was done to determine whether the measured and MEPDG predicted distress/IRI represented the same population of distress/IRI. The paired t-test was performed as follows:

- Hypothesis 3: Paired t-test.
 - a. Perform a paired t-test to test the following null and alternative hypothesis:
 - i. H_0 : Mean measured distress/IRI = mean predicted distress/IRI.
 - ii. H_A : Mean measured distress/IRI \neq mean predicted distress/IRI.

A rejection of the null hypothesis ($p\text{-value} < 0.05$) implied the measured and MEPDG distress/IRI are from different populations. Thus, predicted MEPDG distress/IRI prediction is biased. In such a situation, the identified bias is removed through recalibration.

Note that hypotheses 1 through 3 were performed sequentially. A rejection of any of the null hypothesis implied that the model was biased and, therefore, there was no need for further testing. Models that successfully passed all three tests were deemed to be unbiased.

The results of both the non-statistical and statistical analysis as appropriately applied were used to determine overall MEPDG distress/IRI models adequacy. Where the MEPDG models were deemed inadequate for Ohio conditions, the models were recalibrated. The recalibrated models were evaluated for prediction capacity, accuracy, and bias.

New HMA Pavement Models

HMA Alligator Cracking

Validation and Recalibration

As discussed in chapter 4, the alligator cracking data recorded on the LTPP SPS-1 and SPS-2 projects were confounded with construction-related cracking. It was not possible to separate construction-initiated top-down cracking from fatigue related bottom-up (or alligator) or top-down cracking; hence, the alligator cracking model was not evaluated or recalibrated due to a lack of adequate data for analysis.

HMA Transverse Cracking

Validation

Figure 19 presents a histogram of all measured (including time series) transverse cracking for the LTPP projects evaluated. The plot shows that approximately 90 percent of all measured transverse cracking values ranged from 0 to 20 ft/mi. The information in Figure 19, therefore, shows that the majority of the pavement projects used in analysis had minimal transverse cracking.

Applying conventional statistical tests to such data will not produce meaningful diagnostic statistics. Thus, a simple non-statistical comparison of measured and predicted transverse cracking was done.

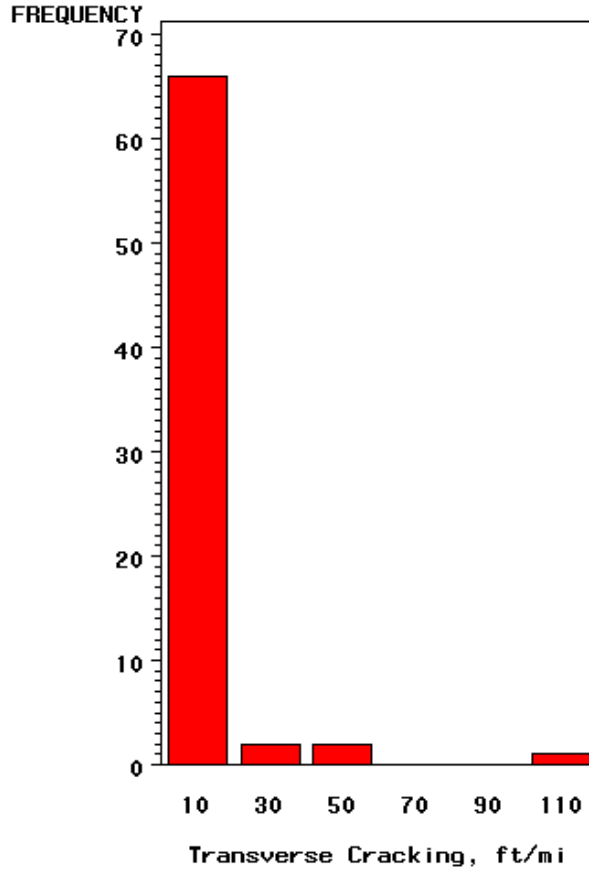


Figure 19. Histogram showing distribution of measured transverse “thermal” cracking.

For this comparison, transverse cracking was categorized into four groups as follows:

- 0-250 ft/mi.
- 250-500 ft/mi.
- 500-1000 ft/mi.
- 1000-2000 ft/mi.

The goal was to determine how often measured and predicted transverse cracking fell in the same grouping. The range of each group was determined using engineering judgment. Results of the comparison are presented in Table 11. Table 12 shows the same information broken down by binder type.

A review of the information presented in Table 11 and Table 12 showed that, for both conventional and SuperPave binders, all measured transverse cracking data fell in the same grouping.

Table 11. Comparison of measured and predicted transverse cracking (percentage of all measurements).

MEPDG Measured Transverse Cracking, ft/mi	MEPDG Predicted Transverse Cracking, ft/mi			
	0-250	250-500	500-1000	1000-2000
0-250	71	0	0	0
250-500	0	0	0	0
500-1000	0	0	0	0
1000-2000	0	0	0	0

Table 12. Comparison of measured and predicted transverse cracking (percentage of all measurements) by binder type.

Binder Type	MEPDG Measured Transverse Cracking, ft/mi	MEPDG Predicted Transverse Cracking, ft/mi			
		0-250	250-500	500-1000	1000-2000
Conventional binder (AC-20)	0-250	63	0	0	0
	250-500	0	0	0	0
	500-1000	0	0	0	0
	1000-2000	0	0	0	0
SuperPave binder (PG 64-22)	0-250	8	0	0	0
	250-500	0	0	0	0
	500-1000	0	0	0	0
	1000-2000	0	0	0	0

*Note that conventional binder was used for the SPS-1 projects and project 0901. Project 0902 & 0903 used SuperPave binders.

Based on the results presented for a limited number of SPS-1 and SPS-9 projects, it is concluded that the nationally calibrated MEPDG transverse cracking model predicted transverse cracking adequately. However, based on the researchers' experience with MEPDG implementation efforts with other agencies, the MEPDG default creep compliance and tensile strength estimates overestimated the true creep compliance of HMA mixes and underestimated thermal cracking. This discrepancy comes into sharper focus when measured thermal cracking from colder climates is compared to the MEPDG predicted thermal cracking using Level 3 defaults. It is recommended that ODOT reassess the thermal cracking model using data from northern Ohio sites before making a final decision.

Recalibration

Although the predictions for the SPS-1 and 9 sites selected are reasonable, given the fact that all these sites are located in a single climatic region, it is recommended that the model's prediction capability be reassessed using data from colder sites in Ohio.

HMA Rutting

Validation

Figure 20 presents a histogram of all measured (including time series) rutting for the HMA pavement projects used in analysis. The plot shows data ranging from 0.06 to 0.41 in and a mean of 0.17 in. Evaluating such data statistically should produce reasonable and meaningful diagnostic statistics that can be used to assess the model's predictive capability, accuracy, and bias. Thus, a statistical comparison of measured and MEPDG predicted rutting was performed. The results, presented in Figure 21 and Table 13, show the following trends:

- Bias in predicted and measured rutting, as indicated by the results of hypothesis testing of items (1) and (3). It is also obvious that the MEPDG over-predicts the rutting.
- A poor correlation between measured and MEPDG predicted rutting.
- SEE less than that reported for the national MEPDG rutting model.

Considering the biased predictions and poor correlation coefficient, an attempt was made to recalibrate the MEPDG rutting model to improve its prediction accuracy. Because the data set is small and all the sections are drawn from a single site, this recalibration effort should be viewed more as a feasibility or model exercise. A more rigorous effort involving a larger data set of sections that are more representative of the diverse design and site factors that exist in Ohio will be needed for the results to be valid for a general design/analysis use.

Recalibration

The first step in recalibration involved a thorough review of the HMA, base, and subgrade rutting predictions to determine if they pass engineering judgment. Findings of this review of predicted rutting along with modifications applied to the MEPDG model coefficients are described below:

- The trends in HMA, base, and subgrade layer rutting were as expected, with the predicted rutting decreasing with increasing HMA thickness.
- Predicted HMA layer rutting ranged from 17 to 44 percent of predicted total rutting for all the projects analyzed. This is surprising considering that most of the LTPP SPS-1 and SPS-9 sections were relatively thick. This indicated that the rutting accumulated in the unbound layers and subgrade needed to be adjusted downwards through calibration. Therefore, unbound base/subgrade submodels coefficients β_{S1} and β_{S2} were modified as needed to improve predicted rutting.

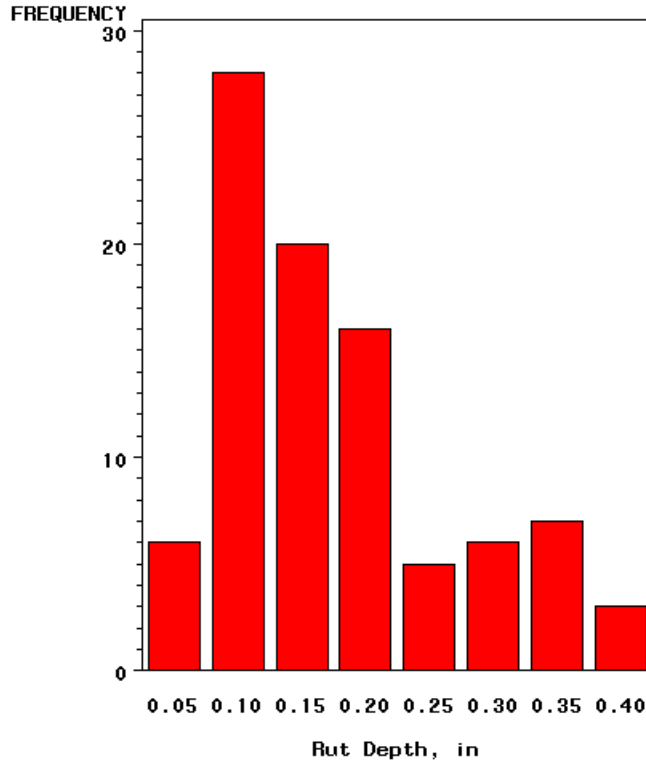


Figure 20. Histogram showing distribution of measured total rutting.

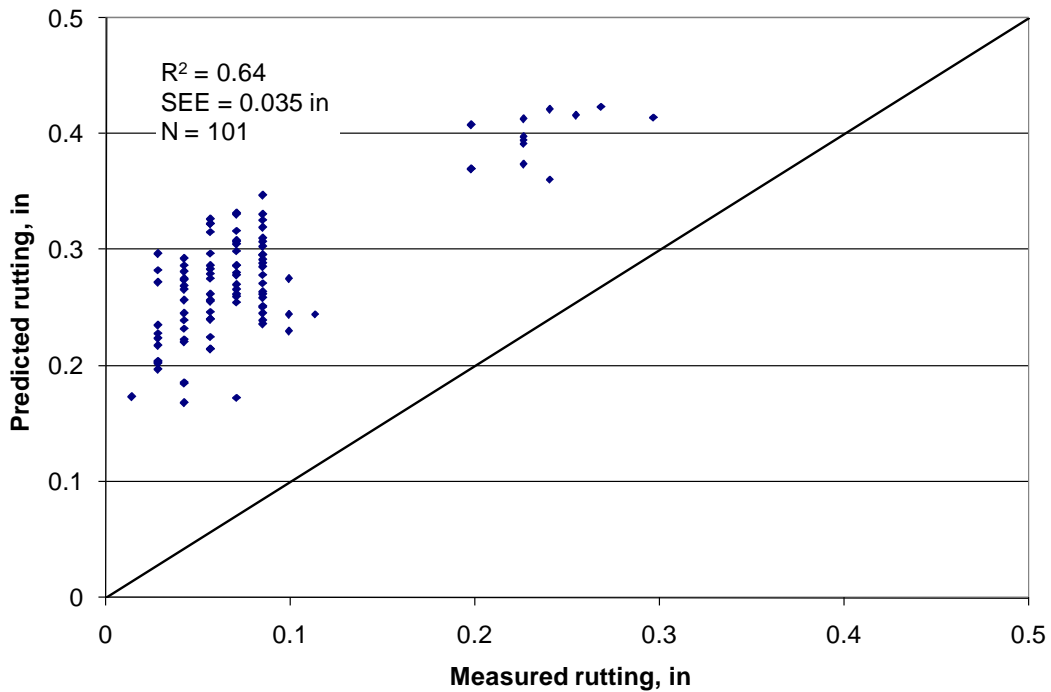


Figure 21. Plot of measured versus MEPDG predicted HMA pavement total rutting.

Table 13. Statistical comparison of measured and predicted rutting data.

Goodness of Fit							
N = 101							
R ² = 0.64							
Adj R ² = 0.64							
SEE = 0.035 in							
Hypothesis Testing							
Hypothesis	DF	Parameter Estimate	Std. Error	t Value	p-value (Pr > t)	95 Percent Confidence Limits	
(1) Ho: Intercept = 0	1	0.2178	0.0059	36.8	<0.0001	0.21	0.23
(2) Ho: Slope = 1.0	1	1.02280	0.0571	13.49	<0.0001	0.65	0.88
(3) Ho: Measured Rutting - MEPDG Predicted Rutting = 0	101			-52.7	<0.0001		

- The slope of the rutting versus age (traffic) curve was not matched well by the MEPDG. As a consequence, the MEPDG over-predicts rutting for the lower magnitudes of measured rutting and under-predicts rutting for the higher magnitudes of measured rutting. This requires an adjustment to the β_{2r} and β_{3r} of the HMA rutting submodel. Adjustments to these coefficients should be based on laboratory investigation of accumulation of permanent deformation with repeated loadings. Such investigations are being performed in NCHRP Project 9-30A project. It is recommended that ODOT follow this research (due for completion in 2010) and implement its findings. ODOT also should plan on performing repeated load permanent deformation testing on its typical mixtures to validate the permanent deformation model in the MEPDG.

Based on the findings of the review, recalibration was limited to modifying the local calibration coefficient β_{1r} of the HMA rutting submodel and the local calibration coefficients β_{S1} and β_{S2} of the base and subgrade rutting submodels (see equations 14 through 21). Recalibration was performed using the selected LTPP SPS-1 and SPS-9 projects described earlier. The recalibrated model, including new model coefficients, is presented below:

$$\text{TRUT} = 0.51 \cdot \text{ACRUT} + 0.32 \cdot \text{BASERUT} + 0.33 \cdot \text{SUBGRUT} \quad (39)$$

Where

- TRUT = Total rutting
- ACRUT = Rutting in the asphalt layers predicted using the 1-40D models (see chapter 2)
- BASERUT = Rutting in the base layer predicted using the 1-40D models (see chapter 2)

- SUBGRUT = Rutting in the subgrade layer predicted using the 1-40D models (see chapter 2)
- β_{1r} = HMA rutting prediction local calibration factor = 0.51
- β_{B1} = Unbound base rutting prediction local calibration factor = 0.32
- β_{s1} = Subgrade rutting prediction local calibration factor = 0.33

A statistical comparison of measured and MEPDG predicted rutting was performed to determine accuracy and precision. The results, presented in Figure 22 and Table 14, indicate the following:

- A fair correlation between measured and MEPDG predicted rutting.
- SEE much less than that reported for the national MEPDG rutting model.
- Significant bias in predicted and measured rutting, as indicated by the results of hypotheses (1) and (3).

Although the goodness of fit of the recalibrated model was adequate, the model predictions still were significantly biased, suggesting that the revised model is still deficient. The presence of bias post recalibration was due mainly to the inability of the MEPDG to match the shape of the rutting versus age (traffic) curve. A more comprehensive evaluation of ODOT HMA pavement mixtures and a larger calibration data set will be necessary to calibrate the models for ODOT conditions.

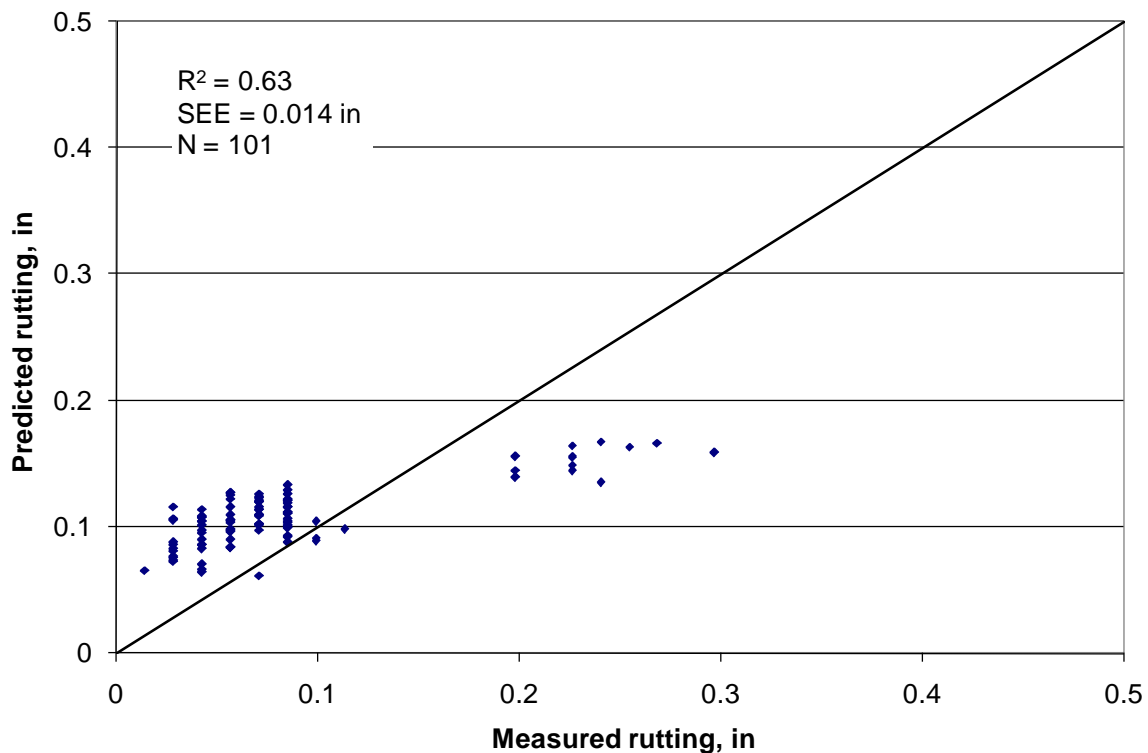


Figure 22. Plot of measured versus MEPDG predicted HMA pavement total rutting.

Table 14. Statistical comparison of measured and recalibrated rutting model predicted rutting data.

Goodness of Fit							
N = 101							
R ² = 0.63							
Adj R ² = 0.63							
SEE = 0.014 in							
Hypothesis Testing							
Hypothesis	DF	Parameter Estimate	Std. Error	t Value	p-value (Pr > t)	95 Percent Confidence Limits	
(1) Ho: Intercept = 0	1	0.083	0.0024	34.4	< 0.0001	0.078	0.087
(2) Ho: Slope = 1.0	1	0.952	0.049	19.4	0.3395	0.855	1.05
(3) Ho: Measured Rutting - MEPDG Predicted Rutting = 0	101			-5.62	< 0.0001		

HMA Smoothness (IRI)

Validation

Figure 23 presents a histogram of all measured IRI for the SPS-1 and SPS-9 projects included in the analysis. The plot shows that the IRI data range from approximately 40 to 180 in/mi and have a mean of 81 in/mi. A statistical comparison of the measured and MEPDG predicted IRI was performed to determine the nationally calibrated model's predictive ability and accuracy. The results are presented in Figure 24 and Table 15 and indicate the following:

- There is significant bias in predicted IRI. It can be gathered that the MEPDG over-predicts the IRI for the lower magnitudes of measured IRI and under-predicts it for the higher magnitudes of measured IRI. In other words, the slope of the predicted versus measured IRI does not match the 1:1 slope represented by the line of equality.
- There is a poor correlation between measured and MEPDG predicted IRI.
- The SEE is less than that reported for the national MEPDG IRI model.

A recalibration effort was needed to remove the identified significant bias. Just as with the rutting model recalibration effort, this recalibration effort should be viewed as an example or model exercise. To be implementable in design, a broader data set including sections representing the diverse site and design factors in Ohio will be needed.

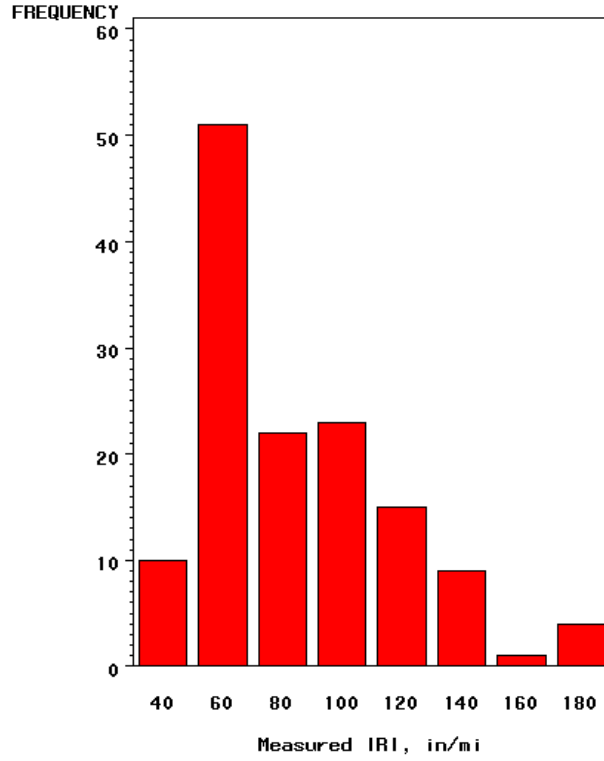


Figure 23. Histogram showing distribution of measured total IRI.

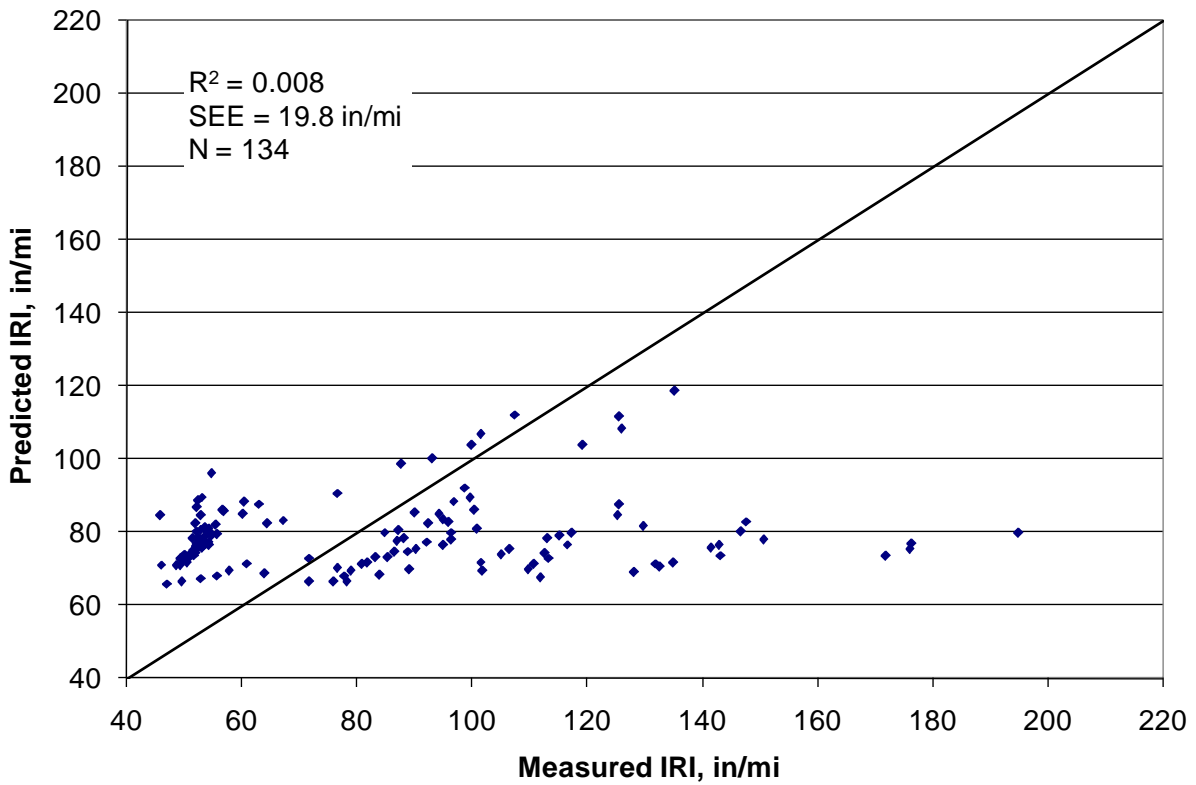


Figure 24. Plot of measured versus MEPDG predicted HMA pavement IRI.

Table 15. Statistical comparison of measured and MEPDG predicted IRI data.

Goodness of Fit							
N = 134							
R ² = 0.008							
Adj R ² = 0.0009							
SEE = 9.8 in/mi							
Hypothesis Testing							
Hypothesis	DF	Parameter Estimate	Std. Error	t Value	p-value (Pr > t)	95 Percent Confidence Limits	
(1) Ho: Intercept = 0	1	76.6	2.48	30.8	<0.0001	71.7	81.5
(2) Ho: Slope = 1.0	1	1.008	0.032	31.2	0.78	0.94	1.07
(3) Ho: Measured IRI - MEPDG Predicted IRI = 0	134			-4.18	<0.0001		

Recalibration

Recalibration involved modifying the original MEPDG HMA IRI prediction model as follows:

$$IRI = IRI_o + \alpha_1(SF) + \alpha_2(FC_{Total}) + \alpha_3(TC) + \alpha_4(RD) \quad (40)$$

where:

- IRI_o = Initial IRI after construction, in/ mi
- SF = Site factor, refer to equation 41
- FC_{Total} = Area of fatigue cracking (combined alligator, longitudinal, and reflection cracking in the wheel path), percent of total lane area. All load related cracks are combined on an area basis - length of cracks is multiplied by 1 foot to convert length into an area basis
- TC = Length of transverse cracking (including the reflection of transverse cracks in existing HMA pavements), ft/ mi.
- NRD = Average rut depth (computed using the recalibrated rutting model presented as equation 39)
- $\alpha_1, \alpha_2, \alpha_3, \alpha_4$ = New model coefficients obtained through recalibration

The site factor is calculated in accordance with the following equation.

$$SF = FROSTH + SWELL * AGE^{1.5} \quad (41)$$

where:

- FROSTH = LN([PRECIP+1]*FINES*[FI+1])
- SWELLP = LN([PRECIP+1]*CLAY*[PI+1])
- FINES = FSAND + SILT
- AGE = pavement age, years

PI	=	subgrade soil plasticity index
PRECIP	=	mean annual precipitation, in.
FI	=	mean annual freezing index, deg. F Days
FSAND	=	amount of fine sand particles in subgrade (percent of particles between 0.074 and 0.42 mm)
SILT	=	amount of silt particles in subgrade (percent of particles between 0.074 and 0.002 mm)
CLAY	=	amount of clay size particles in subgrade (percent of particles less than 0.002 mm)

As shown in equations 40 and 41, all four of the new HMA model coefficients can be modified as needed to improve predicted HMA IRI.

Recalibration also involved reviewing the measured and predicted HMA IRI to determine the possible sources of bias. The review indicated the following:

- The model generally over-predicted IRI for IRI less than 80 in/mi and under-predicted IRI for IRI greater than 80 in/mi.
- Bias still present in the recalibrated rutting model was passed on to the IRI model.

Recalibration was done using the selected LTPP SPS-1 and SPS-9 projects described earlier (project 0159 was excluded because of bad performance data). The recalibrated model, including new model coefficients, is presented below:

$$IRI = IRI_o + 0.066(SF) + 1.37(FC_{Total}) + 0.01(TC) + 17.6(RD) \quad (42)$$

where all variables are as already defined.

A statistical comparison of measured and MEPDG predicted HMA IRI was done to determine recalibrated model prediction capacity, accuracy, and bias. The results are presented in Figure 25 and Table 16 and show the following:

- A very good correlation between measured and predicted smoothness from the recalibrated HMA IRI model.
- SEE was about the same as the original MEPDG HMA IRI model.
- Although both hypotheses (1) and (2) were rejected and hypothesis (3) accepted, the levels of bias reported were more reasonable when compared to the nationally calibrated model.

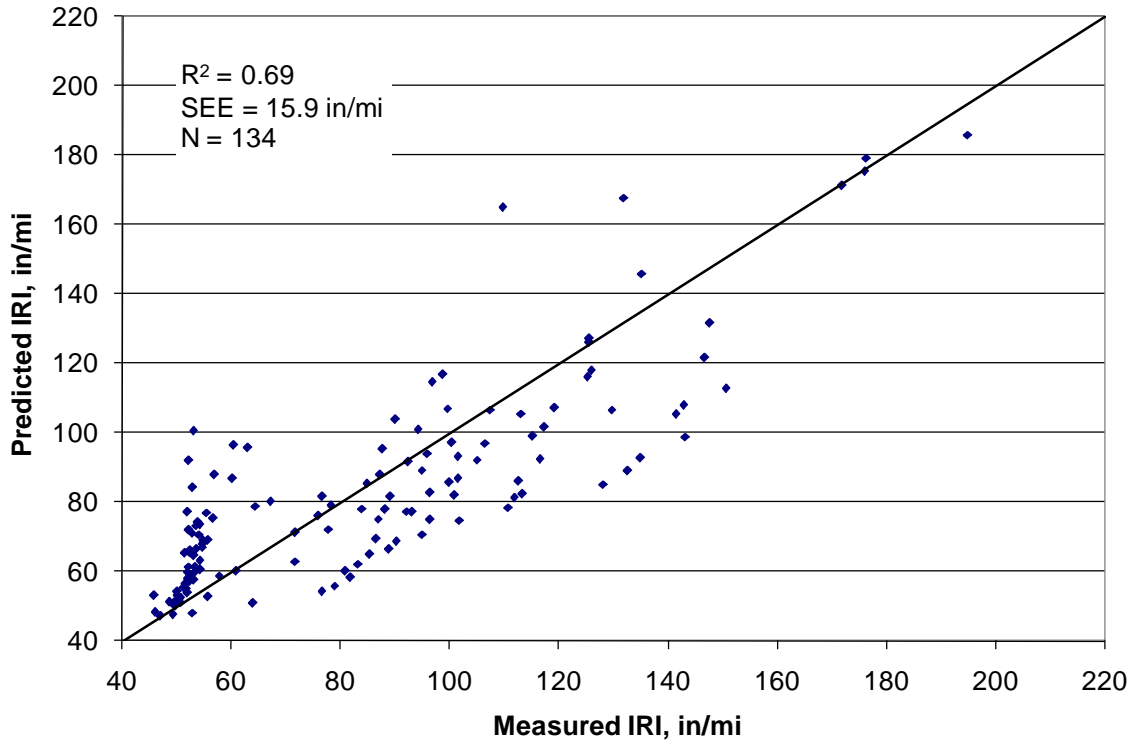


Figure 25. Plot of measured versus MEPDG predicted HMA pavement IRI.

Table 16. Statistical comparison of measured and predicted recalibrated HMA model IRI data.

Goodness of Fit							
N = 134							
R ² = 0.69							
Adj R ² = 0.69							
SEE = 15.9 in/mi							
Hypothesis Testing							
Hypothesis	DF	Parameter Estimate	Std. Error	t Value	p-value (Pr > t)	95 Percent Confidence Limits	
(1) Ho: Intercept = 0	1	22.9	3.67	6.25	< 0.0001	17.7	30.2
(2) Ho: Slope = 1.0	1	0.95	0.017	54.7	< 0.0027	0.912	0.981
(3) Ho: Measured IRI - Recalibrated Model Predicted IRI = 0	134			0.75	0.455		

New JPCP

Transverse Slab Cracking

Validation

Figure 26 presents a histogram of all measured PCC slab transverse cracking for the LTPP projects evaluated. Sixty-six of the 68 reported measurements of percent slabs cracked were zero. Thus, the MEPDG JPCP transverse cracking model was evaluated by comparing measured and predicted percent slabs cracked in a non-statistical manner. The measured transverse cracking was divided into eight groups; the range of each group was determined based on engineering judgment. The goal was to determine how often measured and predicted percent slabs cracked remained in the same group. Measured and predicted percent slabs cracked remaining in the same group implied reasonable and accurate predictions with little or no bias, while measured and predicted distress residing in different groups suggested otherwise. The results of the comparisons are summarized in Table 17.

A vast majority of the measured and predicted transverse cracking (approximately 97 percent) fell within the same measured and predicted transverse cracking grouping. All of these were for pavements with very little cracking distress. There were two data points for which predicted percent slabs cracked was higher than measured. The difference was, however, less than 10 percent and was deemed not significant.

For the levels of cracking evaluated in this analysis, the JPCP transverse cracking model predicted cracking with reasonable accuracy and without significant bias. Higher levels of cracking present on moderate to highly distressed pavements were not evaluated, as none of the projects included in the analysis experienced this level of cracking. Thus, although the JPCP transverse cracking was found to predict the distress reasonably well, there is a the need for additional analysis to include moderate to highly distressed pavements and projects that fully represented Ohio site and pavement design and construction practices.

Recalibration

Recalibration of the MEPDG JPCP transverse cracking model was not warranted at this stage.

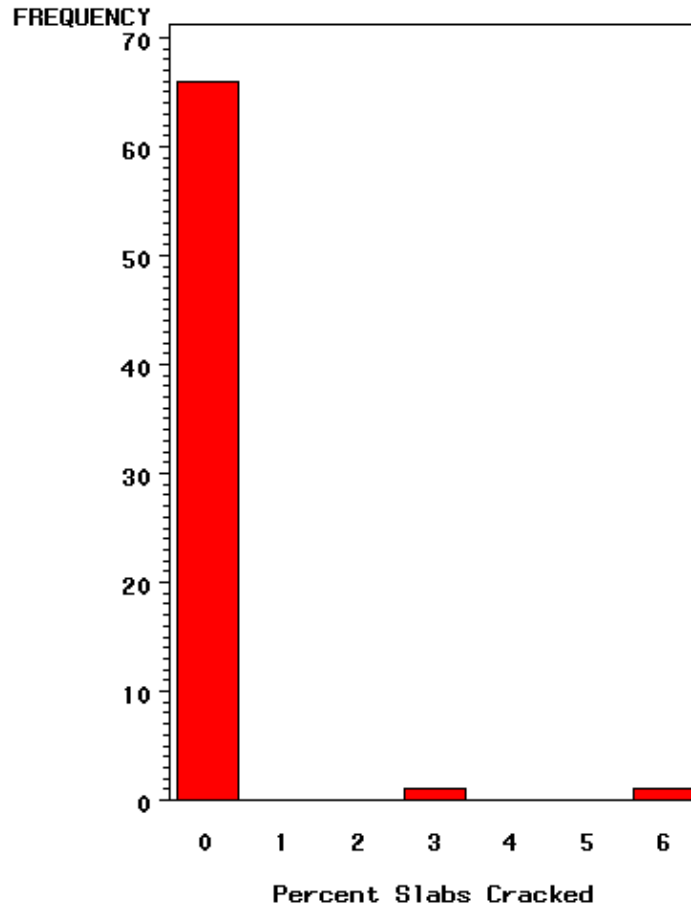


Figure 26. Histogram showing distribution of measured transverse slab cracking.

Table 17. Comparison of measured and predicted transverse slab cracking (percentage of all data points).

Measured Percent Slabs Cracked	MEPDG Predicted Percent Slabs Cracked							
	0-2	2-5	5-10	10-20	20-40	40-60	60-80	80-100
0-2	66	0	0	0	0	0	0	0
2-5	1	0	0	0	0	0	0	0
5-10	1	0	0	0	0	0	0	0
10-20	0	0	0	0	0	0	0	0
20-40	0	0	0	0	0	0	0	0
40-60	0	0	0	0	0	0	0	0
60-80	0	0	0	0	3	8	0	0
80-100	0	0	0	0	0	0	0	0

*Total data points = 68.

Transverse Joint Faulting

Validation

Figure 27 presents a histogram of all measured mean transverse joint faulting for all the SPS-2 and GPS-3 pavement sections included in this analysis. The plot shows that the measured mean joint faulting ranges from 0 to 0.14 in. Evaluating these data should produce reasonable and meaningful diagnostic statistics that can then be used to assess the model's predictive capacity, accuracy, and bias. Thus, a statistical comparison of measured and MEPDG predicted transverse joint faulting was done. The results are presented in Figure 28 and Table 18 and indicate the following:

- A good correlation between measured and MEPDG predicted faulting.
- SEE less than that reported for the national MEPDG faulting model.
- No bias in predicted and measured faulting as indicated by the results of hypotheses (1), (2), and (3).

Therefore, it can be concluded that the MEPDG mean joint faulting model's prediction capacity was very good and had no significant bias.

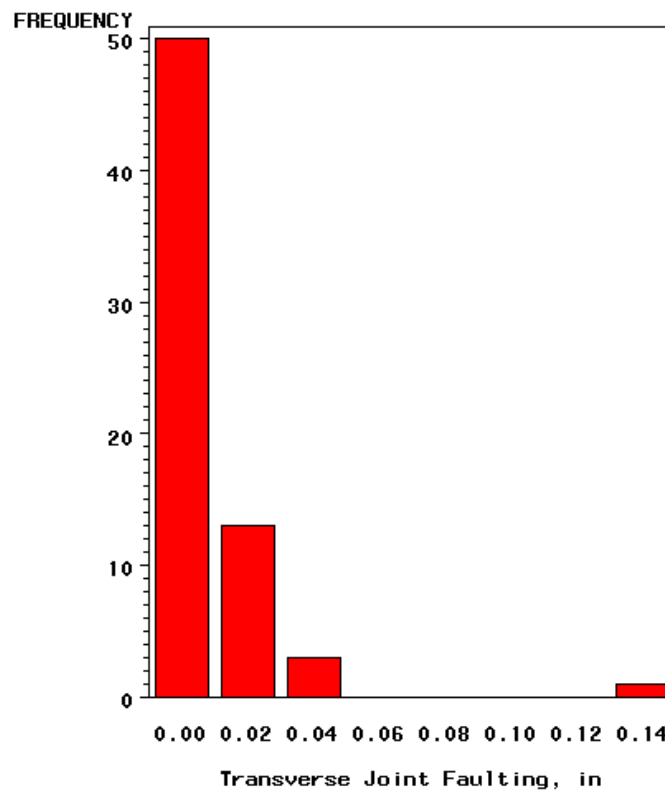


Figure 27. Histogram showing distribution of measured transverse joint faulting for all projects evaluated.

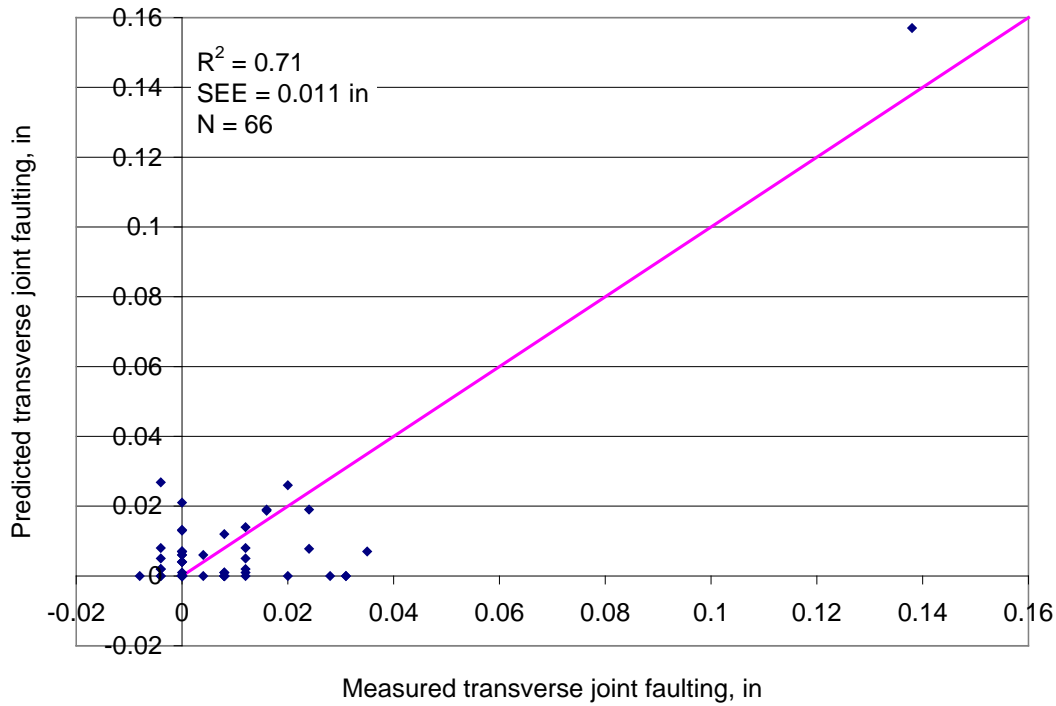


Figure 28. Plot of measured versus MEPDG predicted JPCP faulting.

Table 18. Statistical comparison of measured and MEPDG predicted transverse joint faulting data.

Goodness of Fit							
N = 66							
R ² = 0.71							
Adj R ² = 0.71							
SEE = 0.011 in							
Hypothesis Testing							
Hypothesis	DF	Parameter Estimate	Std. Error	t Value	p-value (Pr > t)	95 Percent Confidence Limits	
(1) Ho: Intercept = 0	1	0.00009745	0.00141	0.07	0.9452	-0.00272	0.00292
(2) Ho: Slope = 1.0	1	0.88807	0.06499	2.97	0.0897	0.75830	1.01783
(3) Ho: Measured Faulting - MEPDG Predicted Faulting = 0	66			-0.55	0.5823		

Recalibration

Recalibration of this model is still warranted given the limited amount of data from sections with higher amounts of faulting distress. In a future validation/calibration effort, it is recommended that data from projects with higher faulting distress be included in the experimental factorial.

JPCP Smoothness (IRI)

Validation

Figure 29 presents a histogram of the measured IRI data for the selected SPS-2 projects included in analysis. The plot shows that the measured IRI ranges from 60 to 250 in/mi with a mean of 81 in/mi. A statistical comparison of the measured and MEPDG predicted IRI was performed. The results are presented in Figure 30 and Table 19.

The results showed the following:

- An excellent correlation between measured and MEPDG predicted IRI.
- SEE less than that reported for the national MEPDG JPCP IRI model.
- Bias in predicted and measured JPCP IRI as indicated by the results of hypotheses (1), (2), and (3).

Although the model's predictive capacity was excellent, there was a need to perform recalibration to remove the significant bias identified.

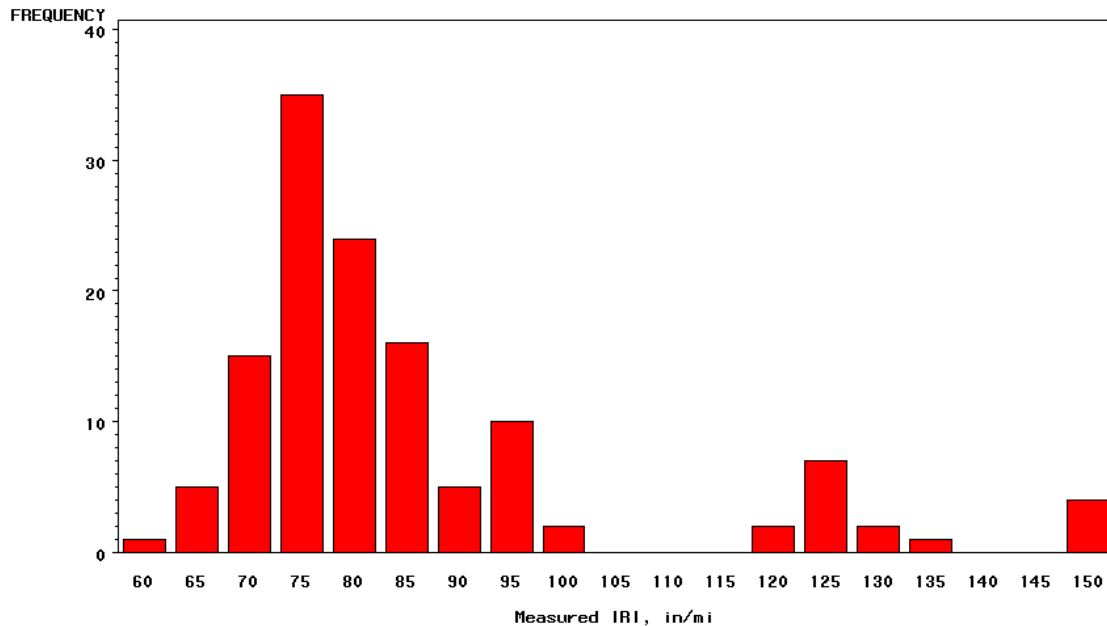


Figure 29. Histogram showing distribution of measured JPCP IRI.

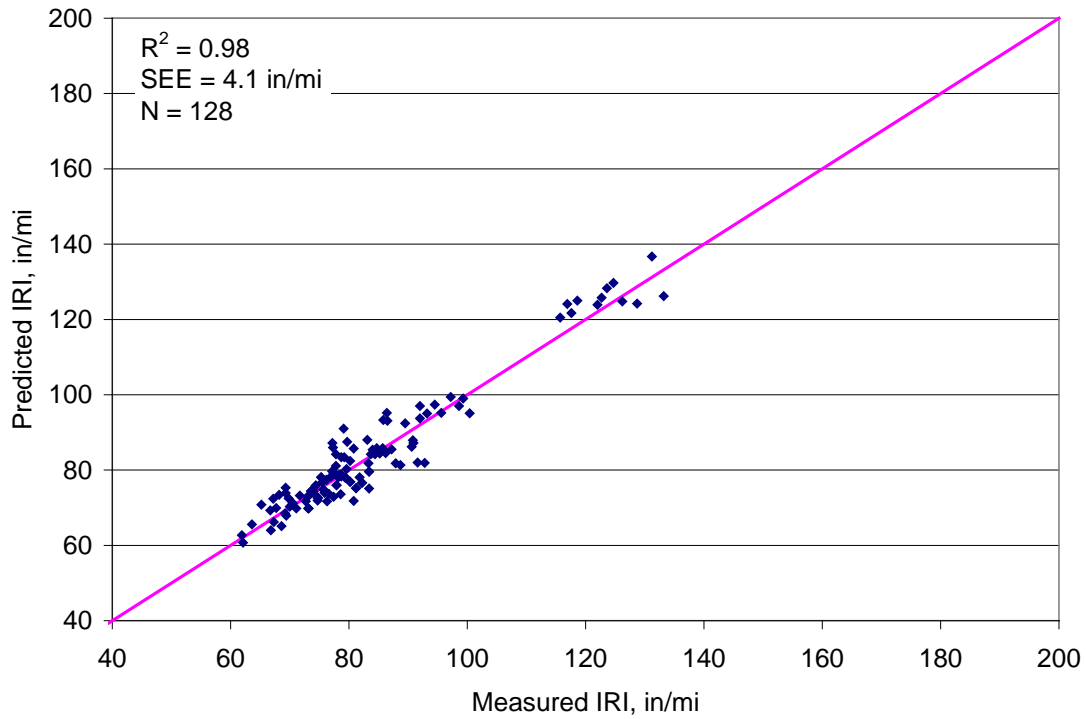


Figure 30. Plot of measured versus MEPDG predicted JPCP pavement IRI.

Table 19. Statistical comparison of measured and MEPDG predicted JPCP IRI data.

Goodness of Fit							
N = 128							
R ² = 0.98							
Adj R ² = 0.98							
SEE = 4.1 in/mi							
Hypothesis Testing							
Hypothesis	DF	Parameter Estimate	Std. Error	t Value	p-value (Pr > t)	95 Percent Confidence Limits	
(1) Ho: Intercept = 0	1	8.04080	1.04733	7.68	<0.0001	5.96833	10.11327
(2) Ho: Slope = 1.0	1	0.90059	0.01110	81.12	<0.0001	0.87862	0.92256
(3) Ho: Measured IRI - MEPDG Predicted IRI = 0	128			17.72	<0.0001		

Recalibration

Recalibration involved modifying the original MEPDG JPCP IRI prediction model as follows:

$$IRI = IRII + C1*CRK + C2*SPALL + C3*TFAULT + C4*SF \quad (43)$$

where:

<i>IRI</i>	=	Predicted IRI, in/mi
<i>IRI_I</i>	=	Initial smoothness measured as IRI, in/mi
<i>CRK</i>	=	Percent slabs with transverse cracks (all severities)
<i>SPALL</i>	=	Percentage of joints with spalling (medium and high severities)
<i>TFAULT</i>	=	Total joint faulting cumulated per mi, in
<i>C1, C2, C3, C4</i>	=	Recalibration coefficients
<i>SF</i>	=	Site factor

$$SF = AGE (1+0.5556*FI) (1+P_{200}) * 10^{-6} \quad (44)$$

where:

<i>AGE</i>	=	Pavement age, yr.
<i>FI</i>	=	Freezing index, °F-days.
<i>P₂₀₀</i>	=	Percent subgrade material passing No. 200 sieve.

As shown in equations 43 and 44, all four model coefficients can be modified as needed to improve predicted JPCP IRI by removing bias.

Recalibration also involved reviewing the measured and predicted JPCP IRI to determine the possible sources of bias. The review indicated that there was no obvious source of bias.

Recalibration was performed using the selected LTPP SPS-2 and GPS-3 projects described earlier. The recalibrated model, including new model coefficients, is presented in equation 45. It should be noted once again that the recalibration exercise undertaken here is limited by the constraints imposed by the data set used. It is anticipated that, before finalizing this model for design use, a wider inference space representing the range of site and design factors of interest to ODOT will be used in a future recalibration effort.

$$IRI = IRII + 0.82*CRK + 3.7*SPALL + 1.711*TFAULT + 5.703*SF \quad (45)$$

All variables are as already defined.

A statistical comparison of measured and predicted JPCP IRI was done to determine recalibrated model prediction capacity and accuracy. The results are presented in Figure 31 and Table 20 and show the following:

- An excellent correlation between measured and predicted IRI from the recalibrated JPCP IRI model.
- SEE was about the same as the original MEPDG JPCP IRI model which was less than that reported for the national MEPDG JPCP IRI model.
- No significant levels of bias as indicated by the results of hypotheses (1), (2), and (3).

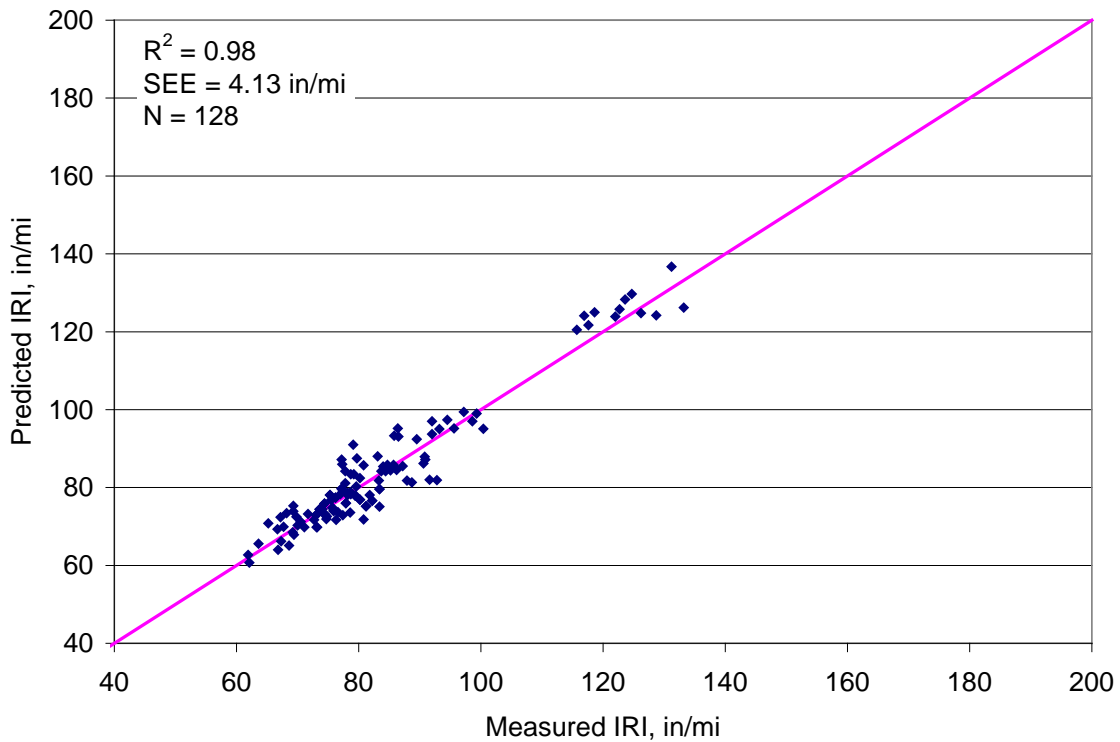


Figure 31. Plot of measured versus recalibrated JPCP IRI model predicted IRI.

Table 20. Statistical comparison of measured and predicted recalibrated JPCP model IRI data.

Goodness of Fit							
N = 128 R ² = 0.98 Adj R ² = 0.98 SEE = 4.13 in/mi							
Hypothesis Testing							
Hypothesis	DF	Parameter Estimate	Std. Error	t Value	p-value (Pr > t)	95 Percent Confidence Limits	
(1) Ho: Intercept = 0	1	2.04752	1.05691	1.94	0.0549	-0.04391	4.13896
(2) Ho: Slope = 1.0	1	0.99389	0.00389	2.46	0.1190	0.98618	1.00159
(3) Ho: Measured IRI – Recalibrated Model Predicted IRI = 0	134			-0.81	0.4200		

*Borderline when compared to a significance level of 0.05.

CHAPTER 5. SENSITIVITY ANALYSIS OF RECALIBRATED MEPDG MODELS

Introduction

A sensitivity analysis is the process of varying model input parameters (subgrade type, base type, PCC strength, etc.) over a practical range and observing the relative change in model response. By doing this for typical Ohio conditions, the MEPDG models can be evaluated for reasonableness.

For this study, a comprehensive sensitivity analysis of the nationally calibrated MEPDG models was done and presented in Volume 3 of this report. Supplemental sensitivity analysis was required to augment the results presented in Volume 3 due to the recalibration of the HMA rutting and IRI models and the JPCP IRI model.

Baseline designs were developed for deep-strength HMA pavement and JPCP using a central Ohio location's site conditions and other inputs that typically would be used. The baseline designs were used in both the comprehensive sensitivity analysis and the supplemental sensitivity analysis described here. A full and detailed description of the baseline designs is presented in Volume 3, along with the range of various input factors around the input baseline values established for the baseline designs.

This supplemental analysis was conducted by varying the design features, material properties, climate, etc. of the baseline design to determine how changes to these MEPDG input parameters influence the prediction of the following recalibrated models:

- New HMA rutting.
- New HMA IRI.
- JPCP IRI.

The goal was to compare predictions from the recalibrated models with those from the nationally calibrated MEPDG models, thereby deducing the effect of all key inputs variables on predictions from the recalibrated models.

Sensitivity Analysis Results for New HMA Pavements Recalibrated Models

Effect of Base Type on MEPDG Predicted HMA Pavement Performance

The base types considered were the DGAB and ATB_301. Both base types were 6 inches thick. Figure 32 and Figure 33 show the effect of base type on new HMA rutting and IRI. The information presented shows that, as reported by the nationally calibrated MEPDG models, unbound aggregate base causes the highest levels of the rutting and IRI. Compared to the nationally calibrated MEPDG models, the recalibrated models

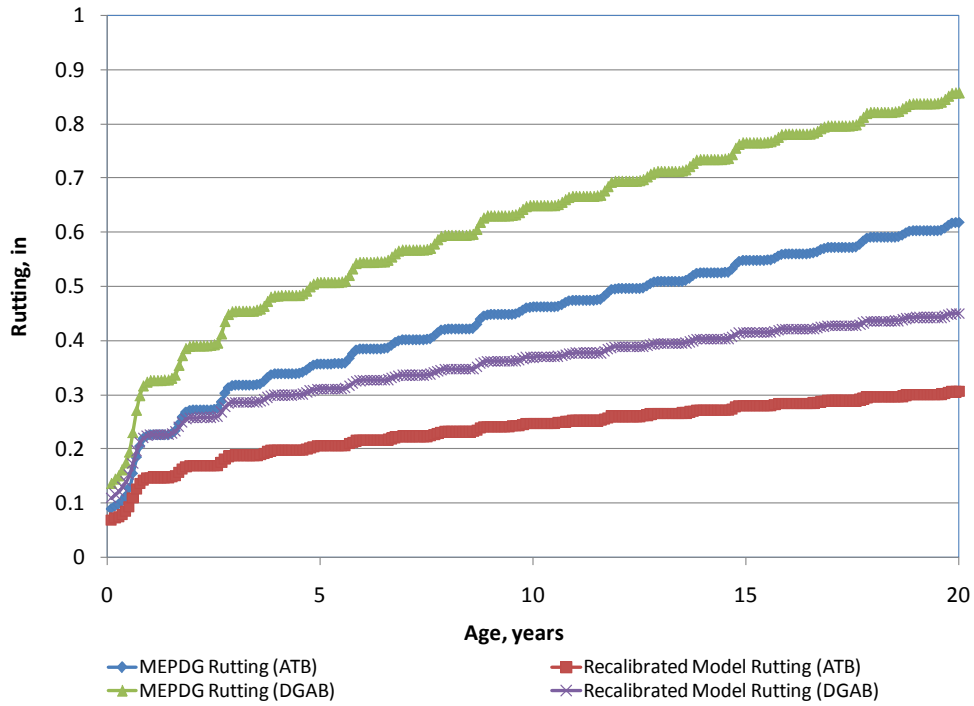


Figure 32. Plot showing the effect of base type on predicted rutting.

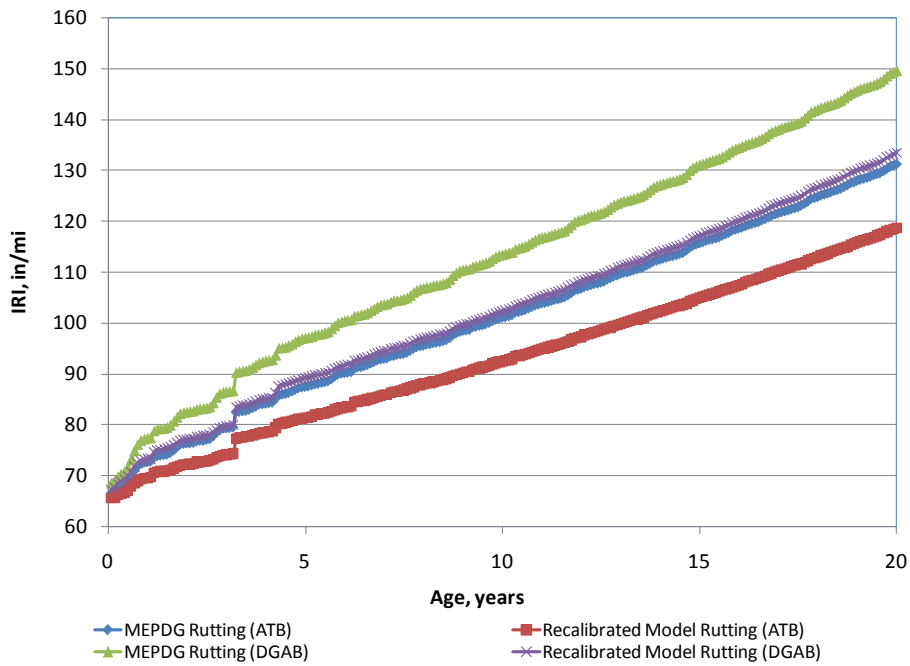


Figure 33. Plot showing the effect of base type on predicted IRI.

predicted less rutting and IRI. An evaluation of the trends in predicted rutting and IRI using the recalibrated models showed reasonable predictions that were in agreement with the trends in pavement deterioration observed in Ohio.

Effect of Climate

The effect of climate on recalibrated models predicted rutting and IRI was determined by selecting representative weather stations from the north (Cleveland) and south (Cincinnati) of the state. The objective was to determine whether the effect of climate on the recalibrated models was reasonable and how it compared with the nationally calibrated models. Climatic conditions were simulated using approximately 9 years of climate data collected from available weather stations. The results of the sensitivity analysis are presented in Figure 34 and Figure 35 for rutting and IRI, respectively.

The trends were similar to those of the nationally calibrated models, with climate having a moderate effect on predicted rutting and IRI. For the recalibrated models, however, the magnitude of the difference in predictions of rutting and IRI due to variation in climate conditions was less than that observed for the nationally calibrated models. Therefore, the recalibrated models were less sensitive to the effect of climate.

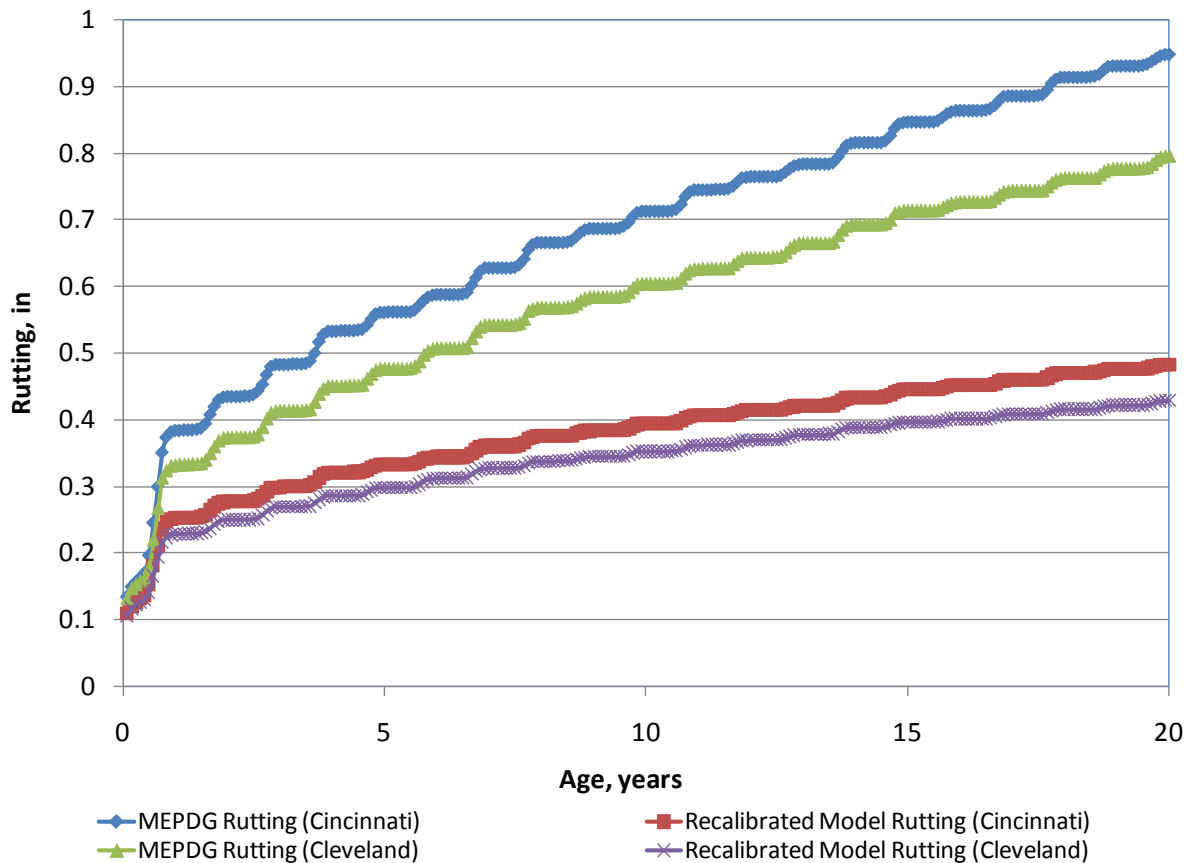


Figure 34. Plot showing the effect of climate on predicted rutting.

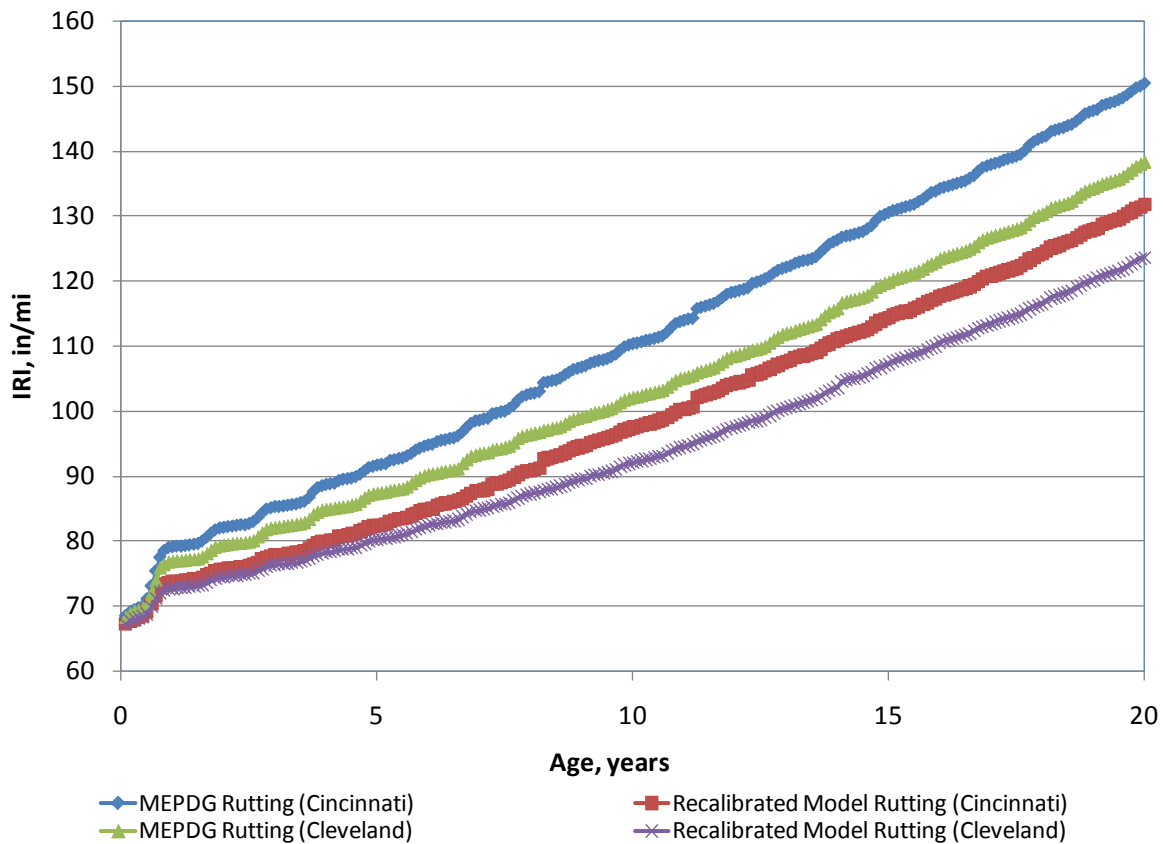


Figure 35. Plot showing the effect of climate on predicted IRI.

Effect of HMA Thickness

HMA thickness had a large effect on rutting and IRI for both the nationally calibrated models and the recalibrated models. These effects are shown in Figure 36 and Figure 37 for HMA thickness ranging from 5 to 11 in. The trends shown by the recalibrated models were reasonable and as expected. The recalibrated models were thus deemed reasonable.

Effect of Subgrade Type

The effect of subgrade type on performance was determined by simulating a new HMA pavement constructed over a fine-grained (A-7-5) and coarse grained (A-1-b) soil foundation.

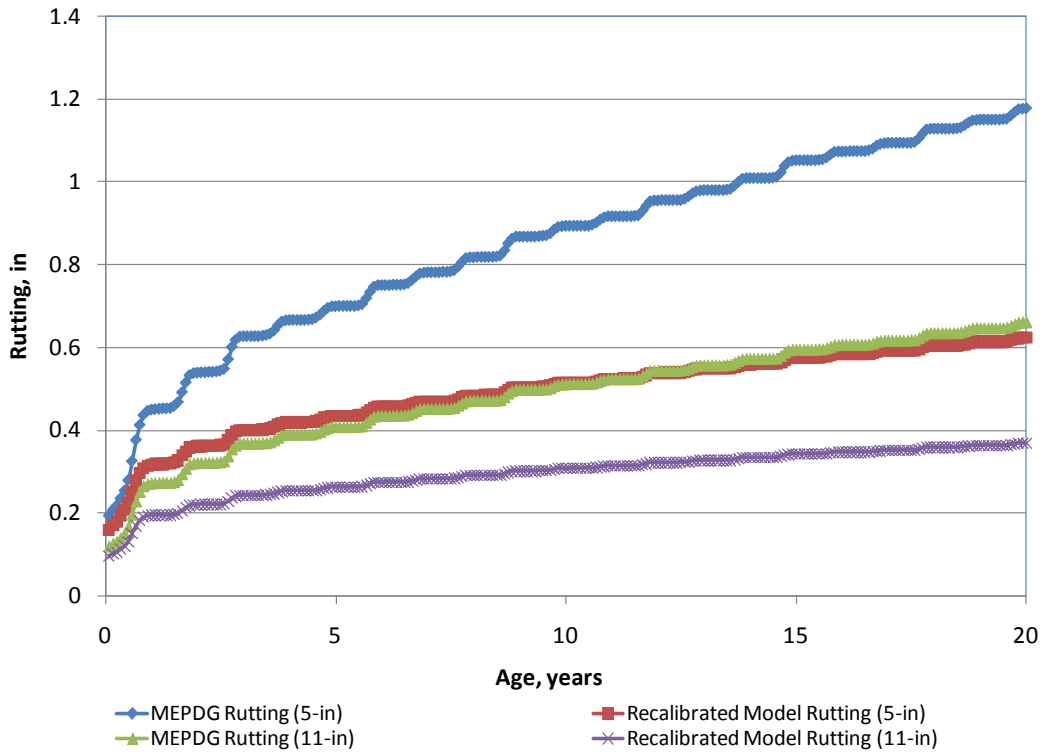


Figure 36. Plot showing the effect of HMA thickness on predicted rutting.

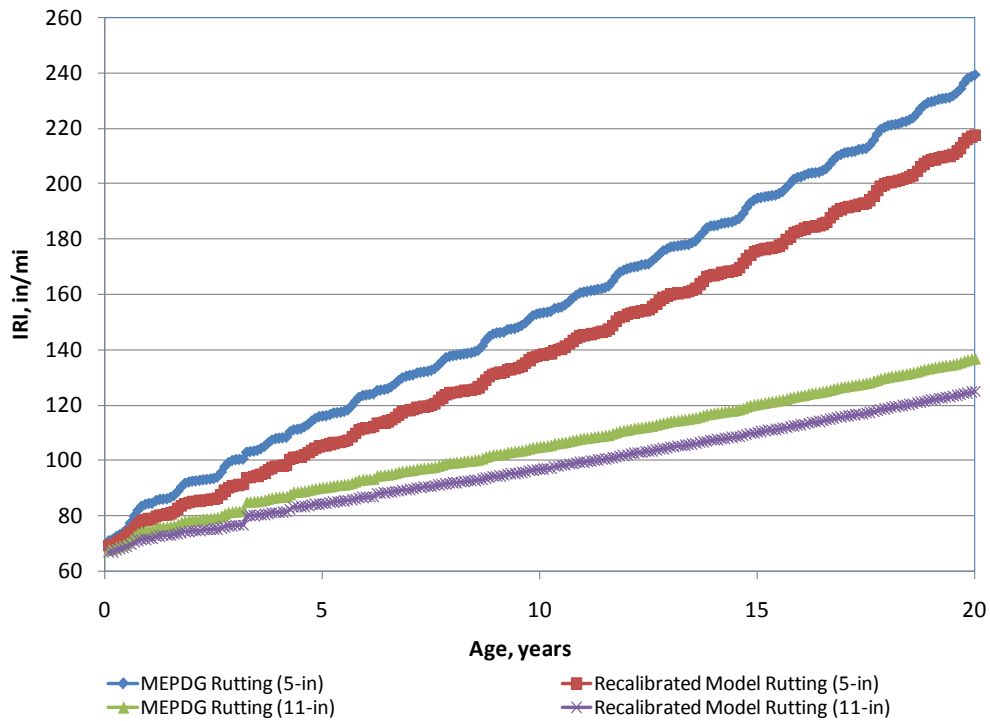


Figure 37. Plot showing the effect of HMA thickness on predicted IRI.

The subgrade soil properties represented by these two soil types are summarized below:

- Coarse-grained soil:
 - Resilient modulus: 26,500 psi.
 - Percent passing the No. 200 sieve size: 13.4 percent.
 - Maximum dry density: 127 pcf.
 - Optimum moisture content: 7.5 percent.
 - Hydraulic conductivity: 0.066 ft/hr
- Fine-grained soil:
 - Resilient modulus: 11,500 psi
 - Percent passing the No. 200 sieve size: 61.1 percent.
 - Maximum dry density: 112 pcf.
 - Optimum moisture content: 14.6 percent.
 - Hydraulic conductivity: 0.00004 ft/hr

The most significant property affecting distress development is the resilient modulus, which affects stress, strains, and deformations in the pavement and subgrade. As the subgrade modulus decreases, tensile strain in the bottom of the HMA layer and vertical strain at the top of the subgrade increase. Figure 38 and Figure 39 present the effect of subgrade soil type on predicted rutting and IRI. In general, the lower the subgrade type/modulus, the higher alligator fatigue cracking, rutting, and IRI. The trends shown by the recalibrated models were reasonable and as expected. The recalibrated models were thus deemed reasonable.

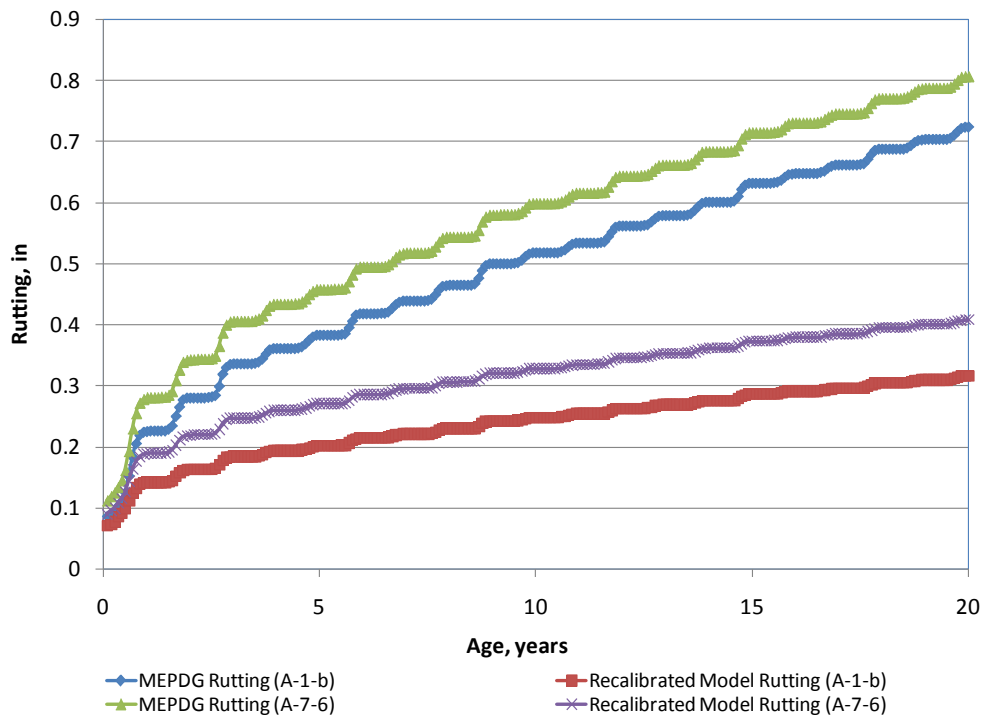


Figure 38. Plot showing the effect of subgrade type on predicted rutting.

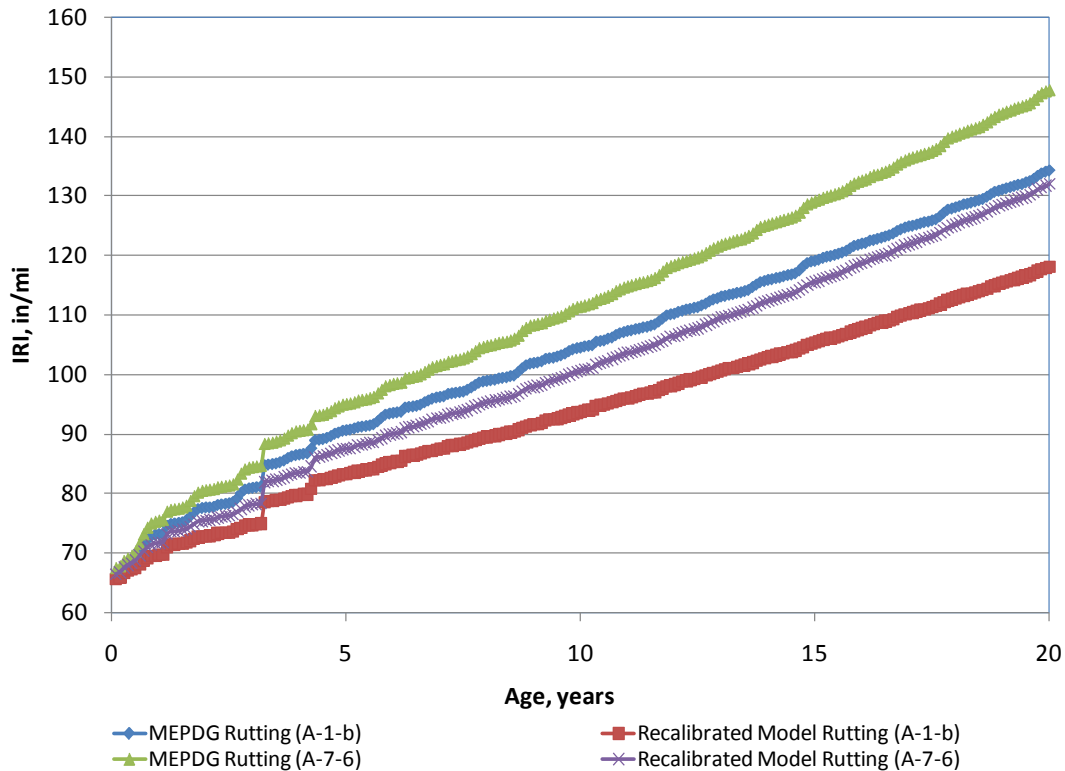


Figure 39. Plot showing the effect of subgrade type on predicted IRI.

Effect of HMA In-Situ Air Voids

Changes in HMA air voids have a considerable effect on rutting and IRI, since air voids affect HMA dynamic modulus – a key input for estimating permanent strain within the HMA layer.

Figure 40 and Figure 41 show the effect of the air voids in the base HMA layer (lowermost HMA layer) on predicted rutting and IRI. As can be seen, an increase of in-situ air void content in the lowermost HMA layer results in a large increase in both rutting and IRI. Figure 42 and Figure 43 show that an increase of in-situ air void content in the uppermost two layers also increases the rate of progression of rutting. IRI shows the same trend but is not affected much by a change of in-situ air void content over this range. The trends shown by the recalibrated models were reasonable and as expected. The recalibrated models were thus deemed reasonable.

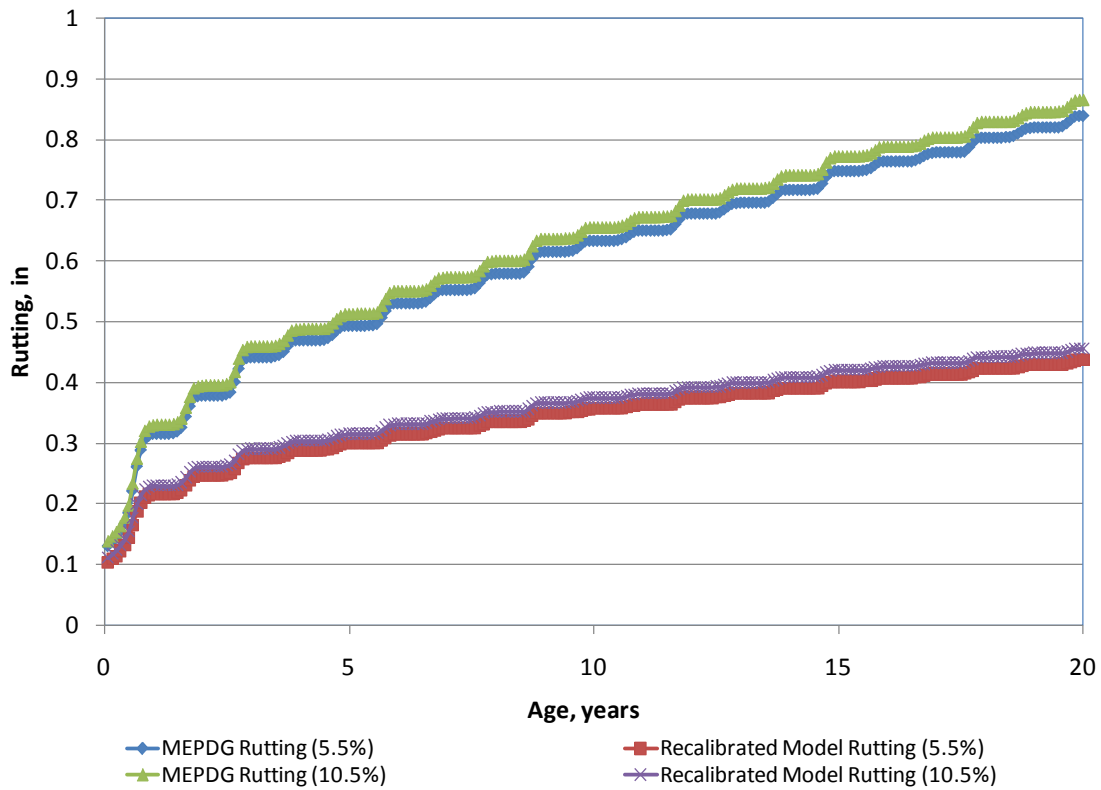


Figure 40. Plot showing the effect of HMA air voids in bottom layer on predicted rutting.

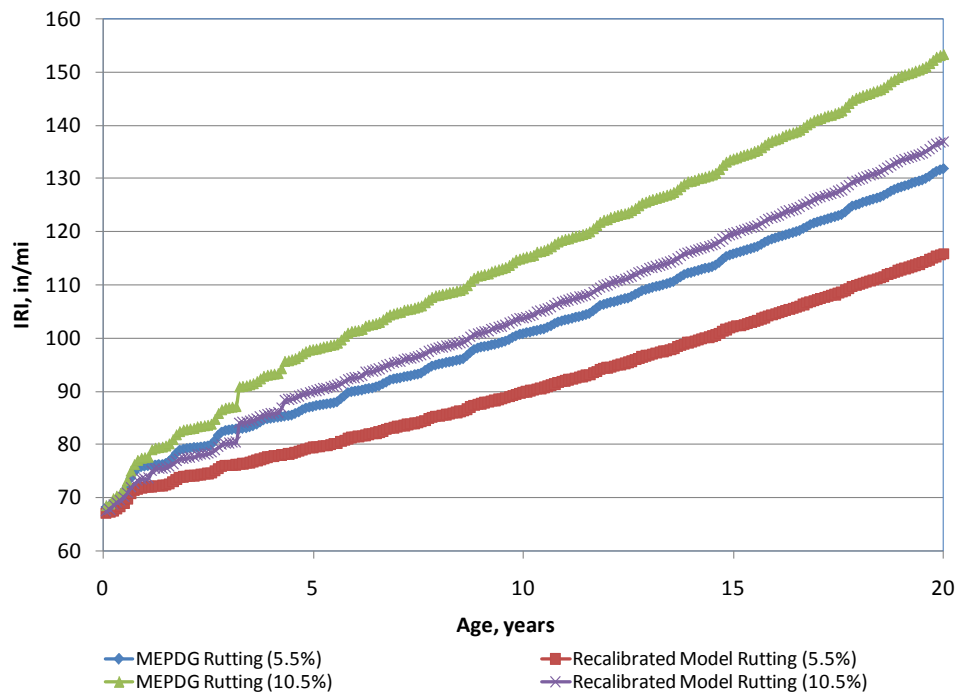


Figure 41. Plot showing the effect of HMA air voids in bottom layer on predicted IRI.

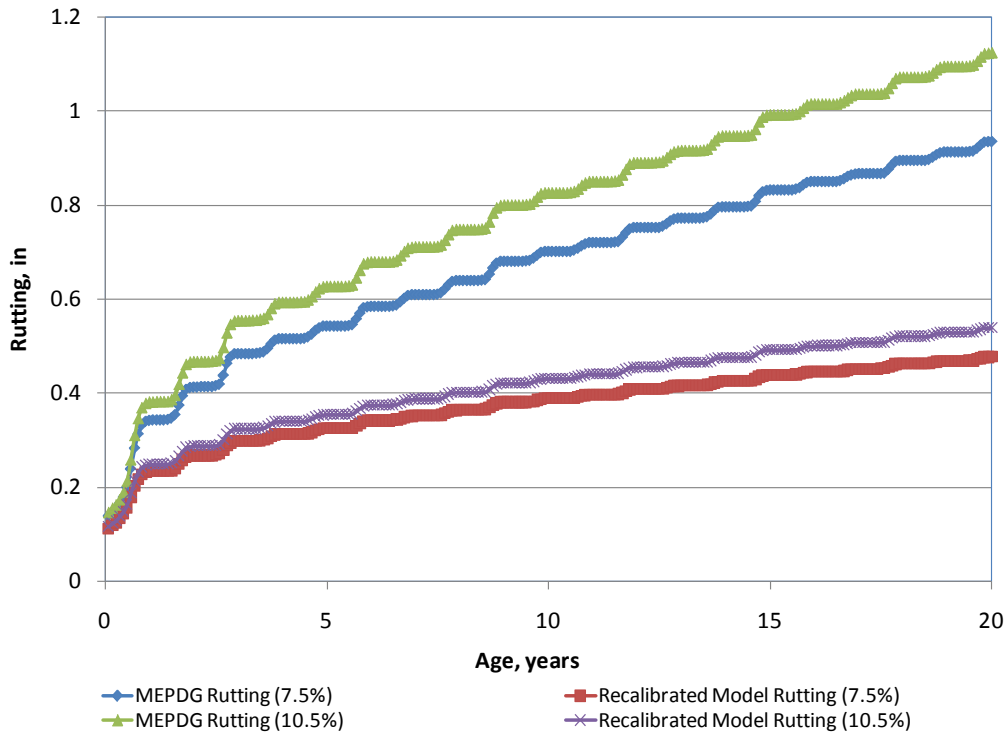


Figure 42. Plot showing the effect of HMA air voids in top layer on predicted rutting.

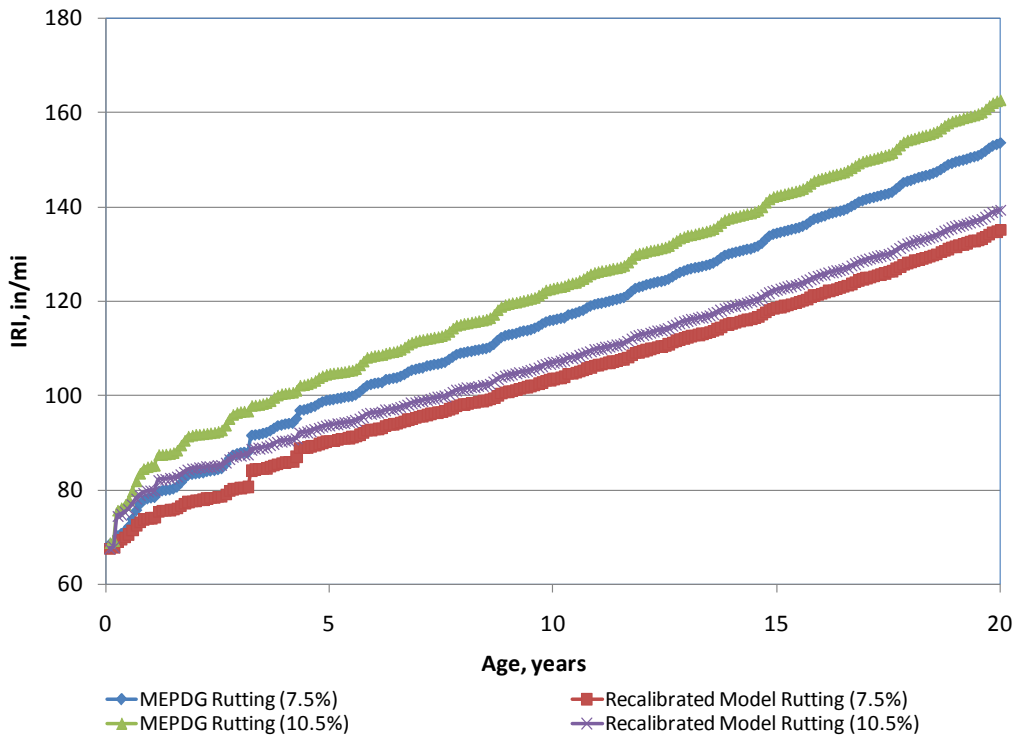


Figure 43. Plot showing the effect of HMA air voids in top layer on predicted IRI.

Sensitivity Analysis Results for New JPCP Recalibrated Models

Effect of Climate

The effect of climate on predicted JPCP IRI was determined by selecting representative weather stations in Cincinnati and Cleveland to determine whether the effect of climate was captured by the recalibrated IRI model. The results of the supplemental sensitivity analysis are presented in Figure 44, which shows that IRI was moderately influenced by climate across Ohio. The trend shown by the recalibrated JPCP IRI model was reasonable and as expected. The recalibrated model was thus deemed reasonable.

Effect of PCC Flexural Strength and Modulus of Elasticity

Concrete strength is expected to have a considerable effect on IRI since it has a significant effect on slab cracking – a key IRI model input. When PCC strength increases for the same mix, the modulus of elasticity also changes. This sensitivity analysis included the natural change in the modulus of elasticity along with strength. (Note that other PCC properties such as shrinkage and CTE also could change with a change in strength, depending on how the strength change was accomplished in the mix design. However, for simplicity, only elastic modulus – which has the strongest and well established correlation with strength by far – has been chosen to co-vary with strength). These two effects tend to negate each other to some extent, in that as the modulus increases the stress also increases. Figure 45 shows that a change in PCC strength and elastic modulus has a moderate effect on IRI. The trend shown by the recalibrated JPCP IRI model was reasonable and as expected. The recalibrated model was thus deemed reasonable.

Effect of PCC Slab Length/Joint Spacing

The standard joint spacing in Ohio is 15 ft, and this was used as the baseline design. Spacing was varied from 12.5 to 20 ft to show its impact. As joint spacing is increased, additional joint opening and curling stresses occur, leading to an expectation of increased joint faulting and slab cracking (key inputs for IRI). Figure 46 shows the sensitivity plot for IRI. As joint spacing increases, smoothness decreases greatly, as expected. The trend shown by the recalibrated JPCP IRI model was reasonable and as expected. The recalibrated model was thus deemed reasonable.

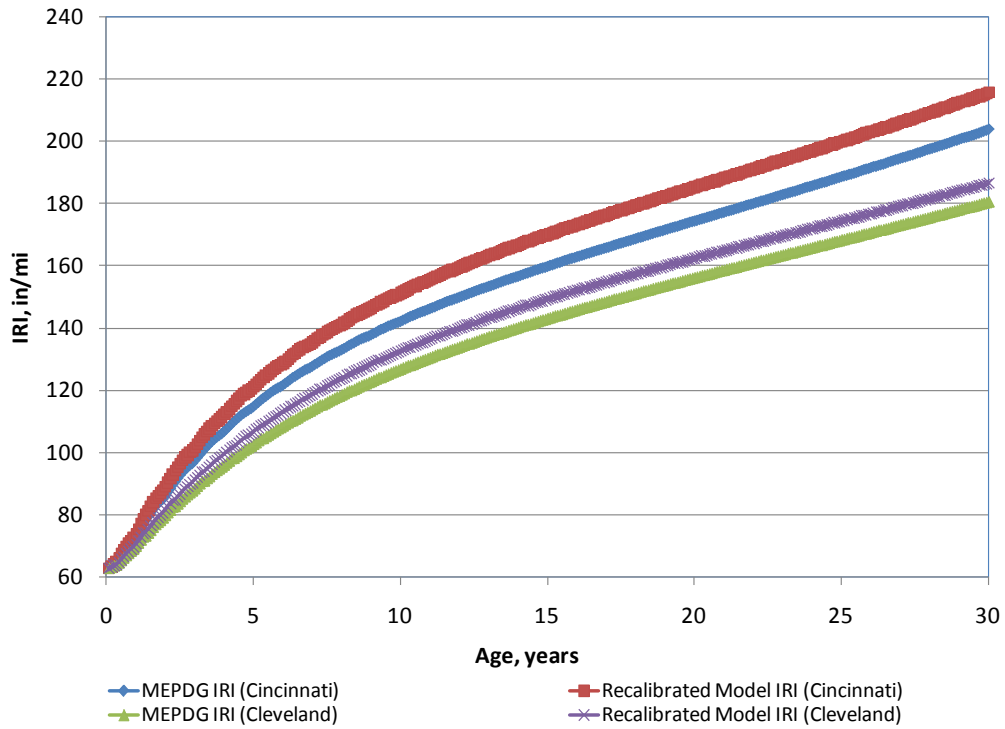


Figure 44. Plot showing the effect of climate on predicted JPCP IRI.

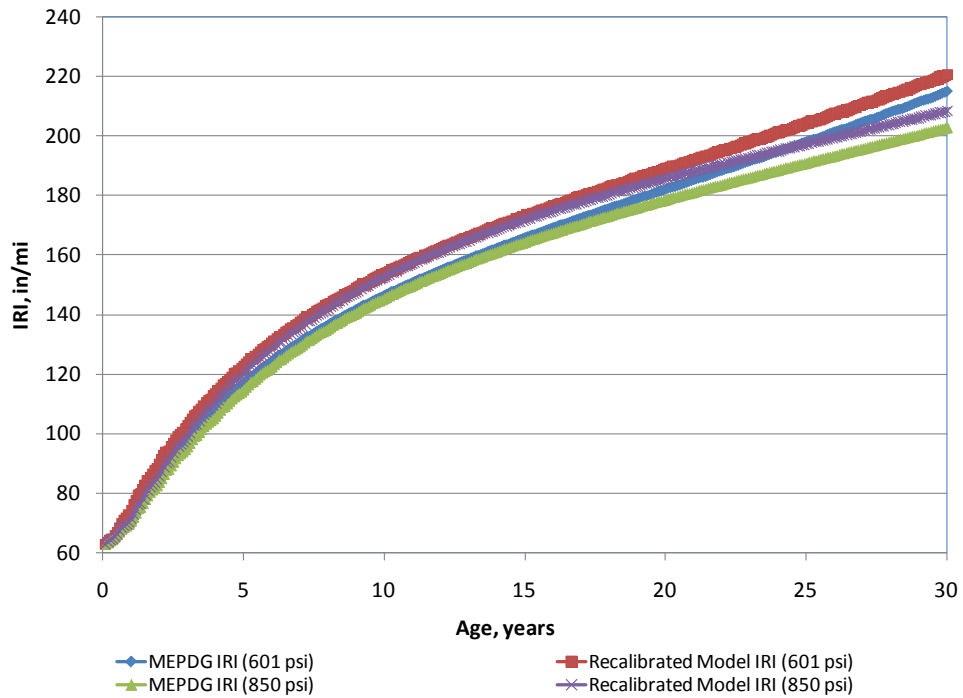


Figure 45. Plot showing the effect of PCC flexural strength and elastic modulus on predicted JPCP IRI.

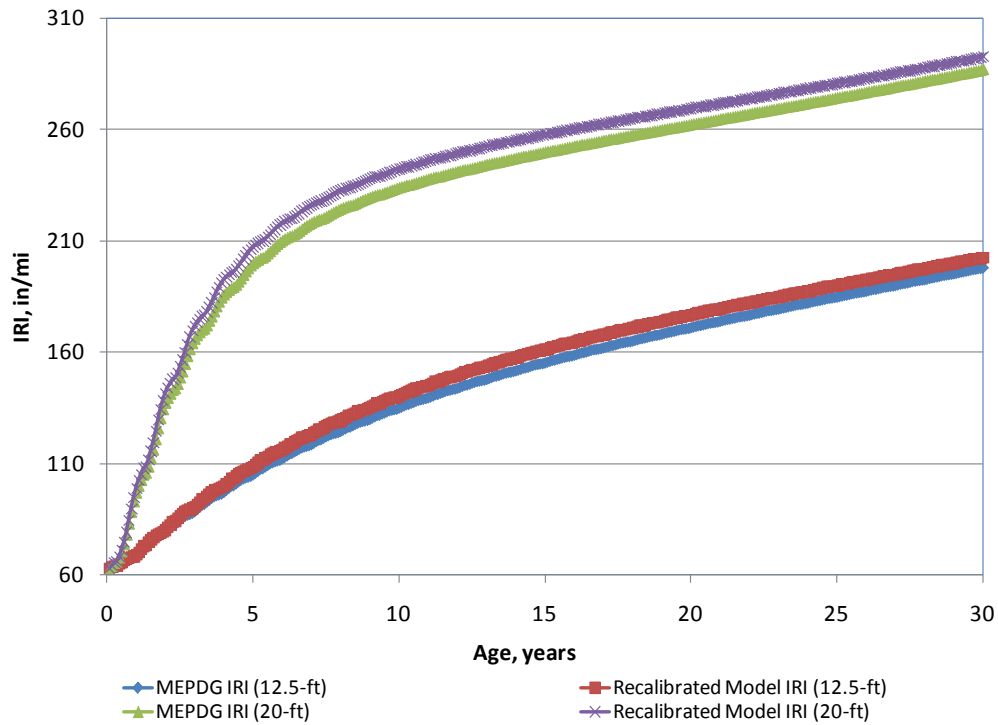


Figure 46. Plot showing the effect of joint spacing on predicted JPCP IRI.

Effect of Subgrade Type

The subgrade properties included in the MEPDG that change with the various subgrade soil types are resilient modulus, gradation, and Atterberg limits. The most significant property affecting distress development is the resilient modulus, which was selected based on AASHTO soil classification as shown in Table 21.

Subgrade type affects joint faulting and slab cracking considerably and has a moderate effect on IRI, as shown in Figure 47. The trend shown by the recalibrated JPCP IRI model was reasonable and as expected. The recalibrated model was thus deemed reasonable.

Table 21. Recommended subgrade/embankment resilient modulus input (at optimum density and moisture) for rigid pavements and rehabilitation of rigid pavements. [Do not use these resilient modulus values for compacted base or subbase course. Use appropriate table for base/subbase course resilient modulus].

Subgrade AASHTO Soil Class	Optimum Dry Density (mean, std. dev.)*	Optimum Moisture Content (mean)*	Design Guide Input Resilient Modulus at Optimum Density/Moist. (mean, std. dev.)**	Design Guide Backcalculated Output Dynamic k-value (mean, std. dev.)**	Recommended Input Subgrade Resilient Modulus (Opt. Density/Moisture Content)
A-1-b	122, 9	11%	14,760, 8,817	335, 92	18,000
A-7-6	102, 8	20	13,218, 322	203, 53	13,000

*Information provided in this table was obtained from the LTPP database (optimum density and moisture).

**Information obtained from Design Guide backcalculation and from use of the Design Guide (input subgrade resilient modulus, Mr, at optimum density and moisture).

***These results are based on about 250 JPCP and CRCP pavements located across the U.S. and used in the calibration of the Design Guide rigid pavements.

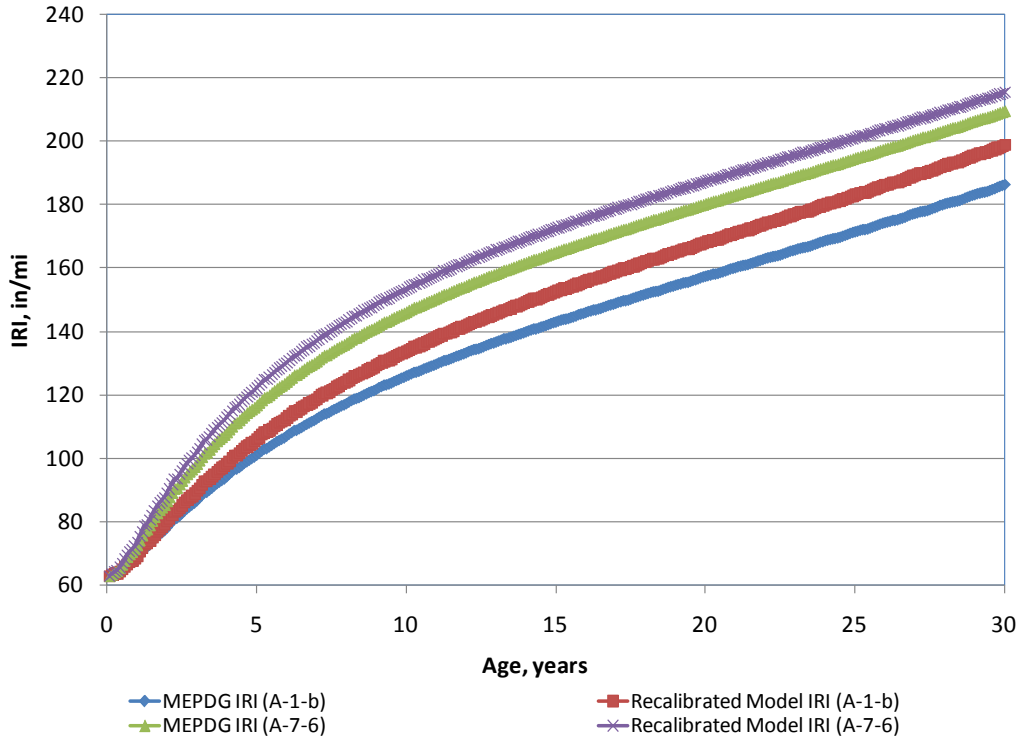


Figure 47. Plot showing the effect of subgrade type on predicted JPCP IRI.

THIS PAGE INTENTIONALLY LEFT BLANK.

CHAPTER 6. SUMMARY AND CONCLUSIONS

Summary

New HMA

Results for the MEPDG models evaluated for new HMA and new JPCP are summarized as follows:

- Alligator fatigue cracking: A full evaluation of this model could not be conducted due to the lack of data.
- Transverse “thermal cracking” cracking: A full statistical analysis could not be conducted because there was no cracking measured on the projects. The non-statistical comparison of predicted and measured cracking data showed that all measured and MEPDG predicted transverse cracking data fell in the same grouping. Thus, on this limited scale, the transverse cracking model performed adequately. A more detailed review to determine the adequacy of MEPDG default HMA creep compliance and tensile strength is needed to determine reasonableness of these defaults throughout Ohio’s climate zones.
- Rutting: The MEPDG rutting model was inadequate (predicted rutting with significant bias) and therefore was recalibrated. Recalibration produced local calibration factors for all three rutting submodels (HMA, base, and subgrade). Local calibration significantly improved the model accuracy but not the bias. Laboratory testing of typical ODOT HMA mixtures and a larger calibration dataset will be needed to refine this model before it can be used.
- HMA IRI: There was poor correlation between measured and MEPDG predicted IRI, while SEE was less than that reported for the national MEPDG IRI model. There was significant bias in predicted and measured IRI. With the model prediction capacity inadequate along with significant bias in predicted IRI, there was the need to perform recalibration to remove the identified significant bias. Local calibration significantly improved on the model accuracy and removed some of the existing bias. The recalibrated model still had some bias in its predictions.

New JPCP

Prediction models for new JPCP are as follows:

- Transverse “fatigue” cracking in the slab: Sixty-six of the 68 reported measurements of percent slabs cracked were zero. Thus, the MEPDG JPCP transverse cracking model was evaluated by comparing measured and predicted percent slabs cracked categorized into eight groups. Results were as follows:

- Approximately 97 percent of the measured and predicted transverse cracking fell within the same measured and predicted transverse cracking grouping. All of these were for pavements with very little cracking distress.
 - There were two data points for which predicted percent slabs cracked was higher than measured. The difference was, however, less than 10 percent and was deemed not significant.
 - For the levels of cracking evaluated in this analysis, the JPCP transverse cracking model predicted cracking with reasonable accuracy and without significant bias. Higher levels of cracking present on moderate to highly distressed pavements were not evaluated, as none of the projects included in the analysis experienced this level of cracking.
 - Although the JPCP transverse cracking was found to predict the distress reasonably well, there is a need for additional analysis to include moderate to highly distressed pavements and projects that more fully represent Ohio site conditions and pavement design and construction practices.
- Transverse joint faulting: The MEPDG model predicted faulting reasonably well as summarized below:
 - A good correlation between measured and MEPDG predicted faulting.
 - SEE less than that reported for the national MEPDG faulting model.
 - No bias in predicted and measured faulting as indicated by the results of hypotheses (1), (2), and (3).

However, although the model was found to predict joint faulting reasonably well, there is a need for additional analysis to include more moderate to highly distressed pavements and projects that more fully represent Ohio site conditions and pavement design and construction practices.

- IRI: Predicted IRI using the MEPDG showed the following:
 - An excellent correlation between measured and MEPDG predicted IRI.
 - SEE less than that reported for the national MEPDG JPCP IRI model.
 - Bias in predicted and measured JPCP IRI as indicated by the results of hypotheses (1), (2), and (3).

Although the model's prediction capacity was excellent, there was a need to perform recalibration to remove the identified significant bias. The new local calibration coefficients are as follows:

Pavement Type	JPCP IRI Model Local Calibration Coefficients			
	CRK (C1)	SPALL (C2)	TFAULT (C3)	SF (C4)
New JPCP	0.82	3.7	14.66	5.703

Local calibration significantly improved model accuracy and removed all significant bias.

Conclusions

The MEPDG models were reviewed thoroughly for use under Ohio conditions using LTPP SPS-1, SPS-2, SPS-9, and GPS-3 projects. All the SPS projects were relatively young, with approximately 10 years of distress/IRI data. The projects were located mostly at the same site and thus did not represent all of Ohio's site conditions or pavement design and construction practices.

A limited review of the MEPDG models indicated that while some of the MEPDG models predicted distress/IRI reasonably, others exhibited significant bias and poor model accuracy. Based on the analysis performed, the original MEPDG and recalibrated models presented in this report appear to predict distress/IRI reasonably well, within limitations including:

- HMA alligator cracking was not evaluated.
- Recalibrated HMA rutting and IRI models still have some bias.
- The HMA rutting, HMA IRI, and JPCP IRI models must be used only with the local calibration coefficients specified.
- The models may be valid only for the limited conditions under which they were evaluated.

A more comprehensive evaluation effort is needed that would include moderately to highly deteriorated pavements.

THIS PAGE INTENTIONALLY LEFT BLANK.

REFERENCES

AASHTO. *Mechanistic-Empirical Pavement Design Guide, Interim Edition: A Manual of Practice*, American Association of State and Highway Transportation Officials, Washington, DC, 2008.

Applied Research Associates, Inc. "Development of the 2002 Guide for the Design of New and Rehabilitated Pavement Structures," Final Report and Software (version 0.70) NCHRP Project 1-37A, Transportation Research Board, Washington, DC, April 2004.

Darter, M.I., et al. NCHRP *Research Digest 308: Changes to the Mechanistic-Empirical Pavement Design Guide Software through Version 0.900*, National Cooperative Highway Research Program, Transportation Research Board, Washington, DC, 2007.

LTPP Data Release Version 22. Federal Highway Administration, Washington, DC, 2008.

Miner, M.A. "Cumulative Damage in Fatigue," *Transactions*, American Society of Mechanical Engineers, Vol. 67, 1945, pp. A159-A164.

Sargand, S.M., et al. *Evaluation of Pavement Performance on DEL 23*, Report No. FHWA/OH-2007/05, Ohio Department of Transportation, Columbus, 2007.

SAS Institute Inc., *SAS 9.1.3 Help and Documentation*, Cary, NC: SAS Institute Inc., 2002-2004.